State of Oregon
Oregon Department of Geology and Mineral Industries
Brad Avy, State Geologist

GEOLOGIC MAP 121

GEOLOGIC MAP OF THE DEVINE RIDGE NORTH 7.5' QUADRANGLE, HARNEY COUNTY, OREGON

by Robert A. Houston[1], Jason D. McClaughry[2], Carlie J. M. Duda[3], and Clark A. Niewendorp[4]

2018

[1] Oregon Department of Geology and Mineral Industries, Springfield Field Office, Springfield Interagency Office, 3106 Pierce Pkwy D, Springfield, OR 97477
[2] Oregon Department of Geology and Mineral Industries, Baker City Field Office, Baker County Courthouse, 1995 3rd Street, Ste. 130, Baker City, OR 97814
[3] Oregon Department of Geology and Mineral Industries, 800 NE Oregon Street, Suite 965, Portland, OR 97232
[4] Retired from Oregon Department of Geology and Mineral Industries, 800 NE Oregon Street, Suite 965, Portland, OR 97232

NOTICE

Cover photograph: A view looking south along South Fork Trout Creek in the northeastern part of the Devine Ridge North 7.5' quadrangle, Harney County (43.86260, -118.884763WGS84 geographic coordinates; 348541.49mE, 4858342.01mN WGS84 UTM Zone 11 coordinates). The dacite rocks exposed in the background are the part of the oldest rock unit in the quadrangle. Photo credit: Robert A. Houston, 2017.

Oregon Department of Geology and Mineral Industries Geologic Map 121
Published in conformance with ORS 516.030.

For additional information:
Administrative Offices
800 NE Oregon Street, Suite 965
Portland, OR 97232
Telephone (971) 673-1555
Fax (971) 673-1562
www.oregongeology.org
https://www.oregon.gov/dogami

TABLE OF CONTENTS

LIST OF FIGURES

LIST OF TABLES

GEODATABASE

DRN2018_NCGMP09_v10.1.gdb

See the appendix for geodatabase description.
Geodatabase is Esri® version 10.1 format.

SHAPEFILES AND SPREADSHEETS

Shapefiles

Bedding: DRN2018_Bedding.shp
Geochemistry: DRN2018_Geochemistry.shp
Geochronology: DRN2018_Geochronology.shp
Magnetic polarity: DRN2018_Magnetics.shp
Reference map: DRN2018_RefMap.shp
Water Wells: DRN2018_WaterWells.shp
Cross Section Lines: DRN2018_XSectionLines.shp

Spreadsheets

DRN2018_DATA.xlsx master file contains:

- Bedding: DRN2018_Bedding.xlsx
- Geochemistry: DRN2018_Geochemistry.xlsx
- Geochronology: DRN2018_Geochronology.xlsx
- Magnetic polarity: DRN2018_Magnetics.xlsx
- Water Wells: DRN2018_WaterWells.xlsx

40Ar39ArAnalyticalData folder contains:

- Graph: 40Ar39ArDataGraph (.xlsx and .pdf)
- Summary: 40Ar39ArDataSummary (.xlsx)
- Table: 40Ar39ArDataTable (.xlsx and .pdf)

See the digital publication folder for files.
Metadata is embedded in the geodatabase and shapefiles and is also provided as separate .xml format files.

MAP PLATE

Plate 1. Geologic map of the Devine Ridge North 7.5' quadrangle, Harney County, Oregon, scale 1:24,000

1.0 INTRODUCTION

The Oregon Department of Geology and Mineral Industries (DOGAMI) mapped the geology of the Devine Ridge North 7.5′ quadrangle, Harney County, Oregon, during 2017 and 2018. This mapping is part of a multi-year geologic study of the Harney Basin, designated a high priority by the Oregon Geologic Mapping Advisory Committee (OGMAC; **Figure 1-1**; Plate 1). Key objectives of this project are: 1) provide an updated and spatially accurate geologic framework for the Devine Ridge North 7.5′ quadrangle; 2) correlate lithologic units to surrounding areas; 3) improve the understanding of the structural and lithologic controls on groundwater aquifers; and 4) describe the occurrence of geologic resources (aggregate, industrial, mineral, and energy) and geologic hazards within the quadrangle. This study was supported in part by a grant from the STATEMAP component of the National Cooperative Geologic Mapping Program (G17AC00210). Additional funds were provided by the State of Oregon.

The core products of this study are this report, an accompanying geologic map and cross sections, and an Esri™ ArcGIS™ ArcMap™ geodatabase. The geodatabase presents new geologic mapping in a digital format, consistent with the U.S. Geological Survey (USGS) National Cooperative Geologic Mapping Program 2009 draft standard format for digital publication of geologic maps, version 1.1 (NCGMP, 2010). It contains spatial information about geologic polygons, contacts, and structures, and basic data about each geologic unit such as age, lithology, mineralogy, and structure. The geologic map and cross sections, showing the distribution of bedrock lithology, critical structural relationships, and surficial geology, are at a scale of 1:24,000 (Plate 1).

Figure 1-1. Location map of the Devine Ridge North 7.5′ quadrangle, showing status map of geologic mapping completed, in progress, and planned in the Harney Basin. Green-shaded area encompasses 2017 to 2018 geologic mapping in the Devine Ridge North 7.5′ quadrangle (this study) and the Devine Ridge South 7.5′ quadrangle (Niewendorp and others, 2018). Orange-shaded quadrangles include areas where geologic mapping is currently being conducted by Portland State University (EDMAP). The blue-shaded quadrangle includes areas that have been mapped by DOGAMI with funding from OWRD and STATEMAP between 2016 and 2017. Red-shaded Poison Creek and Burns 7.5′ quadrangles are being mapped for STATEMAP during 2018 and 2019. Pink-shaded quadrangles include targets of future geologic mapping by DOGAMI. Lake label abbreviations are as follows: HL—Harney Lake; ML—Malheur Lake.

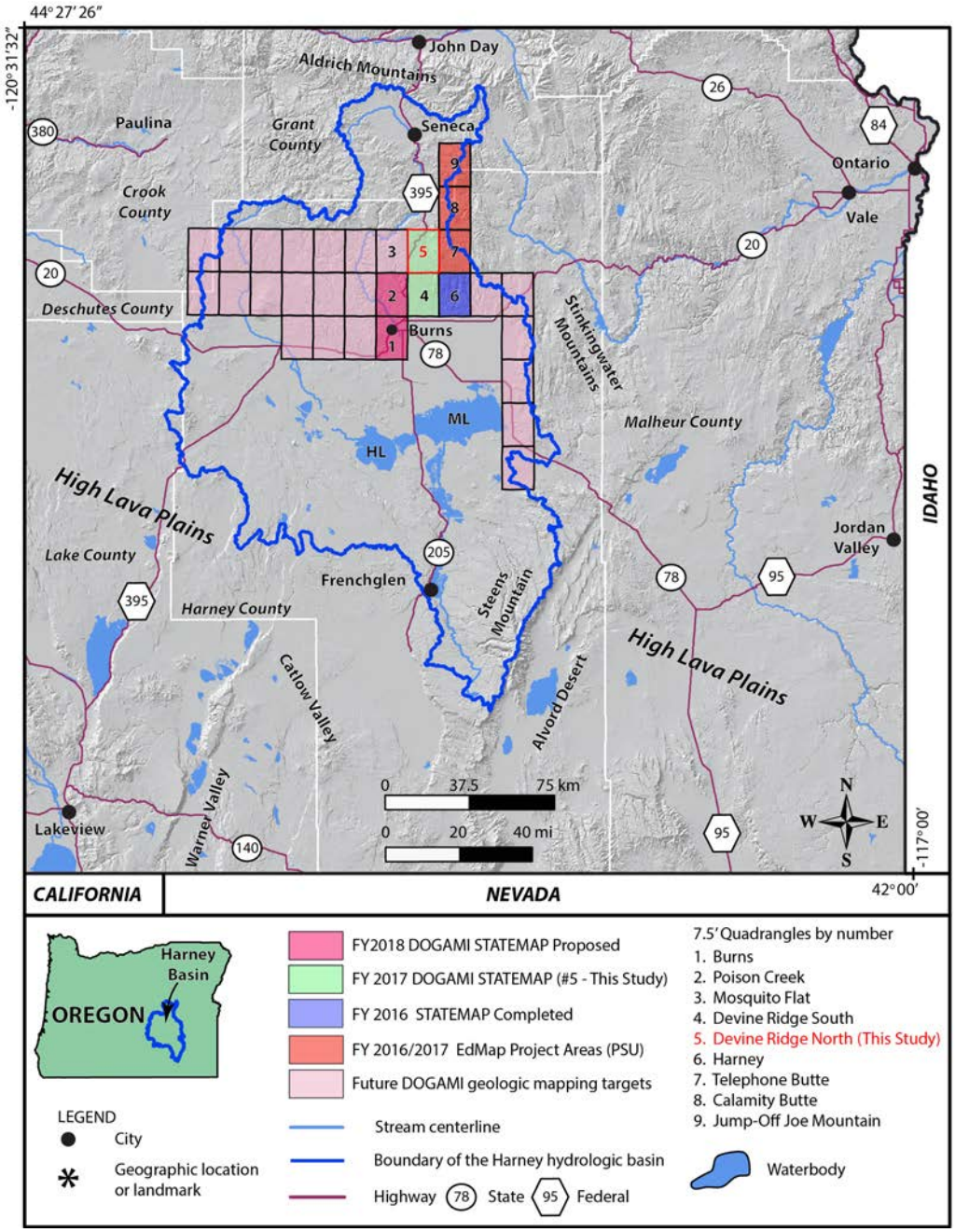

2.0 GEOGRAPHIC, ECOLOGIC, AND REGIONAL GEOLOGIC SETTINGS

The Harney Basin encompasses an area of approximately 13,566 km^2 (5,247 mi^2) in southeastern Oregon (**Figure 1-1**). The basin is internally drained and fed by several creeks and rivers, including Silver Creek, Silvies River, and the Donner und Blitzen River (**Figure 1-1**). These tributaries drain into numerous plains, marshes, and lakes, including Harney and Malheur Lakes, which lie near the geographic center of the basin. Topographic relief is substantial, ranging from a high of 2,967 m (9,733 ft) at the summit of Steens Mountain to a low of 1,248 m (4,093 ft) at Harney Lake in the center of the basin. Climate in the Harney Basin is semi-arid.

The Harney Basin straddles the boundary between the Blue Mountains, High Lava Plains, and Basin and Range physiographic provinces (Walker and MacLeod, 1991; **Figure 2-1**). The Blue Mountains Uplift province (BMU) extends into the northern part of the Harney Basin (**Figure 2-1**). The High Lava Plains province (HLP) transects the central part of the basin and is characterized by multiple episodes of late Miocene and younger bimodal volcanism (MacLeod and others, 1976; Jordan and others, 2004). The northern part of the Basin and Range province (BRP) extends into the southern third of the basin and is marked by large displacement (>150 m; >500 feet) north-northeast to northwest trending normal faults (e.g., Winter Rim fault, Abert Rim fault, Hart Mountain fault, Steens Mountain fault). BRP deformation began during the Miocene (~17 Ma; Donath, 1962; Thompson and Burke, 1974).

The Brothers fault zone (BFZ) lies across the southern part of the basin as a wide diffuse zone interpreted as an intracontinental transform fault separating the extended crust of the BRP from comparatively un-extended BMU crust to the north (Lawrence, 1976; **Figure 2-1**). The Steens fault extends across the eastern end of the BFZ. The western end is obscured by Holocene ash deposits (Lawrence, 1976). Lawrence described the BFZ as a series of longer (as much as 20 km; 12.4 miles) discontinuous en echelon faults (Reidel shears) trending ~N50°W and less abundant shorter (5 km, 3.1 miles) N30°E faults expressed as horst and graben structures (Lawrence, 1976). Faults in the BFZ largely dip steeply northeast, downdropping rock of the region northeast of the lineament down to the northeast. Iademarco (2009) and Trench (2008) suggested en echelon faults in the BFZ formed from ~7 Ma to 5 Ma. Trench (2008) suggested east-west extension in the Basin and Range Province is transitioned to the BFZ by way of dextral oblique strike-slip horsetail fractures and structural clockwise rotation about a pole located in northeastern Oregon.

The stratigraphic sequence in the Harney Basin includes a diverse assemblage of middle Miocene and younger lavas, fluvial and lacustrine sedimentary rocks, and widespread ash-flow tuffs that unconformably overlie a deeply eroded basement of Eocene to late Oligocene volcanic and sedimentary rocks and pre-Cenozoic accreted terranes (**Figure 2-2**).

Significant geologic units in the Harney Basin include the 16.7 Ma Steens Basalt of the Columbia River Basalt Group (CRBG; Camp and others, 2013), middle to late Miocene ash-flow tuffs, and late Miocene and Pliocene basaltic flows. Rocks of the Steens Basalt, the earliest lavas to erupt as part of the CRBG, are exposed in the southern part of the Harney Basin and cover much of southeastern Oregon and parts of southwestern Idaho to northern Nevada (**Figure 2-2**). The 14.6 and 15.8 Ma Picture Gorge Basalt (Watkins and Baksi, 1974) of the CRBG largely occurs in north-central Oregon and extends south to the northern part of the Harney Basin (Cahoon and Streck, 2017). Three voluminous tuffs, the 9.63 Ma Devine Canyon Ash-flow Tuff (Ford and others, 2013; S. L. Isom and M. J. Streck, unpub. data, 2017), 8.41 Ma Prater Creek Ash-flow Tuff (Jordan and others, 2004), and 7.05 Ma Rattlesnake Tuff (Streck and Grunder, 1995), overlie the CRBG and are important stratigraphic markers where exposed. The areal extent of the Rattlesnake Tuff is as much as 40,000 km^2 (15,444 miles^2). The caldera sources for these tuffs are not

exposed and but are thought on the basis of thickness and distribution to reside in the Harney Basin to the south and southwest of the study area (Greene, 1972; Streck, 1994; Khatiwada and Keller, 2015). Locally, Pliocene olivine-basalts of the High Lava Plains and several late Pleistocene to Holocene volcanic fields that occur along the northwest-trending Brothers fault zone overlie the ash-flow tuffs (**Figure 2-2**). Central and marginal parts of the Harney Basin are covered by sequences of Quaternary sediments (<100 m thick). The northern region of the basin can be generally described as a south dipping block on the flank of the Strawberry Mountains. Pre-Tertiary basement rocks are exposed less than 8 km (5 mi) to the northwest of the study area.

Figure 2-1. Physiographic province map of Oregon, showing location of the Brothers fault zone, selected Basin and Range faults, and the study area. Abbreviations: CR – Coast Range; HC – High Cascades; KM – Klamath Mountains; WC – Western Cascades; WV – Willamette Valley. Solid black lines demarcate physiographic provinces (after Walker, 1977). Blue lines are selected major Basin and Range type normal faults, showing normal displacement direction. White line marks the location of the Harney hydrologic basin. Basemap: 10-m hillshade DEM.

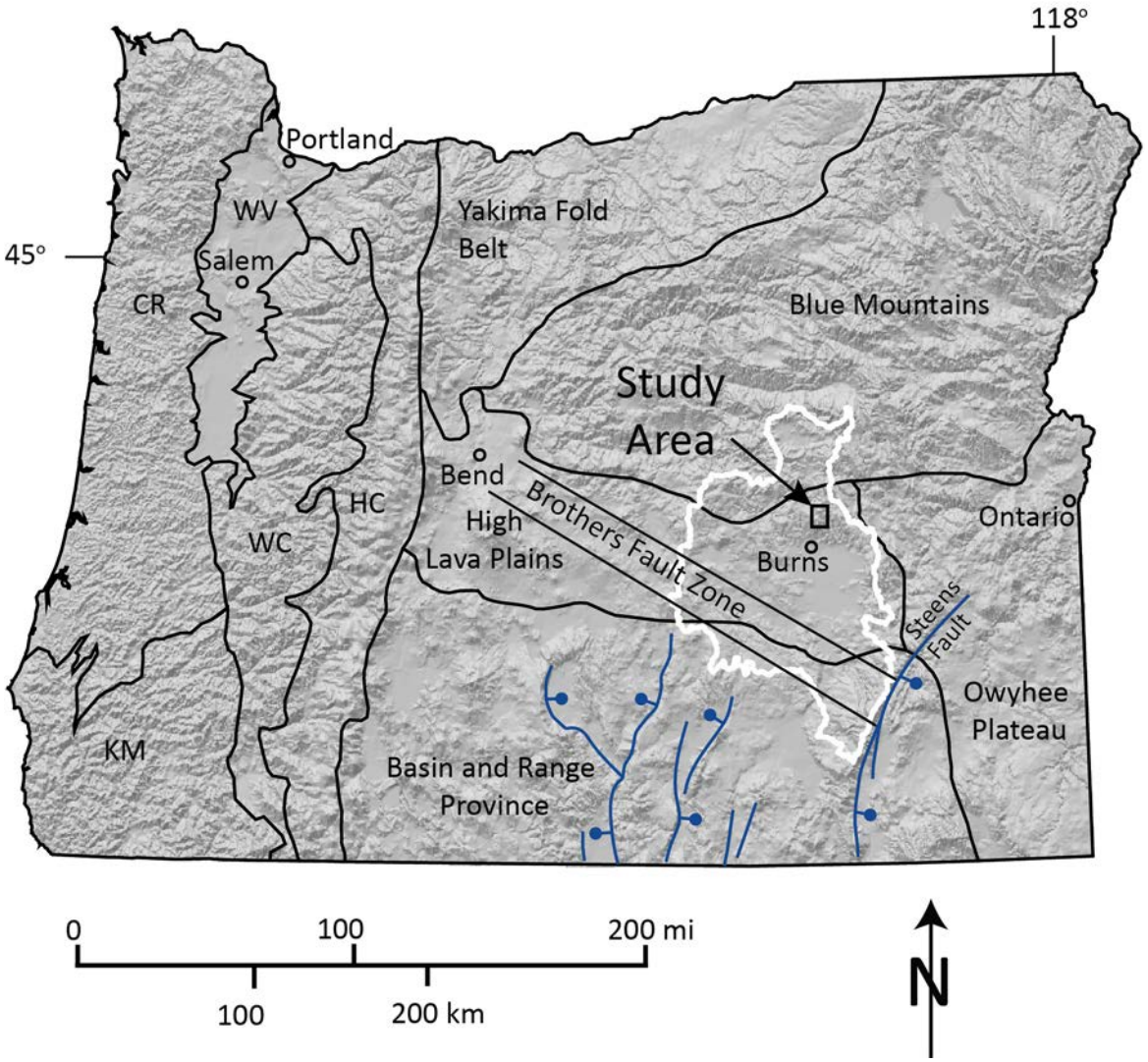

Figure 2-2. Generalized geology of southeastern Oregon. Generalized geologic map of southeastern Oregon, after Smith and Roe (2015).

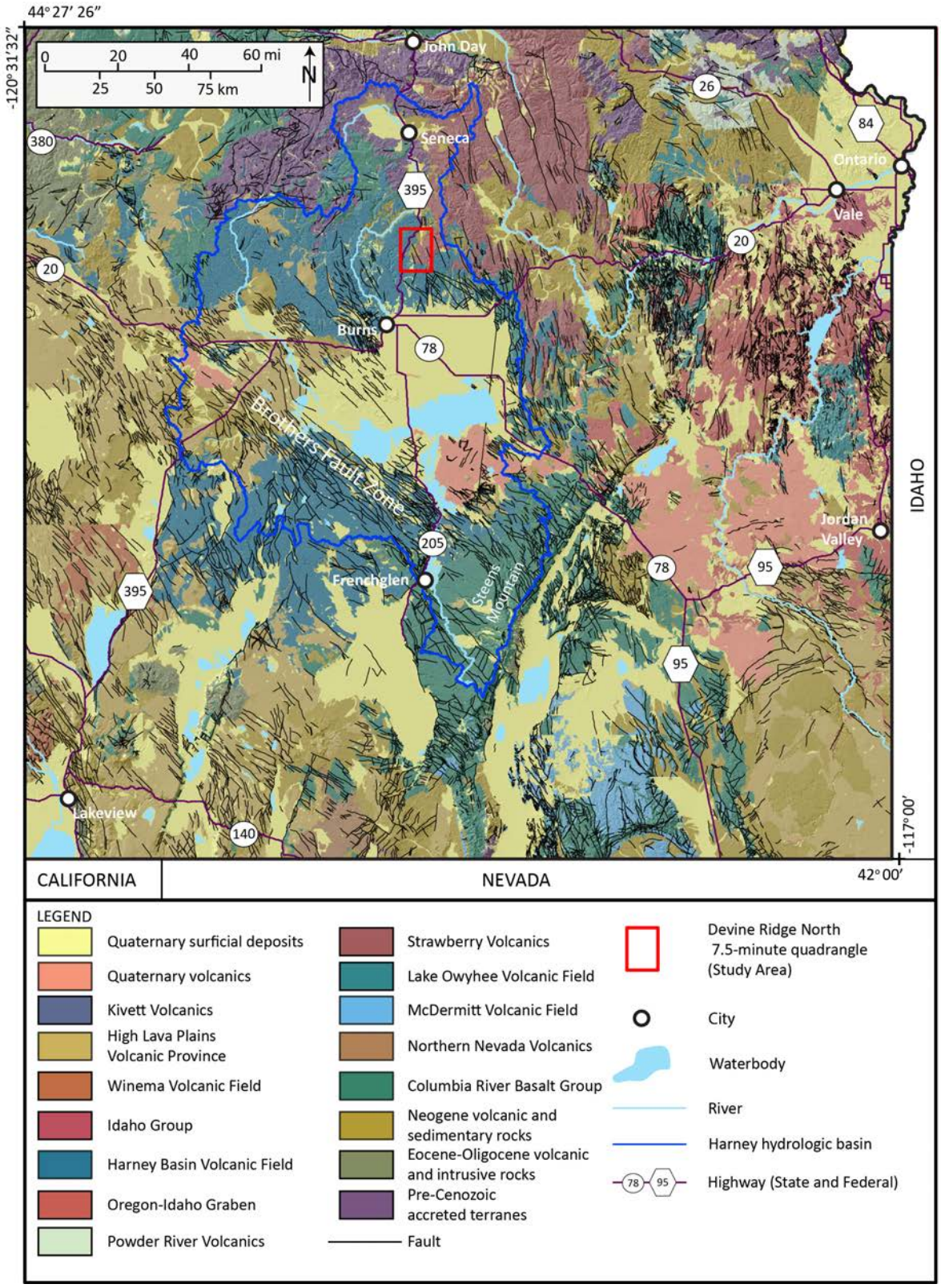

3.0 PREVIOUS WORK

This report builds on previous regional geologic mapping, groundwater studies, and natural resource investigations by Russell (1884), Piper and others (1939), Wagner (1944 unpublished report, Valley View Prospect [cinnabar, geodes], DOGAMI), Wallace and Calkins (1956), Walker and Repenning (1965), Brown and Thayer (1966) Greene (1972), Greene and others (1972), Greene (1973), Niem (1974), Lawrence (1976), Walker (1979), Brown and others (1980), Brown (1982), Gray and others (1983), McGrane (1985), Minor and others (1987a,b), Walker and MacLeod (1991) Johnson (1994), Sheppard (1994), Sherrod and Johnson (1994), Streck and Grunder (1995), Johnson (1996, 1998), Johnson and others (1998a,b), Camp and others (2003), Streck and Ferns (2004), Trench (2008), Meigs and others (2009), Milliard (2010), Boschmann (2012), Ferns and McClaughry (2013), Ford and others (2013), Camp and others (2013), Khatiwada and Keller (2015), Streck and others (2015), Isom (2017), S. L. Isom and M. J. Streck (unpub. data, 2017), Niewendorp and others (2018), Houston and others (unpub. data, 2018), M. Cruz and M. J. Streck (unpub. data, 2018). The index map shown in **Figure 3-1** summarizes the sources of regional geologic maps used during the preparation of the Devine Ridge North 7.5′ quadrangle geologic map (Plate 1).

Figure 3-1. Sources of geologic maps used during the preparation of this report. See DataSourcePolys feature class in the geodatabase. Basemap: 10-m shaded relief DEM.

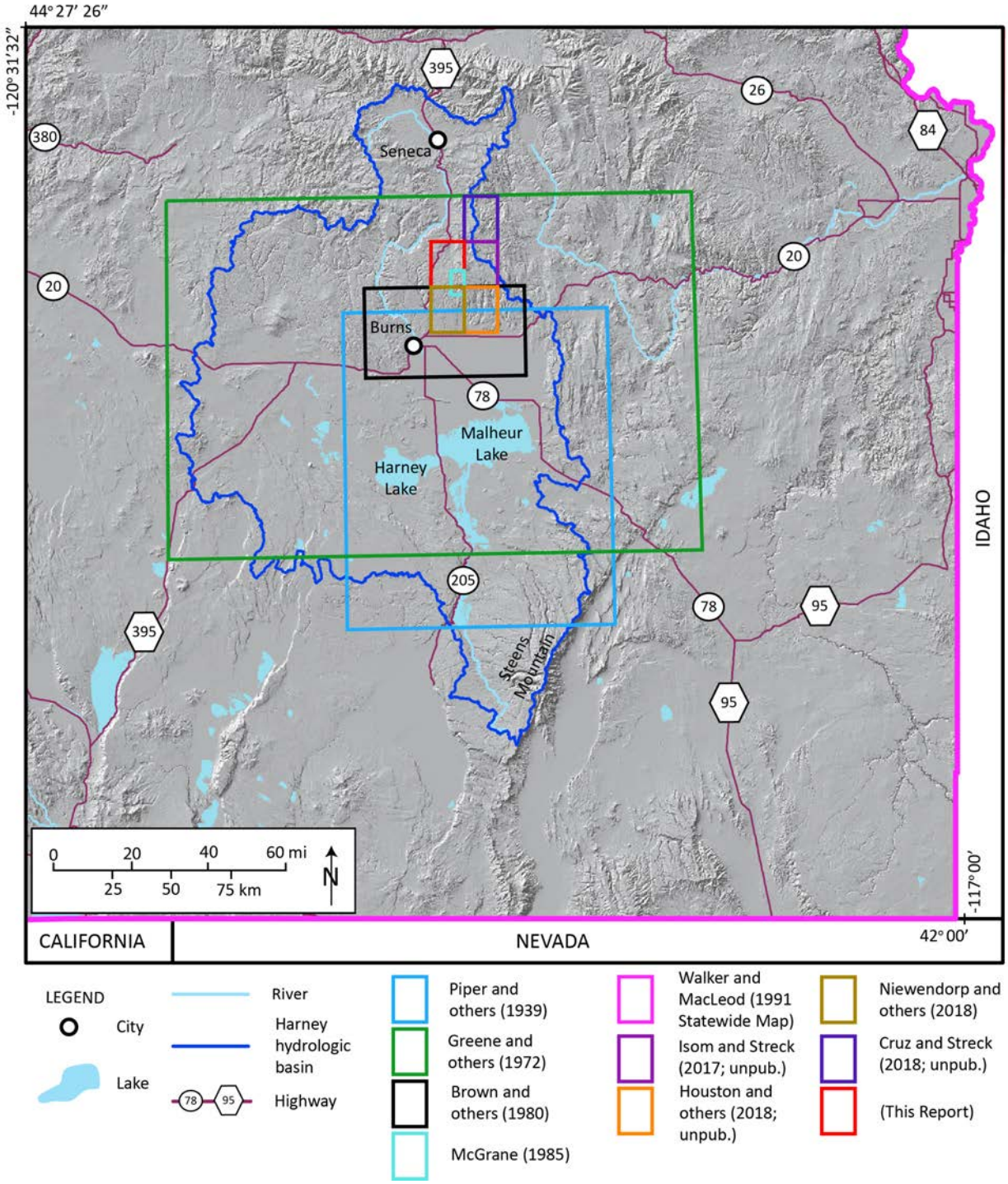

4.0 METHODOLOGY

Geologic data were collected digitally using a GPS-enabled Apple® iPad® 4 and an GPS-enabled Apple iPhone® 7, both loaded with Geometry Pty Ltd iGIS Pro, a geographic information system software package compatible with Esri ArcGIS. Geologic mapping used shaded relief raster images, USGS digital raster graphics (DRGs), and digital orthophoto imagery (2016) obtained from Google Earth™ as basemaps. Fieldwork conducted during this study consisted of data collection along roads, combined with transects following lithologic contacts and faults across public and private timber and rangelands. Standard geologic methods for collecting samples and measuring attitudes of inclined bedding, geologic features, and faults were employed. Digitization and the final digital Esri ArcGIS ArcMAP format geologic database was completed at a minimum scale of 1:24,000.

Mapping was supported by new and compiled X-ray fluorescence (XRF) geochemical analyses of whole-rock samples, thin-section petrography, and field and remotely collected strike and dip measurements of inclined bedding (Plate 1). Whole-rock geochemical samples were prepared and analyzed by XRF at the Washington State University GeoAnalytical Lab, Pullman, Washington, under the direction of Dr. Scott Boroughs. Analytical procedures for the Washington State University GeoAnalytical Lab are described by Johnson and others (1999) and can be obtained online at https://s3.wp.wsu.edu/uploads/sites/2191/2017/06/Johnson-Hooper-and-Conrey.pdf. Major element determinations were normalized to a 100-percent total on a volatile-free basis and recalculated with total iron expressed as FeO*. Whole-rock geochemical data are useful in classifying volcanic rocks, as many lavas are too fine grained and glassy to be adequately characterized by mineralogical criteria alone. Descriptive rock unit names for volcanic rocks are based in part on the online British Geological Survey classification schemes (Gillespie and Styles, 1999; Robertson, 1999; Hallsworth and Knox, 1999) and normalized major element analyses plotted on the total alkali ($Na_2O + K_2O$) versus silica (SiO_2) diagram (TAS) of Le Bas and others (1986), Le Bas and Streckeisen (1991), and Le Maitre and others (1989, 2004). The magnetic polarity of strongly magnetized lavas was determined at numerous outcrops using a handheld digital magnetometer. A new $^{40}Ar/^{39}Ar$ radiometric age-date determination was prepared and analyzed by Drs. Anthony Koppers and Daniel Miggins at the College of Oceanic and Atmospheric Sciences, Oregon State University, Corvallis, Oregon. Duncan and others (1997) describe the $^{40}Ar/^{39}Ar$ methodology used to collect new isotopic ages; additional information is available at http://geochronology.coas.oregonstate.edu/.

Microsoft Excel® spreadsheets tabulating geochemical analyses, water wells, and strike and dip measurements are provided as part of this publication and accompany the geodatabase. The appendix contains a summary of data collection methods and the field list for the spreadsheets mentioned above.

In this report, volcanic rocks with fine-grained (<1 mm [0.04 in]; Mackenzie and others, 1997; Le Maitre and others, 2004), average crystal or particle size in the groundmass are characterized in the following manner:

- A "coarse groundmass" if the average crystal or particle size is <1 mm (0.04 in) and can be determined using the naked eye (>~0.5 mm [0.02 in]).
- A "medium groundmass" if crystals of average size cannot be determined by eye but can be distinguished by using a hand lens (>~0.05 mm [0.02 in]).
- A "fine groundmass" if crystals or grains of average size can be determined only by using a microscope (or by hand lens recognition of phyllite-like sparkle or sheen in reflected light, indicating the presence of crystalline groundmass).

- A “glassy groundmass” if the groundmass has (fresh), or originally had (altered), groundmass with the characteristics of glass (conchoidal fracture; sharp, transparent edges; vitreous luster; etc.).
- Mixtures of crystalline and glassy groundmass are described as intersertal; ratios of glass to crystalline materials may be indicated by textural terms including holocrystalline, hypocrystalline, hyalophitic, and hyalopilitic.
- Microphenocrysts are defined as crystals larger than the overall groundmass and < 1 mm across (0.04 in).

Grain size of clastic sedimentary rocks is described following the Wentworth (1922) scale. Hand samples of unconsolidated sediments and clastic sedimentary rocks were compared in the field and/or in the laboratory to graphical representations (comparator) of the Wentworth scale to determine average representative grain size in various parts of a respective sedimentary geologic unit. Colors given for hand-sample descriptions are from the Geological Society of America Rock-Color Chart Committee (1991).

Subsurface geology shown in the geologic cross section (Plate 1) incorporates lithologic interpretations from water-well drill records available through the Oregon Water Resources Department (OWRD) Groundwater Resource Information Distribution (GRID) system (Plate 1; Appendix). Water wells were not physically located. However, an attempt was made remotely to locate water wells and other drill holes that have well logs archived by OWRD. Approximate locations were estimated by using a combination of sources, including internal OWRD databases of located wells, Google Earth™, tax lot maps, street addresses, and aerial photographs. The accuracy of the locations ranges widely, from errors of 1.1 km (0.7 mi) possible for wells located only by section and plotted at the section centroid to a few tens of feet for wells located by address or tax lot number on a city lot with bearing and distance from a corner. A well log ID is queried in the database (e.g., HARN-51852) to retrieve an image of the well log from the OWRD website (https://apps.wrd.state.or.us/apps/gw/well_log/). A database of well logs with interpreted subsurface geologic units for the Devine Ridge North 7.5′ quadrangle is provided with the geodatabase.

To allow the interested reader to visit these sites in the field or to visualize remotely the area by using Google Earth™, map coordinates are provided for outcrop photographs shown in report figures. Locations are provided in two coordinate systems: (1) Geographic (datum = WGS84, units = decimal degree); and (2) Universal Transverse Mercator (UTM) Zone 11 (datum = WGS84, units = meters). Decimal degree coordinates can be entered into the “Fly to” box (e.g., 45.661323, -121.471230) in the search toolbar, and Google Earth™ will automatically locate and “fly” to the specified site.

5.0 EXPLANATION OF MAP UNITS

The suite of terrestrial sedimentary and volcanic bedrock units in the Devine Ridge North 7.5′ quadrangle ranges in age from late Miocene to late Oligocene (**Figure 5-1**; Plate 1). Bedrock geologic units are locally covered along drainages and on some slopes in the project area by Pleistocene and Holocene surficial deposits. Widely separated stratigraphic units were grouped on the basis of apparent stratigraphic position, lithology, and chemical composition. Unit names follow local stratigraphic nomenclature when available, but when formal rock names are lacking, informal names are given because of composition or sites of good exposure. **Figure 5-1** depicts a time-rock chart showing age ranges for late Cenozoic bedrock and surficial units.

5.1 Overview of map units

UPPER CENOZOIC SURFICIAL DEPOSITS

Qf modern fill and construction material (upper Holocene)
Qa alluvium (Holocene and Upper Pleistocene[?])
Qaf fan deposits (Holocene and Upper Pleistocene[?])
Qls landslide deposits (Holocene and Upper Pleistocene[?])
Qao older alluvium (Holocene and Upper Pleistocene[?])
Qt strath-terrace deposit (Holocene and lower Pleistocene[?])

Angular unconformity to disconformity

UPPER TO LOWER CENOZOIC VOLCANIC AND SEDIMENTARY ROCKS

UPPER TO MIDDLE MIOCENE VOLCANIC AND SEDIMENTARY ROCKS

Tmtr Rattlesnake Tuff (upper Miocene) 7.05 ± 0.01 Ma ($^{40}Ar/^{39}Ar$); 7.093 ± 0.015 Ma ($^{40}Ar/^{39}Ar$)
Tmtp Prater Creek Ash-flow Tuff (upper Miocene) 8.41 ± 0.16 ($^{40}Ar/^{39}Ar$)
Tmtd Devine Canyon Ash-flow Tuff (upper Miocene) 9.63 ± 0.05 Ma ($^{40}Ar/^{39}Ar$)
Tmst tuffaceous sedimentary rocks (upper Miocene[?] and middle Miocene[?])

Nonconformity

MIDDLE TO LOWER MIOCENE VOLCANIC ROCKS

Tmdc Dinner Creek Tuff (middle or lower Miocene) 15.9 ± 0.09 Ma ($^{40}Ar/^{39}Ar$); 16.16 ± 0.02 Ma ($^{40}Ar/^{39}Ar$)
Tmb basalt-basaltic andesite (lower Miocene[?])

Angular unconformity to disconformity

UPPER OLIGOCENE VOLCANIC ROCKS

Toa andesite (upper Oligocene) 24.75 ± 0.15 Ma ($^{40}Ar/^{39}Ar$)
Tor rhyolite (upper Oligocene [?])
Toda dacite (upper Oligocene [?])

Figure 5-1. Time-rock chart of the Devine Ridge North 7.5' quadrangle showing the 15 geologic units shown on the geologic map and in geologic cross sections in the Devine Ridge North 7.5' quadrangle.

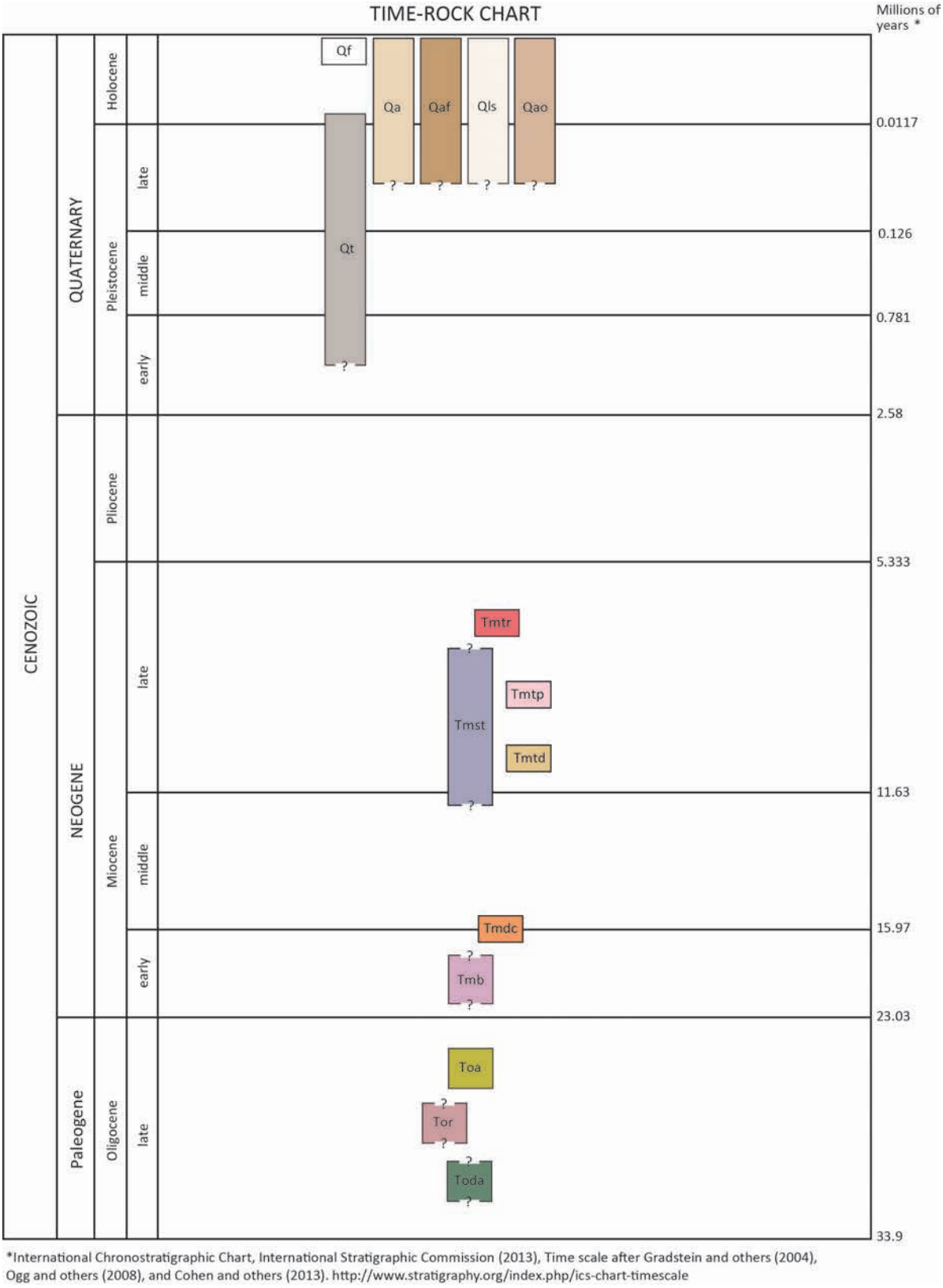

*International Chronostratigraphic Chart, International Stratigraphic Commission (2013), Time scale after Gradstein and others (2004), Ogg and others (2008), and Cohen and others (2013). http://www.stratigraphy.org/index.php/ics-chart-timescale

5.2 Upper Cenozoic surficial deposits

Upper Cenozoic sedimentary and volcanic rocks are locally covered by Pleistocene and Holocene surficial deposits in the Devine Ridge North 7.5′ quadrangle (**Figure 5-1**; Plate 1). Important surficial units include alluvial, landslide, and fan deposits. Surficial units within the project area are delineated on the basis of geomorphology as interpreted from a combination of field observations, shaded relief raster images, USGS digital raster graphics (DRGs) and digital orthophoto imagery (2016).

Qf **modern fill and construction material (upper Holocene)**— Artificial or constructed fill deposits of poorly sorted and crudely layered mixed gravel, sand, clay, and other engineered fill (Plate 1). These deposits usually contain rounded to angular clasts ranging from small pebbles to boulders up to several meters across. The orientation of clasts is typically less uniform than is found in naturally occurring imbricated or bedding-parallel gravel. Deposits mapped as modern fill and construction material in the map area are generally associated with dams, road embankments, culvert fills, and mined land (**Plate 1**). The thickness of fill-deposits may exceed 30 m (98 ft).

Qa **alluvium (Holocene and Upper Pleistocene[?])**—Unconsolidated gravel, sand, silt, and clay deposited along active stream channels and on adjacent floodplains (**Figure 5-2**; Plate 1). Gravels deposited as imbricated, massive to cross-stratified accumulations on smaller mid-channel islands and bars are the most common type of near-channel alluvium along major tributaries. Thickness of alluvial deposits is generally less than 5 m (16 ft); bedrock units may be locally exposed in the bottoms of stream channels within areas mapped as unit **Qa**. The unit is assigned Holocene and late Pleistocene age on the basis of stratigraphic position and a lack of more precise age indications.

Figure 5-2. Annotated photograph of representative alluvium, older alluvium, and fan deposits within the study area. Locally older alluvium (Qao) and alluvium (Qa) are preserved along South Fork Trout Creek. The active channel is eroding the toe of a fan deposit (Qaf). Bedrock in the background is dacite (Toda) (43.862466, –118.884357 WGS84 geographic coordinates; 348573.7018mE, 4858323.1645mN WGS84 UTM Zone 11 coordinates).

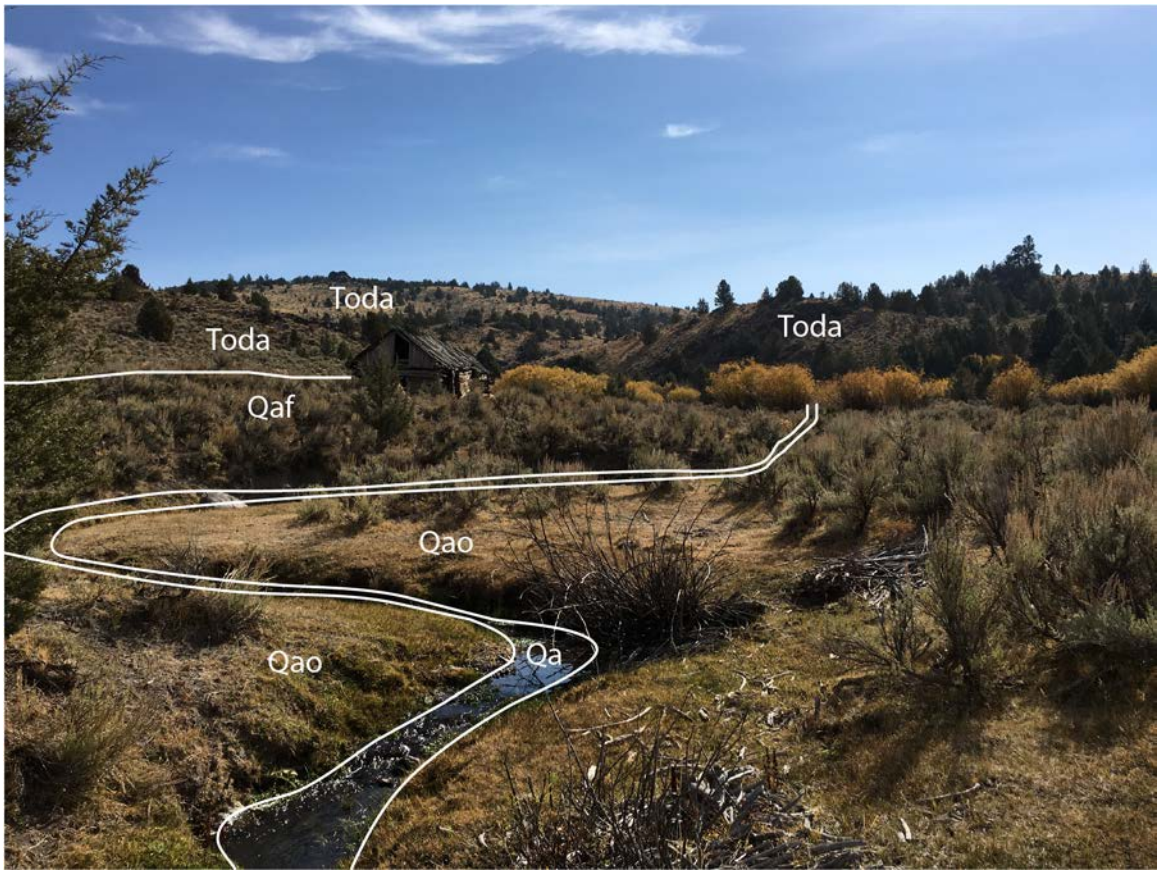

Qaf **fan deposits (Holocene and Upper Pleistocene[?])**—Unconsolidated deposits of boulders, cobbles, pebbles, granules, sand, silt, clay, and woody debris preserved in fan-shaped accumulations at the transition between low-gradient valley floodplains and steeper upland drainages (**Figure 5-2**; Plate 1). Fan surfaces are characterized by anastomosing, intermittent fluvial channels formed where pools or obstructions such as log jams or debris flow levees create flow diversions. Sediment accumulates on the fan surface through normal fluvial deposition, avulsions, and lateral migration as streams emerge from upland settings and the gradient falls below the threshold for further sediment transport. Fans also accumulate during episodic high-discharge events as accumulations of soil, colluvium, large woody debris, or as landslide deposits are remobilized and transported down slope as fast- moving sediment gravity flows (hyperconcentrated floods and debris flows). The unit may locally include rapidly deposited talus from rockfall in steep drainages. Fans typically have a steep gradient at the apex, moderate gradient through the middle section, and low gradient near the toe. Individual fans generally cover less than 1 hectare (2.47 acres). The local thickness of alluvial fan deposits is variable but is probably <15 m (50 ft). Fan deposits are considered to be Holocene and late Pleistocene in age on the basis of stratigraphic position and a lack of more precise age indicators.

Qls **landslide deposits (Holocene and Upper Pleistocene[?])**—Unconsolidated, chaotically mixed masses of rock and soil deposited by landslides (e.g., slumps, slides, earth flows, rock avalanches; Plate 1). Deposits may consist of individual slide masses or may form large complexes resulting from multiple generations of landslide activity. Recent landslide terrain is characterized by sloping hummocky surfaces, locally marked by closed depressions, springs, wet seeps, and scarps. Active or recently active landslides are marked by marginal levees and open ground fissures; tilted trees and bent trunks may be common on the surface. Toes of more recent deposits retain convex-up, fan-shaped morphologies. Slides are often traceable uphill to headwall scarps or slip surfaces. In more deeply seated landslides, these head scarps commonly expose bedrock. The unit locally includes rock fall, large talus piles, shallow-seated landslides of colluvium, rapidly emplaced debris flow deposits, and more deeply seated bedrock slides. Quaternary landslide complexes in the map area are moderate in extent covering as much as 70 hectares (173 acres). Thickness of landslide deposits is highly varied but may be more than several tens of meters in larger deposits. Large areas mapped as Quaternary landslide deposits typically include many discrete deposits of varying age that are not differentiated here. Landslide deposits are typically referred to as clay, boulders, rock, or rock and clay in water well logs. The unit is assigned a Holocene and late Pleistocene age on the basis of stratigraphic position and a lack of more precise age indications.

Qao **older alluvium (Holocene and Upper Pleistocene[?])**—Moderately dissected, unconsolidated, well- to poorly sorted and stratified gravel, sand, silt, and clay deposited in active stream channels and on adjoining flood plains (**Figure 5-2**; Plate 1). These deposits are recognized and mapped along Trout Creek and its tributaries, where deposits reside adjacent to incised drainages filled with younger Quaternary alluvium (**Qa**). Thickness likely does not exceed 6 m (20 ft). The unit is assigned a Holocene and late Pleistocene age on the basis of stratigraphic position and a lack of more precise age indications.

Qt **strath-terrace deposit (Holocene and Upper Pleistocene[?])**—Unconsolidated, well- to poorly sorted gravel, sand, silt, and clay deposited on an eroded paleosurface of tuffaceous sedimentary rocks (**Tmst**) and Rattlesnake Tuff (**Tmtr**) (**Figure 5-3**; Plate 1). The terrace gravels are less than 1 m (3 ft) thick in the northern part of the quadrangle adjacent to Trout Creek. Subsequent channel incision has isolated this strath-terrace deposit approximately 3 m (10 ft) above the modern alluvial (**Qa**) deposits in the active stream channel. The unit is assigned a Holocene and lower Pleistocene age on the basis of stratigraphic position and a lack of more precise age indicators.

Figure 5-3. Photograph of strath-terrace deposit in the northern part of the map area. (A) Tuffaceous sedimentary rocks (Tmst) are overlain by a thin (as much as 1 m; 3 ft) mantling of strath-terrace gravel (Qt) (43.871768, -118.923235 WGS84 geographic coordinates; 345473.4811mE, 4859428.3099mN WGS84 UTM Zone 11 coordinates). *(Figure continued on following page.)*

(Figure 5-3, continued) **Photograph of strath-terrace deposit in the northern part of the map area. (B) Strath-terrace gravel deposit overlying Rattlesnake Tuff (Tmtr). Gravels (Qt) are as much as 1 m (3 ft) in thickness (43.86939, -118.923726 WGS84 geographic coordinates; 345427.8186mE, 4859165.1114mN WGS84 UTM Zone 11 coordinates).**

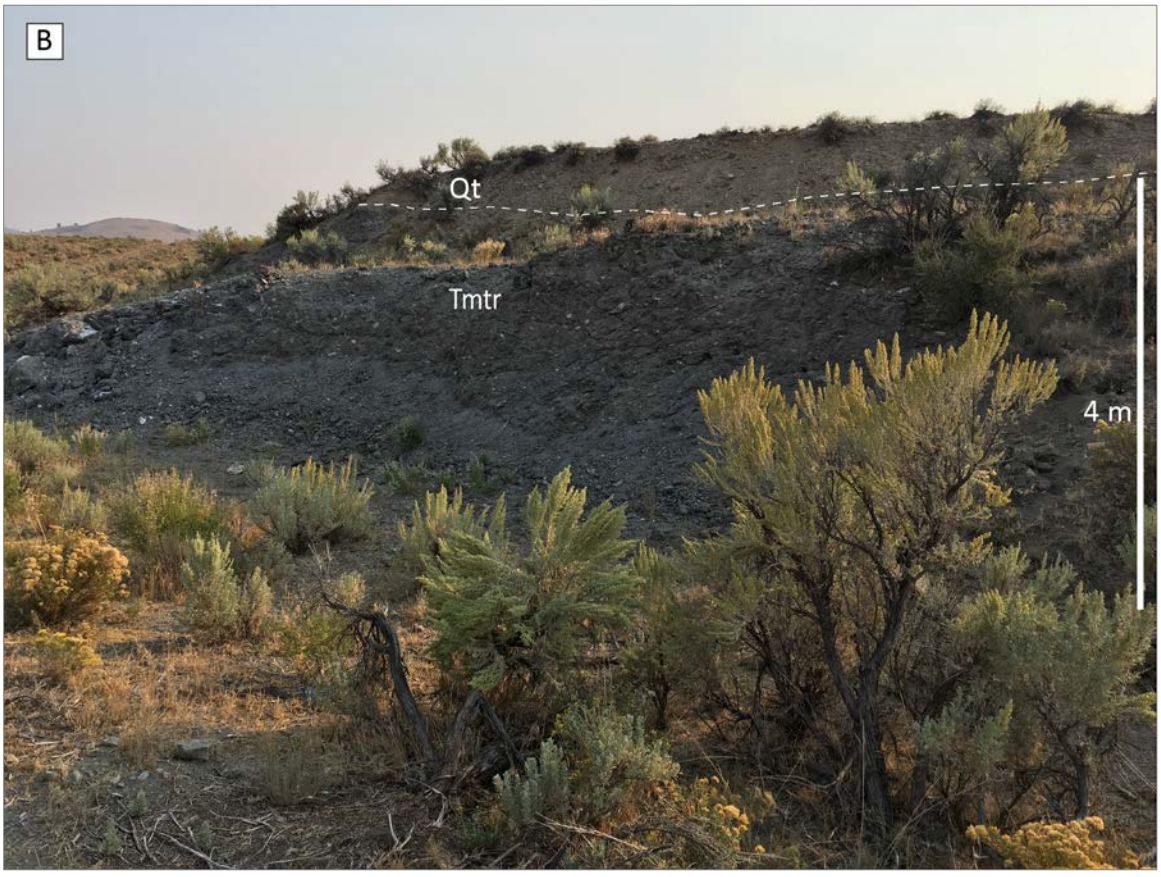

Angular unconformity to disconformity

5.3 Cenozoic volcanic and sedimentary rocks

5.3.1 Upper Miocene and upper Oligocene volcanic and sedimentary rocks

The upper Miocene volcanic and sedimentary stratigraphy contains three laterally extensive ash-flow tuffs that were deposited within a continuous sequence of tuffaceous sedimentary rocks. The felsic tuffs (**Tmtr**, **Tmtp**, **Tmtd**, and **Tmdc**) overlie a lower Miocene and upper Oligocene succession of basalt and basaltic trachy-andesite (**Tmb**), andesite (**Toa**), and dacite (**Toda**). Locally, the dacite is intruded by irregular rhyolitic bodies and dikes (**Tor**).

X-ray fluorescence (XRF) geochemical analyses of whole-rock samples were obtained on 97 samples from the Devine Ridge North 7.5′ quadrangle and are plotted against samples from both Devine Ridge South (DRS) and Harney (Harn.) quadrangles on total alkali ($Na_2O + K_2O$) vs. silica (SiO_2) (**Figure 5-4**), TiO_2 vs. P_2O_5, and Nb vs. Zr elemental variation diagrams (**Figure 5-5**). Major and trace element abundances of representative samples for lithologic units are listed in **Table 5-1**. The following section will present field, hand sample, petrographic, and geochemical characteristics for the early to late Miocene volcanic and sedimentary rocks.

Figure 5-4. Total alkali ($Na_2O + K_2O$) vs. silica (SiO_2) plot classification (TAS), showing whole-rock XRF analyses on volcanic rocks from the upper Miocene to upper Oligocene sampled from the Devine Ridge North (DRN; filled symbols) Devine Ridge South (DRS; symbols not filled), and Harney (Harn.; symbols not filled) 7.5' quadrangles (normalized to 100 percent anhydrous). TAS graph fields are from Le Bas and others (1986) and Le Maitre and others (2004).

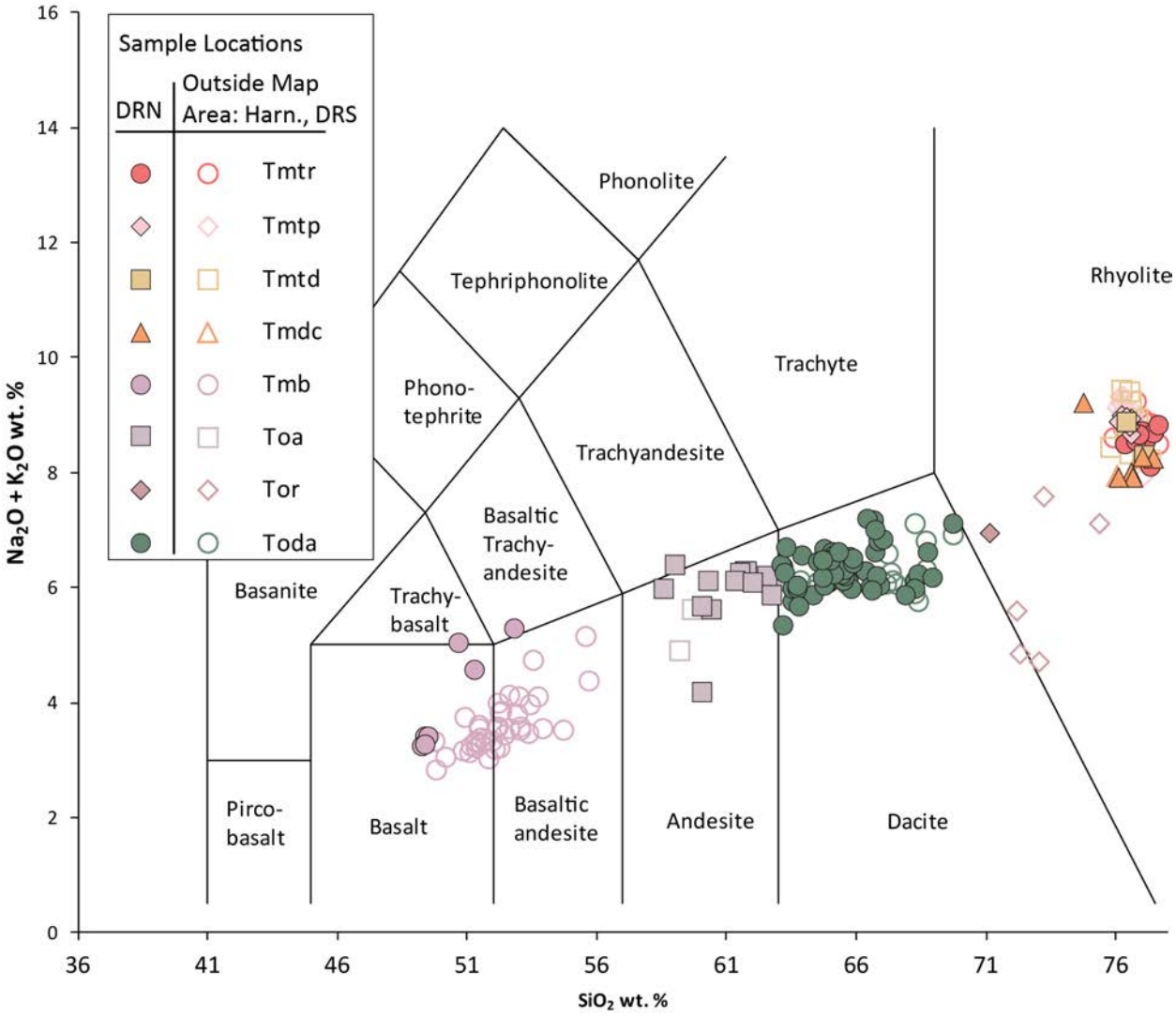

Table 5-1. Representative XRF analyses for late Miocene to late Oligocene volcanic rocks sampled from the Devine Ridge North 7.5' quadrangle.

Sample No.	HBH162-17	HBH286-17	HBH194-17	HBH307-17	HBH066-17	HBH012-17	HBH040-17	HBH042-17
Formation	na	na	na	na	Dinner Creek Tuff	Devine Canyon Ash-flow Tuff	Prater Creek Ash-flow Tuff	Rattlesnake Tuff
Map Unit	dacite	rhyolite	andesite	basalt-basaltic andesite	Dinner Creek Tuff	Devine Canyon Ash-flow Tuff	Prater Creek Ash-flow Tuff	Rattlesnake Tuff
Map Label	Toda	Tor	Toa	Tmb	Tmdc	Tmtd	Tmtp	Tmtr
UTM_N (NAD 83)	4849288.618	4848018.48	4859397.489	4846410.828	4852142.9	4856499.234	4851407.698	4851791.882
UTM_E (NAD 83)	344588.2028	345014.1536	345103.3431	348410.2025	346186.1825	342057.8598	339329.5779	339591.4944
Age (Ma)	nd	nd	24.75	nd	16	9.63	8.41	7.05
Map No.	G43	G98	G109	G5	G70	G100	G58	G63
Oxides, weight percent								
SiO_2	65.23	71.17	62.66	49.32	76.70	76.48	76.26	77.20
Al_2O_3	16.43	15.67	17.53	16.82	12.64	11.65	11.98	12.17
TiO_2	0.66	0.42	0.80	1.57	0.18	0.23	0.17	0.17
FeO*	4.11	2.73	5.58	11.44	2.26	2.32	2.26	1.61
MnO	0.07	0.05	0.06	0.19	0.03	0.05	0.06	0.07
CaO	4.64	2.39	5.41	10.41	0.26	0.36	0.24	0.20
MgO	2.08	0.46	1.49	6.84	0.01	0.03	0.04	0.05
K_2O	3.15	3.16	2.00	0.51	3.77	5.17	4.56	4.47
Na_2O	3.38	3.79	4.17	2.69	4.14	3.67	4.43	4.05
P_2O_5	0.25	0.16	0.29	0.22	0.02	0.04	0.01	0.02
Total_I	97.23	96.86	98.08	97.23	97.75	97.42	99.05	98.59
LOI	2.24	2.42	1.29	2.24	1.53	1.36	0.31	0.51
Trace elements, parts per million								
Ni	23	13	38	71	5	6	7	7
Cr	24	10	36	145	3	4	3	4
Sc	10	6	13	38	4	2	2	5
V	96	48	110	312	8	7	6	7
Ba	1,257	1,270	1,002	240	1,422	103	79	754
Rb	46	59	32	7	74	98	103	90
Sr	711	406	661	268	32	13	13	16
Zr	125	110	148	81	466	803	508	310
Y	11	16	22	26	86	100	62	77
Nb	7.0	8.7	8.1	5.1	25.4	57.9	45.1	30.9
Ga	17	16	18	17	22	27	23	20
Cu	28	24	45	114	4	8	5	9
Zn	66	63	85	77	146	163	98	92
Pb	14	16	12	2	15	22	13	17
La	25	31	25	10	62	98	57	40
Ce	40	45	46	20	69	186	118	69
Th	4	6	5	1	8	9	11	8
Nd	19	23	21	12	65	88	46	48
U	2	4	1	2	3	4	4	3

Major element determinations have been normalized to a 100-percent total on a volatile-free basis and recalculated with total iron expressed as FeO*; nd is no data or element not analyzed; na is not applicable or no information; Total I is total initial unnormalized major elements weight percent; LOI is loss on ignition.

Figure 5-5. Elemental variation diagram showing niobium versus zircon of units Tmdc, Tmtd, Tmtp, and Tmtr sampled from the Devine Ridge North (DRN – filled symbols), Devine Ridge South (symbols not filled), and Harney (symbols not filled) 7.5' quadrangles.

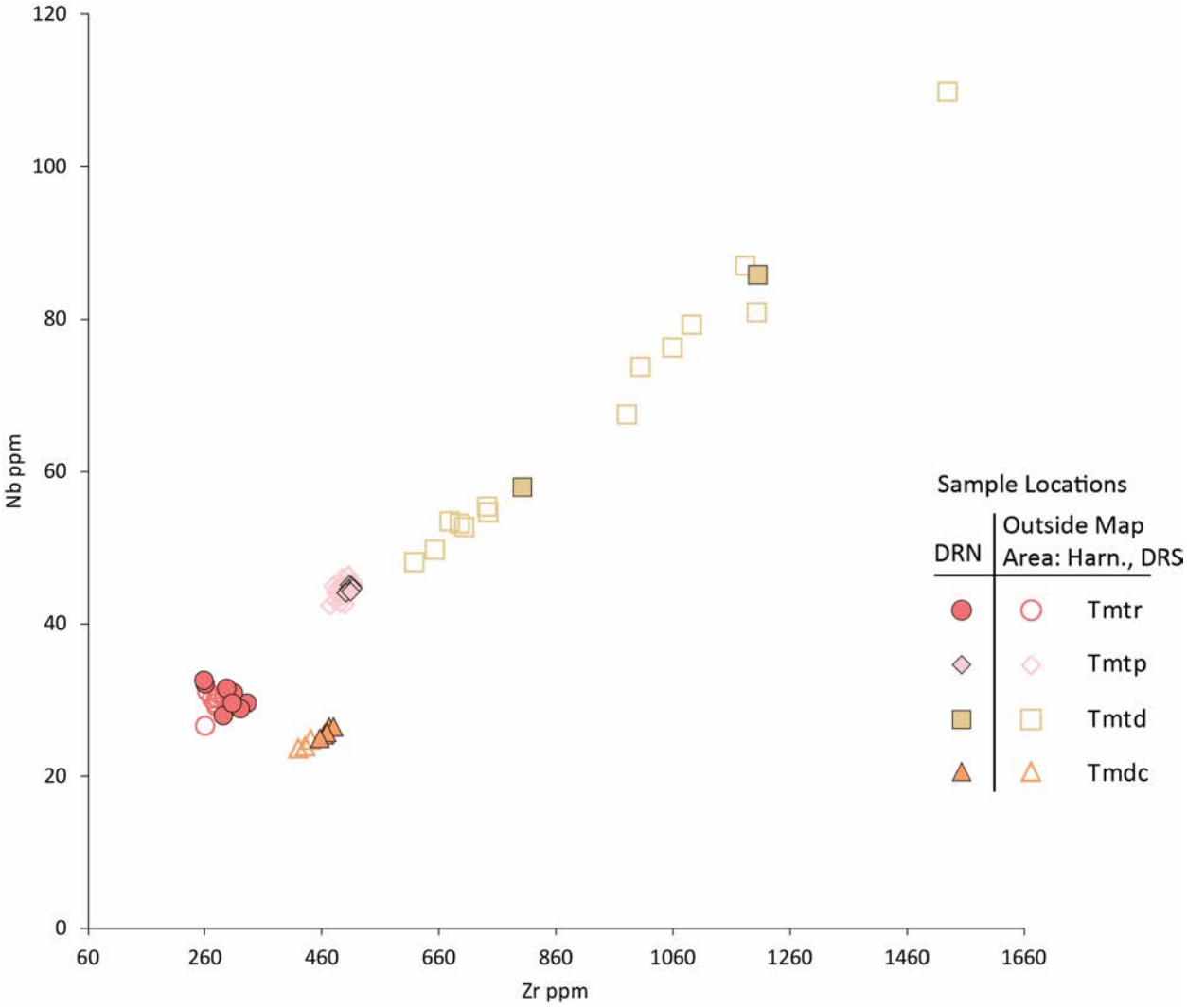

Tmtr **Rattlesnake Tuff (upper Miocene)**—Vitric, crystal-poor, pumice- and lithic-rich tuff exposed primarily in the western part of the map area (**Figure 5-6A**; **Figure 5-6B**; Plate 1). The tuff is 10 to 20 m (32 to 65 ft) thick in the map area and occurs as a single cooling unit. Welded sections form prominent cliff exposures (**Figure 5-6A**; Plate 1). Within the study area, crystallization facies include a vapor phase, pervasively devitrified zone, and a spherulitic and lithophysal zone (Streck and Grunder, 1995). The basal contact and associated non-welded, laminated basal surge deposits are poorly exposed and are overlain by a densely welded vitric tuff (**Figure 5.6C**). Locally, lithophysae increase in abundance up section from the <2 m (6.5 ft) thick basal vitrophyre zone. The lithophysal zone grades upward to a hackly jointed, massively bedded tuff with a eutaxitic texture defined by aligned fiamme. Devitrified, moderately flattened black, white, and banded fiamme occur up to 10 cm (3.9 in) in diameter. Poly-compositional lithic fragments consist of

angular, moderate reddish brown (10R 4/6) fragments as much as 1 cm (0.5 in) in length that are supported in a devitrified glass shard and crystal groundmass.

Typical hand samples are very pale orange (10YR 8/2), to very light gray (N7), to medium gray (N5), and light brownish gray (5YR 6/1), containing < 3 percent quartz, subhedral to euhedral, zoned anorthoclase and anhedral to euhedral clinopyroxene (ferrohedenbergite) microphenocrysts and phenocrysts < 2 mm (0.01 in) distributed within a vitric groundmass. The tuff is petrographically characterized by ~2 percent quartz and feldspar phenocrysts, ~1 percent ferrohedenbergite phenocrysts, ~15 percent lithic fragments, ~15 percent pumice, and 55 percent devitrified glass-shard groundmass (**Figure 5-6D** through **Figure 5-6G**). The original vitroclastic texture of the tuff is retained, but is locally overprinted by very fine elongated crystals forming axiolitic structures (**Figure 5-6D** through **Figure 5-6G**). Samples obtained from this unit have rhyolitic compositions with 76.01 to 79.69 weight percent SiO_2, 10.63 to 12.72 weight percent Al_2O_3, 3.13 to 4.40 weight percent Na_2O, and 4.12 to 5.57 weight percent K_2O (**Table 5-1**). The tuff also contains relatively moderate amounts of barium (365 to 808 ppm Ba), zirconium (261 to 312 ppm Zr), yttrium (83 to 115 ppm Y), and niobium (26.5 to 31.04 ppm Nb).

The unit is equivalent to the Rattlesnake Ash-flow Tuff formally described by Walker (1979) and later renamed to Rattlesnake Tuff by Streck and Grunder (1995) (**Figure 5-6**). Regionally, the Rattlesnake Tuff occurs as a thick deposit that covered at least 35,000 km^2 (13,500 mi^2) (Streck and Grunder, 1995). Although no caldera source related to the tuff is exposed, from pumice size and distance correlations, Streck (1994) proposed a vent located in the western part of the Harney Basin. The Rattlesnake Tuff has a reversed magnetic polarity (Parker, 1974; Thormahlen, 1984; Smith, 1986a,b; Streck, 1994) and is assigned a late Miocene age on the basis of stratigraphic position and $^{40}Ar/^{39}Ar$ ages of 7.05 ± 0.1 Ma (Streck, 1994) and 7.093 ± 0.015 Ma (Jordan and others, 2002).

Figure 5-6. Outcrop, hand sample, and petrographic photographs of the Rattlesnake Tuff (Tmtr). (A) Typical outcrop of Rattlesnake Tuff forming a prominent cliff exposure, 12 to 18 m (40 to 60 ft) in height. Locally, the unit dips gently (2° to 3°) to the south. View is looking north (43.679069, -118.859215 geographic coordinates; 350136.6722mE, 4837908.3119mN WGS84 UTM Zone 11 coordinates). *(Figure continued on following pages.)*

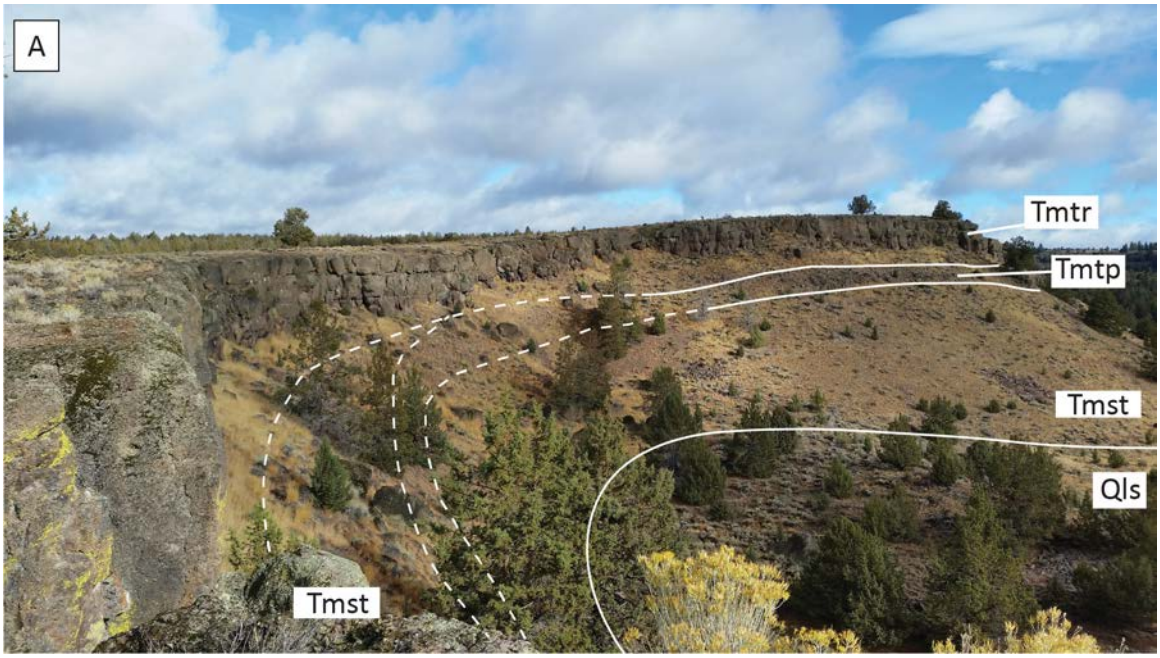

(Figure 5-6, continued) **Outcrop, hand sample, and petrographic photographs of the Rattlesnake Tuff (Tmtr). (B) Pumice-rich Rattlesnake Tuff, containing white and black pumice fragments that are partially collapsed. Hammer for scale is 28 cm (11 in) in length (43.820992, -118.993432 WGS84 geographic coordinates; 4853922.3758mN, 339697.2309mE, WGS84 UTM Zone 11 coordinates). (C) Basal vitrophyre, showing vitric texture and moderate compaction foliation. Quarter for scale is 24 mm (0.96 in) in diameter (43.778925, -118.988513 WGS84 geographic coordinates; 339980.5129mE, 4844868.5625mN WGS84 UTM Zone 11 coordinates).** *(Figure continued on following pages.)*

(Figure 5-6, continued) **Outcrop, hand sample, and petrographic photographs of the Rattlesnake Tuff (Tmtr). (D) Photomicrograph of subhedral feldspar (anorthoclase; 0.5 mm), and anhedral clinopyroxene (0.1 mm) microphenocrysts distributed within a vitric groundmass of glass shards in plane-polarized light. Scale bar is 1 mm (0.04 in) in length. Sample number: HAH0170-16. (E) Same view as (D) under cross-polarized light. Abbreviations: Af - alkali feldspar, Px - pyroxene.** *(Figure continued on following page.)*

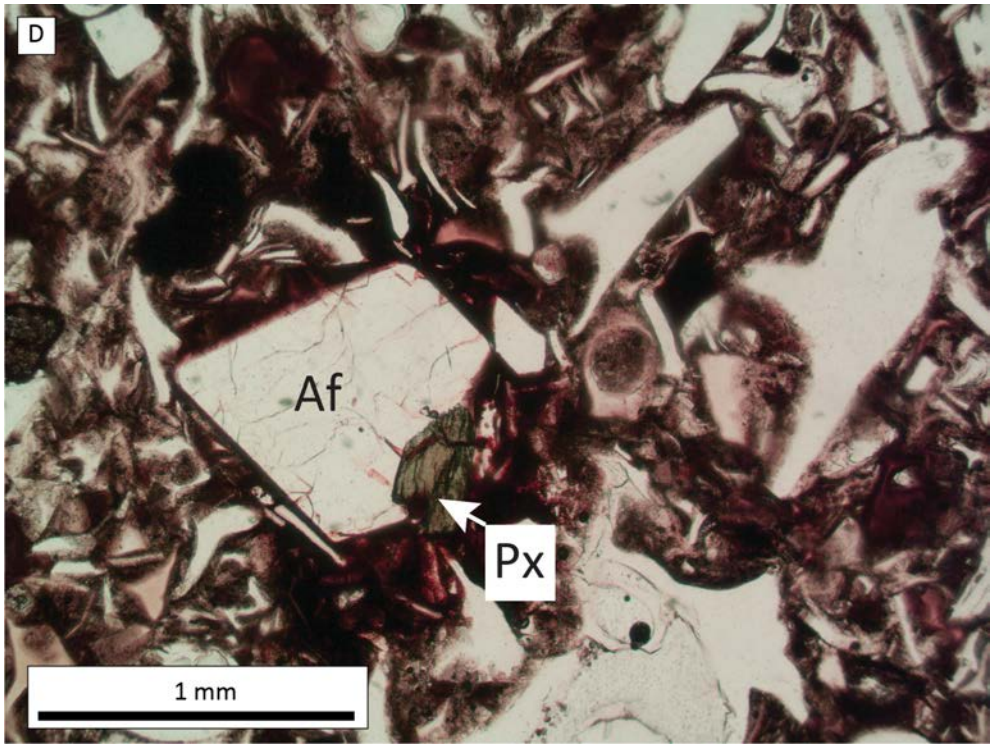

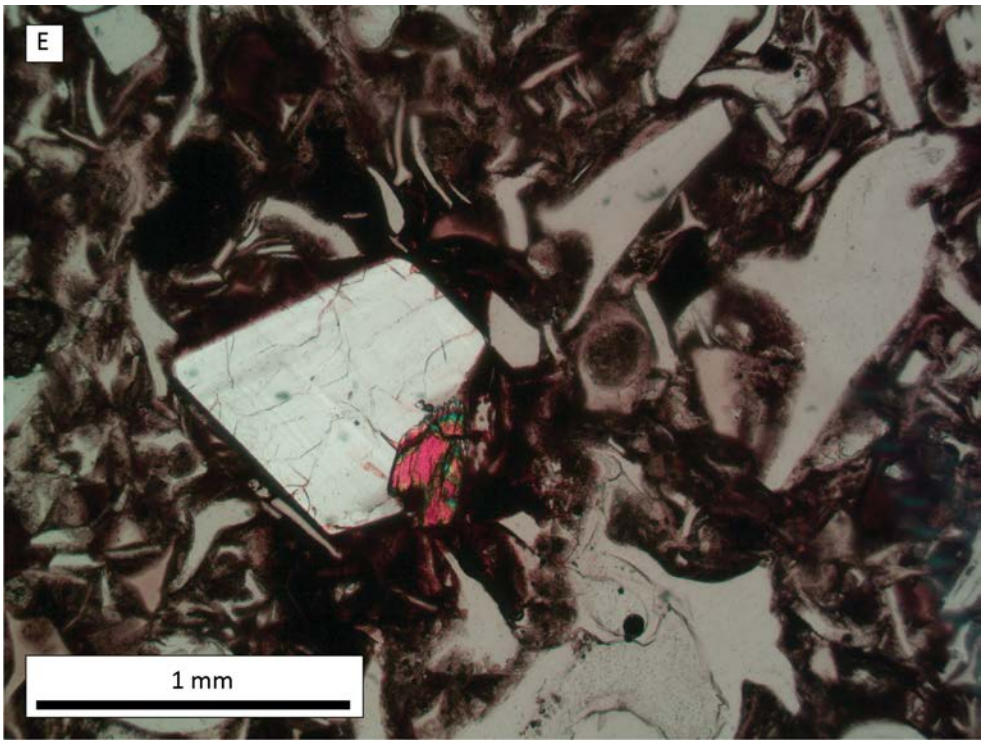

(Figure 5-6, continued) **Outcrop, hand sample, and petrographic photographs of the Rattlesnake Tuff (Tmtr). (F) Photomicrograph of a mafic lithic fragment surrounded by glass shards displaying compaction foliation under plane-polarized light. Scale bar is 1 mm (0.04 in) in length. Sample number: HAH0170-16. (G) Same view as (I) under cross-polarized light. Sample number: HAH0170-16. Abbreviations: Af - alkali feldspar, qtz - quartz, Lithic Frag. - lithic fragment.**

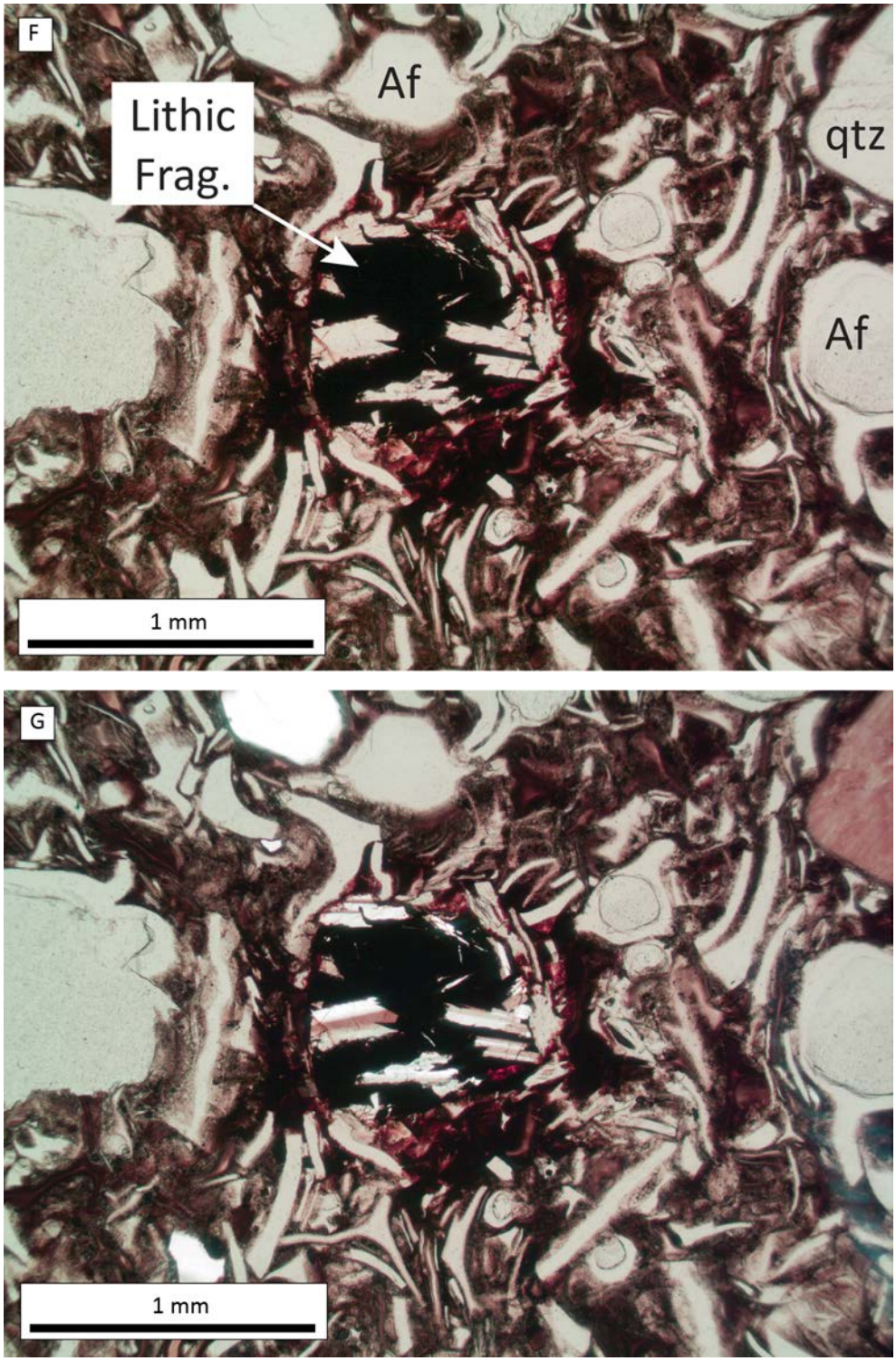

Tmtp **Prater Creek Ash-flow Tuff (upper Miocene)**—Devitrified, welded, crystal-poor ash-flow tuff forming prominent cliff exposures in the western and southern parts of the quadrangle (Plate 1). The ash-flow tuff is 10 to 20 m (32 to 65 ft) thick in the map area and occurs as a single cooling unit. The tuff is massive and densely welded and exhibits a eutaxitic texture and a distinctive platy jointing (**Figure 5-7A**). Locally, a lithophysal section of the tuff exhibits lenticular or crescent-shaped vesicles in the plane of compaction foliation (**Figure 5-7B**; **Figure 5-7C**). Abundant flattened pumice (fiamme) range in size up to 5 cm (2 in.) with a compaction ratio of 10:1 (**Figure 5-7D**; **Figure 5-7E**). Lithics are minor (<3%) and consist of angular poly-compositional lithic fragments as much as 2 cm (0.78 in) in length.

Typical fresh hand samples are pinkish gray (5YR 8/1) to light brown (5YR 5/2) and moderate reddish brown (10R 4/6) when weathered. The tuff contains rare, less than 1 percent by volume, crystal fragments of sanidine and quartz <0.5 mm (0.01 in; **Figure 5-7F** through **Figure 5-7I**). The densely welded devitrified tuff commonly exhibits a distinctive spotted appearance (**Figure 5-7D**). In thin section, the tuff is characterized by less than 1 percent sanidine and quartz crystal fragments in a devitrified glass-shard groundmass. Locally, the tuff is zeolitized. Samples obtained from this unit are rhyolitic in composition with 76.06 to 79.89 weight percent SiO_2, 11.41 to 12.13 weight percent Al_2O_3, 4.15 to 4.73 weight percent Na_2O, and 3.49 to 4.64 weight percent K_2O (Table 5 1). The tuff also contains variable amounts of barium (66 to 1,610 ppm Ba), and moderate amounts of zirconium (420 to 514 ppm Zr), yttrium (51 to 101 ppm Y), and niobium (23.6 to 45.9 ppm Nb). The Prater Creek Ash-flow Tuff has reversed magnetic polarity and is assigned a late Miocene age on the basis of an $^{40}Ar/^{39}Ar$ age of 8.41± 0.16 Ma (Jordan and others, 2004). The Prater Creek Ash-flow Tuff has an estimated eruptive volume of ~200 km^3 (48 $mile^3$; Parker, 1974).

Figure 5-7. Outcrop, hand sample, and petrographic description of the Prater Creek Ash-flow Tuff (Tmtp). (A) Tmtp forms a cliff exposure. The tuff exhibits a platy joint set that is parallel to the eutaxitic texture orientation. Hammer for scale is 28 cm (11 in) in length (43.807407, -118.962544 WGS84 geographic coordinates; -118.962544mE, 4852354.1785mN WGS84 UTM Zone 11 coordinates). *(Figure continued on following pages.)*

(Figure 5-7, continued) **Outcrop, hand sample, and petrographic description of the Prater Creek Ash-flow Tuff (Tmtp). (B) Devitrified tuff with abundant lithophysae as much as 5 cm (2 in) in diameter. Hammer for scale is 28 cm (11 in) in length (43.778442, -118.983518 WGS84 geographic coordinates; 340318.01mE, 4849191.6539mN WGS84 UTM Zone 11 coordinates).** *(Figure continued on following pages.)*

(Figure 5-7, continued) **Outcrop, hand sample, and petrographic description of the Prater Creek Ash-flow Tuff (Tmtp). (C) Hand sample of lithophysal tuff showing lenticular or crescent-shaped lithophysae in the plane of compaction foliation. Quarter for scale is 24 mm (0.96 in) in diameter (43.778442, -118.983518WGS84 geographic coordinates; 340318.01mE, 4849191.6539mN WGS84 UTM Zone 11 coordinates).** *(Figure continued on following pages.)*

(Figure 5-7, continued) **Outcrop, hand sample, and petrographic description of the Prater Creek Ash-flow Tuff (Tmtp). (D) Pinkish gray to reddish brown, densely welded devitrified tuff with distinctive spotted weathering appearance. Alkali feldspar crystals are rare, less than 1 percent by volume. Quarter for scale is 24 mm (0.96 in) in diameter (43.807407, -118.962544 WGS84 geographic coordinates; 342145.3572mE, 4852354.1785mN WGS84 UTM Zone 11 coordinates).** *(Figure continued on following pages.)*

(Figure 5-7, continued) **Outcrop, hand sample, and petrographic description of the Prater Creek Ash-flow Tuff (Tmtp). (E) Densely welded devitrified tuff with abundant fiamme (black arrows) as much as 2 cm (0.75 in). Quarter for scale is 24 mm (0.96 in) in diameter (43.806743, -118.953649 WGS84 geographic coordinates; 342859.1205mE, 4852263.4552mN WGS84 UTM Zone 11 coordinates).** *(Figure continued on following pages.)*

(Figure 5-7, continued) **Outcrop, hand sample, and petrographic description of the Prater Creek Ash-flow Tuff (Tmtp). (F) Photomicrograph, in plane-polarized light, of two fiamme displaying eutaxitic texture surrounded by a groundmass of vitric ash and glass shards. Fiamme #2 measures about 4 mm long by 0.2 mm wide, exhibiting a 20:1 compaction ratio. Scale bar is 1 mm (0.04 in) in length. Sample number: HAH064-16. (G) Same view as (F) under cross-polarized light. Sample number: HAH064-16.** *(Figure continued on following page.)*

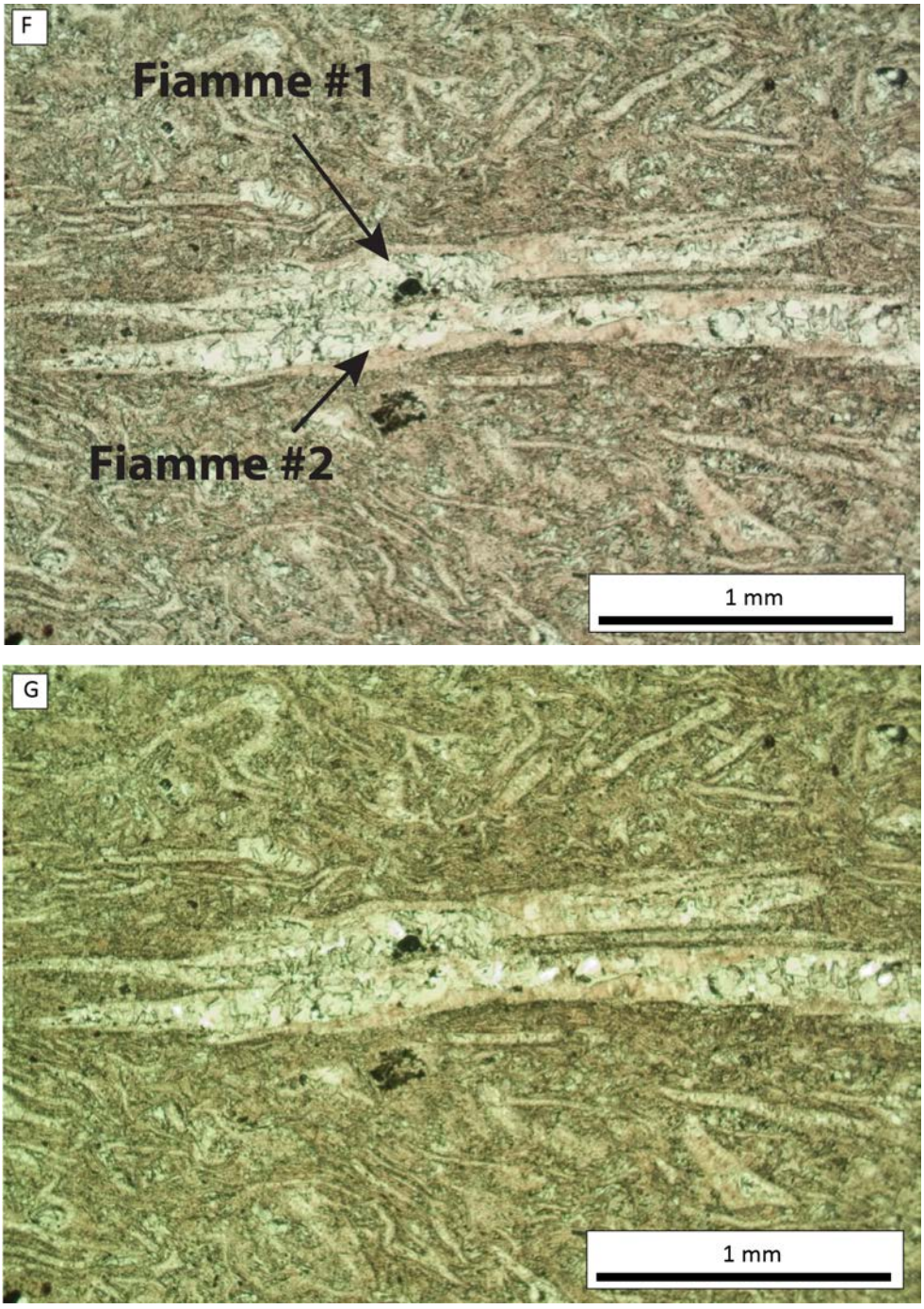

(Figure 5-7, continued) **Outcrop, hand sample, and petrographic description of the Prater Creek Ash-flow Tuff (Tmtp). (H) Photomicrograph of broken sanidine crystal fragment (labeled Sa; 0.25 mm) surrounded by a devitrified groundmass of vitric ash and glass shards. Eutaxitic texture is evident in plane-polarized light. Scale bar is 1 mm (0.04 in) in length. Sample number: HAH023-16. (I) Same view as (H) under cross-polarized light. Sample number: HAH023-16.**

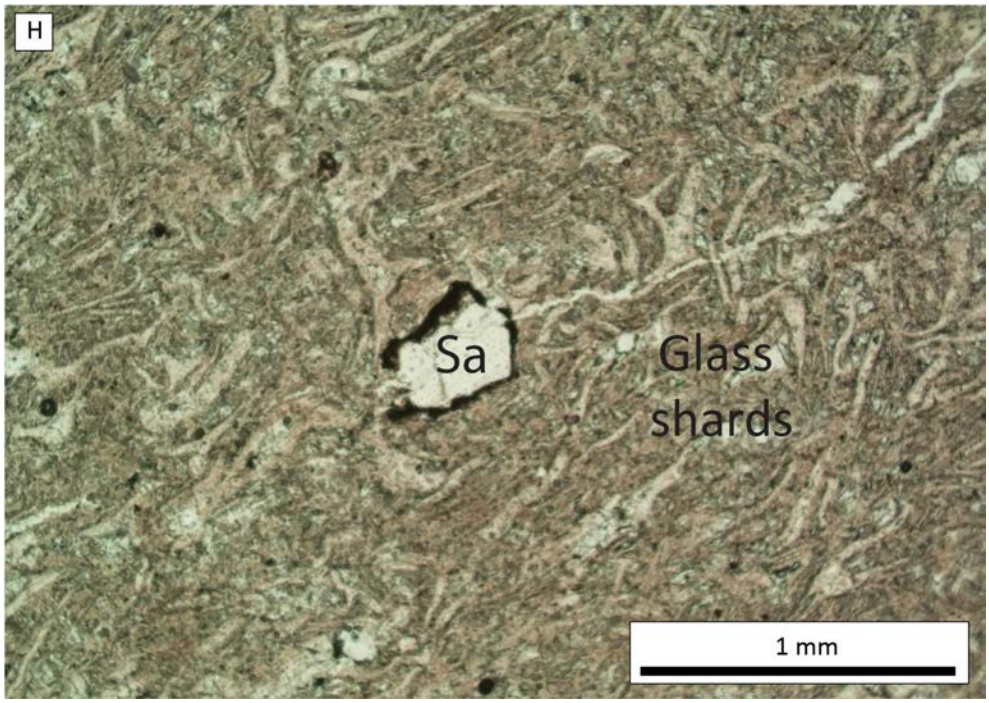

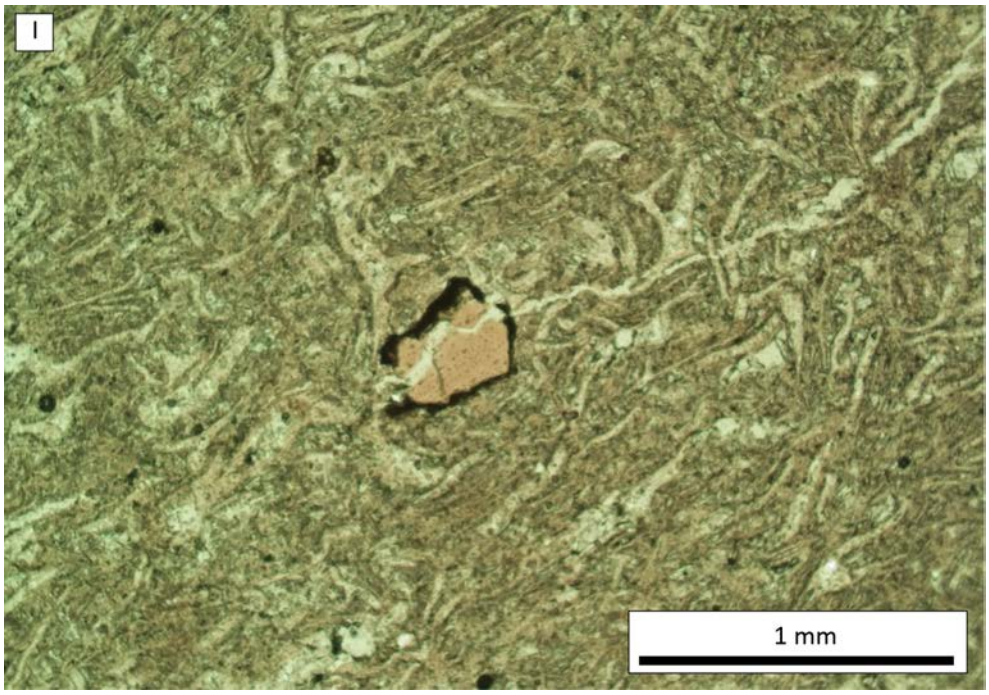

Tmtd **Devine Canyon Ash-flow Tuff (upper Miocene)**—Crystal-rich vitric tuff forming a prominent cliff exposure in the western and southern parts of the quadrangle (**Figure 5-8A** through **Figure 5-8H;** Plate 1). The densely welded zone weathers to form a distinctive apron of very large (as much as 10 m [30 ft] diameter) boulders (**Figure 5-8B**). Large (as much as 30 cm [12 in]) flattened glassy pumice exhibiting compaction ratios as much as 15:1 are common (**Figure 5-8C** through **Figure 5-8F**). Rare limb casts occur near the basal section of the tuff (**Figure 5-8E**). The tuff weathers to produce alkali feldspar-rich sand, which is useful to map the unit in areas of poor exposure. Within the Harney Basin, thickness of the ash-flow tuff is as much as 30 m (100 ft); however, within the study area, unit thicknesses of ~10 m (30 ft) are more typical.

Hand samples of the ash-flow tuff are light gray (N7 to N8) to greenish gray (5GY 5-6/1). Where outcrops are abundant in phenocrysts, the rock is medium to light gray (N5-N7) with pinkish, yellowish, and greenish gray (5 YR 8/1, 5Y 8/1, 5GY 6/1) with a streaked and mottled appearance. Petrographically, the tuff contains as much as 30 percent crystals and crystal fragments of dominantly alkali feldspar (sanidine; Greene, 1973; Smith and MacKenzie, 1958), minor quartz, and rare pyroxene, ilmenite, and magnetite. Alkali feldspar phenocrysts recognized by cleavage and twinning, have abundance ranges from as much as 30 to 35 percent by volume, whereas quartz content ranges from 0 to 7 percent (**Figure 5-8G,H**). Greene (1973) noted that alkali feldspar and quartz generally increase in abundance up section. Most of the phenocrysts are broken and exhibit rounding or embayment textures by resorption (**Figure 5-8G,H**). Rare pyroxene phenocrysts are green and yellow green (pleochroic) in color. Additionally, the unit contains occasional lithic fragments.

Samples obtained from this unit have rhyolitic chemical composition of 76.28 to 76.64 weight percent SiO_2, 10.70 to 11.23 weight percent Al_2O_3, 1.99 to 3.08 weight percent Na_2O, and 6.14 to 6.81 weight percent K_2O (Table 5 1). Additionally, relatively low amounts of barium (8.74 to 62.52 ppm Ba), and high amounts of zirconium (746 to 1,531 ppm Zr), yttrium (96 to 193 ppm Y), and niobium (54.5 to 109.7 ppm Nb) are characteristic of the tuff. Isom (2017) concluded based on the range in zirconium, yttrium, and niobium (**Figure 5-2A**) that the tuff was erupted from a geochemically zoned magma chamber. The Devine Canyon Ash-flow Tuff is believed to have covered more than 18,600 km^2 with a total erupted volume of approximately 195 km^3 from a concealed source within the Harney Basin (Greene, 1973; Parker, 1974). The Devine Canyon Ash-flow Tuff is assigned a late Miocene age on the basis of stratigraphic position and an $^{40}Ar/^{39}Ar$ age of 9.63 ± 0.05 Ma (Ford and others, 2013).

Figure 5-8. Outcrop and petrographic description of the Devine Canyon Ash-flow Tuff (Tmtd) exposed in the map area. (A) Devine Canyon Ash-flow Tuff, cliff exposures range up to 15 m (50 ft) in height (43.827794, -118.946789 WGS84 geographic coordinates; 343465.8791mE, 4854588.5465mN WGS84 UTM Zone 11 coordinates). *(Figure continued on following pages.)*

(Figure 5-8, continued) **Outcrop and petrographic description of the Devine Canyon Ash-flow Tuff (Tmtd) exposed in the map area. (B) The unit typically sheds large distinctive boulders downslope, recognizable in aerial photography (43.777322, -119.000291 WGS84 geographic coordinates; 339028.3872mE, 4849085.4555mN WGS84 UTM Zone 11 coordinates).** *(Figure continued on following pages.)*

(Figure 5-8, continued) **Outcrop and petrographic description of the Devine Canyon Ash-flow Tuff (Tmtd) exposed in the map area. (C) Densely welded, crystal-rich vitric ash-flow tuff with elongated fiamme (black arrows) as much as 50 cm in length. Fiamme compaction ratios average 10:1 ratio. Two distinct pumice populations are evident based on phenocryst abundance. Hammer for scale is 28 cm (11 in) in length (43.827961, -118.957642 WGS84 geographic coordinates; 4854627.7293mN, 342593.7106mE WGS84 UTM Zone 11 coordinates).** *(Figure continued on following pages.)*

(Figure 5-8, continued) **Outcrop and petrographic description of the Devine Canyon Ash-flow Tuff (Tmtd) exposed in the map area. (D) Commonly, large fiamme easily weather out on exposed surfaces. Quarter for scale is 24 mm (0.96 in) in diameter (43.820416, -118.963174 WGS84 geographic coordinates; 4853800.1792mN, 342128.9659mE, WGS84 UTM Zone 11 coordinates).** *(Figure continued on following pages.)*

(Figure 5-8, continued) **Outcrop and petrographic description of the Devine Canyon Ash-flow Tuff (Tmtd) exposed in the map area. (E) Rare limb casts occur near the basal contact. Hammer head is in the “up” direction. Limb cast is 12 cm (5 in) in diameter and extends approximately 1 m (3 ft) into the outcrop. Hammer for scale is 28 cm (11 in) in length (43.827794, -118.946789 WGS84 geographic coordinates; 343465.8791mE, 4854588.5465mN WGS84 UTM Zone 11 coordinates). (F) Hand sample (weathered) of Tmtd exhibiting abundant alkali feldspar crystals, as much as 30 percent by volume, and eutaxitic texture. Quarter for scale is 24 mm (0.96 in) in diameter (43.87381, -118.955374 WGS84 geographic coordinates; 342896.5324mE, 4859715.7023mN WGS84 UTM Zone 11 coordinates).** *(Figure continued on following page.)*

(Figure 5-8, continued) **Outcrop and petrographic description of the Devine Canyon Ash-flow Tuff (Tmtd) exposed in the map area. (G) Photomicrograph of a subhedral to anhedral alkali feldspar (Af; 3 mm) displaying Carlsbad twinning and rounded quartz crystal (Qtz; 1 mm) phenocryst fragment distributed within a vitric groundmass of glass shards in plane-polarized light. Scale bar is 1 mm (0.04 in) in length. Sample number: HAH011-16. (H) Same view as (G) under cross-polarized light. Sample number: HAH011-16.**

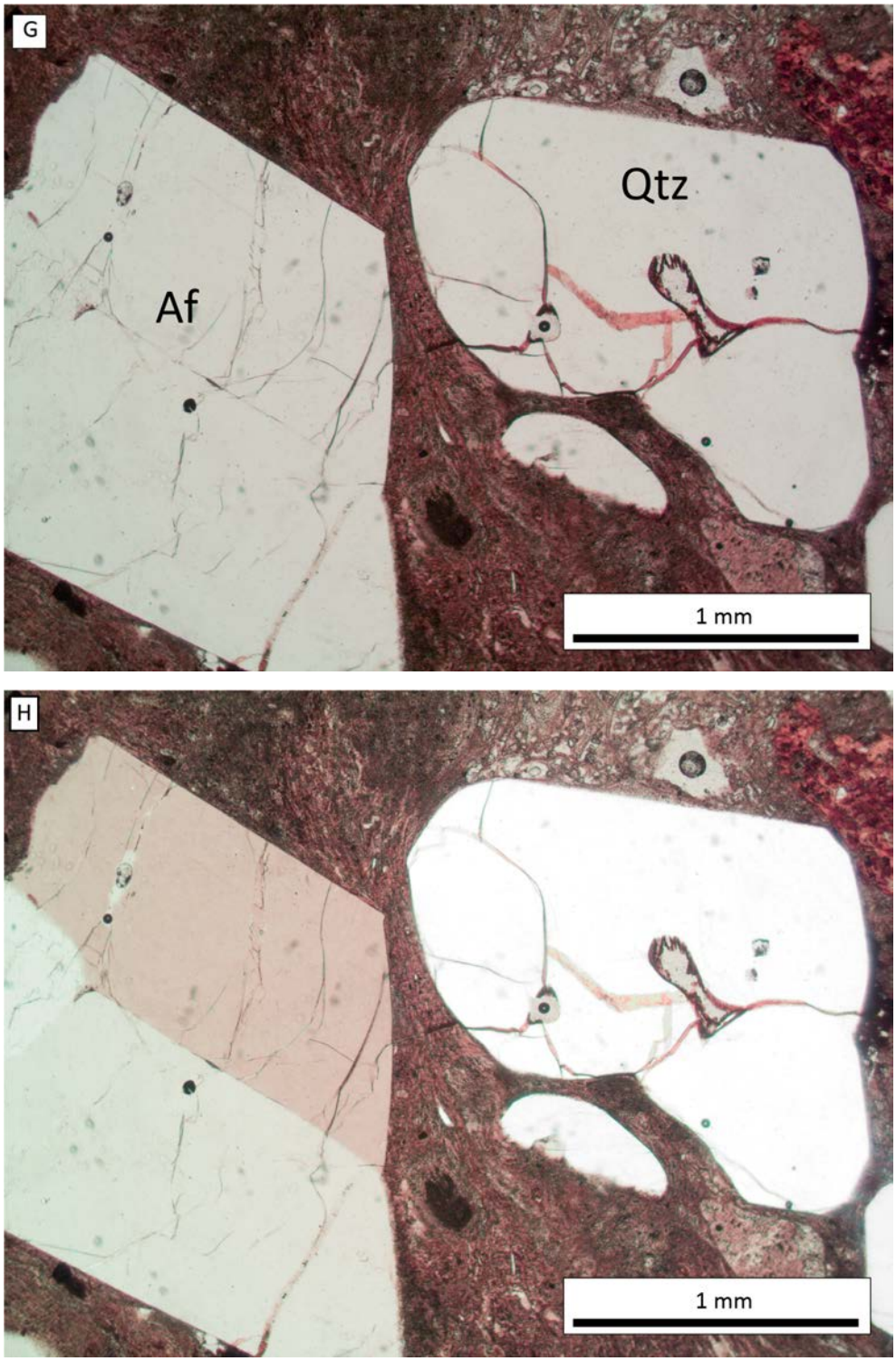

Tmst **tuffaceous sedimentary rocks (upper to middle Miocene [?])**—Tuffaceous mudstone, siltstone, sandstone, and conglomerate and fluvially reworked tuff beds (**Figure 5-9A** through **Figure 5-9C**). The unit is as much as 110 m (360 ft) thick. Fine to coarse grained, thinly bedded and well to poorly sorted sandstone layers contain ripple marks and trough cross-bedding. Conglomerate sequences are generally less than 1 m (3 ft) thick (**Figure 5-9B,C**). The tuffaceous sedimentary rocks are interbedded with the Devine Canyon Ash-flow Tuff and the Prater Creek Ash-flow Tuff. The unit is capped by the Rattlesnake Tuff (**Figure 5-9A**). The relative ages of these tuff units provide excellent chronostratigraphic control. Precise age of the unit is unknown in areas where exposure is poor, and direct relationships to interbedded and precisely dated tuff marker beds are unclear. This unit is partially equivalent to Danforth Formation (unit Td) of Piper and others (1939); Tst sedimentary rocks of Greene (1972); overlying sedimentary rocks of Tdv (welded tuff of Devine Canyon) of Greene (1972); overlying sedimentary rocks of Tdv (welded tuff of Devine Canyon) of Greene and others (1972); Tst (tuffaceous sedimentary rocks and tuff) of Walker (1977); and Tmst-1, -2, and -3 (tuffaceous sedimentary rocks) of Brown and others (1980). From stratigraphic relationships and age dates on bracketing tuff marker beds, the unit is assigned a middle to late Miocene age.

Figure 5-9. Outcrop description of tuffaceous sedimentary rocks (Tmst) exposed in the map area. (A) Tuffaceous sedimentary rocks form a vegetated slope. Tmtp is Prater Creek Ash-flow Tuff. Steeper slopes occur where sedimentary rocks are more indurated or contain ash-flow tuff units (43.67229843, -118.999304 WGS84 geographic coordinates; 338828.0537mE, 4837165.667mN WGS84 UTM Zone 11 coordinates). *(Figure continued on following page.)*

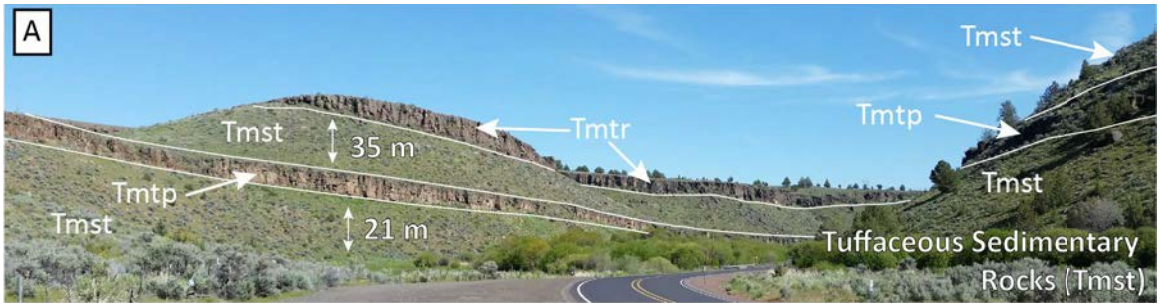

(Figure 5-9, continued) **Outcrop description of tuffaceous sedimentary rocks (Tmst) exposed in the map area. (B) Unconsolidated, poorly sorted conglomerate sequence may locally exceed 4.5 m (15 ft) (43.846861, -118.952741 WGS84 geographic coordinates; -118.952741mE, 4856717.4988mN WGS84 UTM Zone 11 coordinates). (C) Fluvially reworked tuff overlies a poorly sorted clast-supported conglomerate. The reworked tuff is overlain by a thin (1.5 m; 5 ft) tuffaceous siltstone and sandstone (43.846861, -118.952741 WGS84 geographic coordinates; -118.952741mE, 4856717.4988mN WGS84 UTM Zone 11 coordinates).**

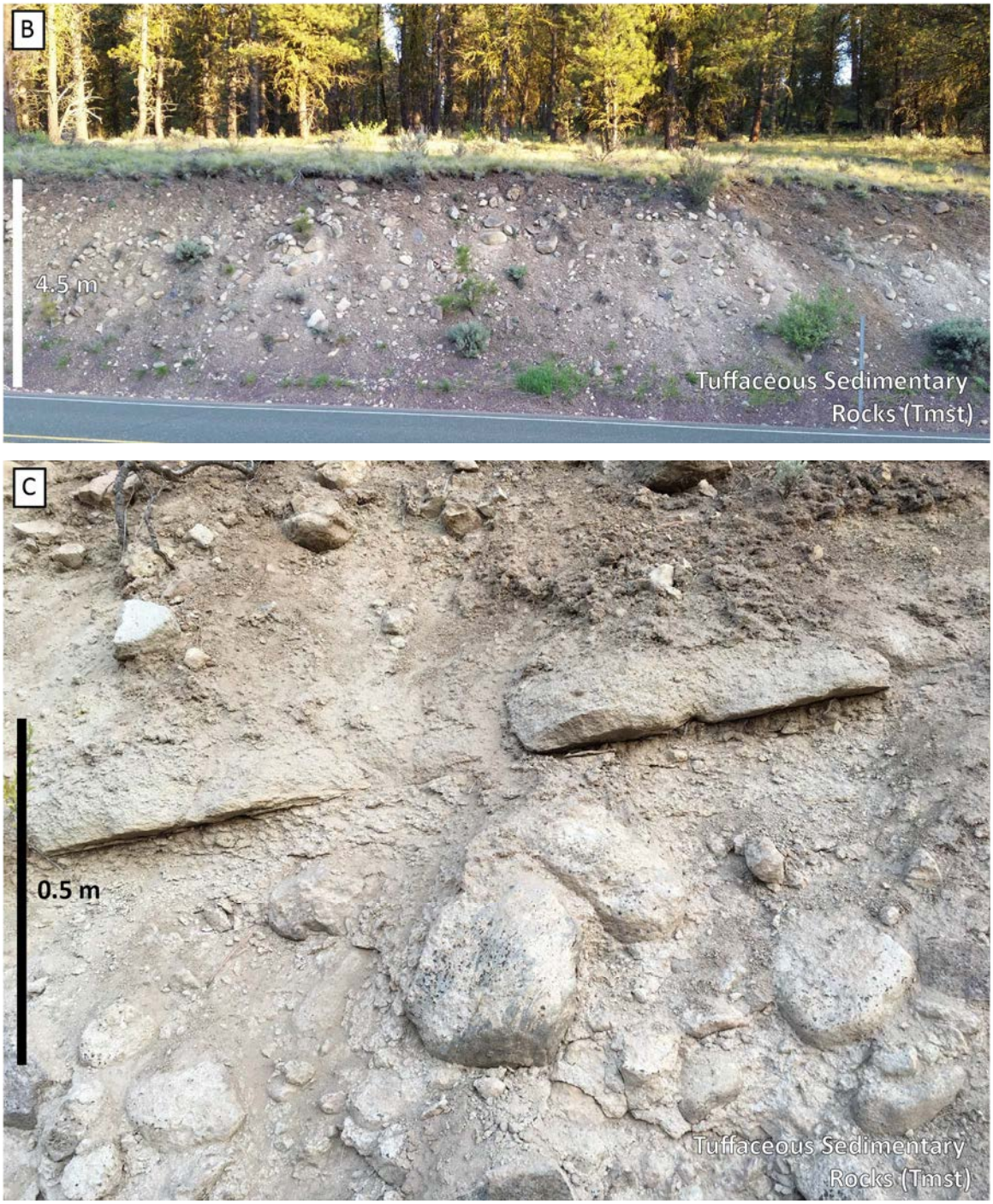

Nonconformity

5.3.2 Middle Miocene and late Oligocene volcanic and sedimentary rocks

Tmdc **Dinner Creek Tuff (middle or lower Miocene)**—Massive, crystal poor, pumice and lithic rich, moderately to densely welded rhyolitic ash-flow tuff (**Tmdc**) occurring in the map area to a limited extent (**Figure 5-10A** and **Figure 5-10B;** Plate 1). Locally, multiple small (<1 hectare; 2.5 acres) closed basins, as much as 6 m (20 ft) deep, are evident when gently dipping surface exposures of the Dinner Creek Tuff slope are near parallel to slope (**Figure 5-10A**). The tuff commonly has a pinkish gray (5YR 8/1) devitrified ash groundmass. The tuff contains white pumice and lithic fragments as much as 3 cm (1 in) in diameter (**Figure 5-10C** and **Figure 5-10D**). The pumice fragments do not exhibit textures related to compaction. Within the study area the tuff is poorly exposed and likely discontinuous. Estimated thickness ranges from 10 to 20 m (32 to 65 ft). The tuff contains angular light gray (N8 to N7) pumice fragments up to 2 cm (0.75 in) in size, minor lithic fragments, sparse, <5 percent, angular fragments of anhedral plagioclase and clinopyroxene, and minor quartz as much as 2 mm (0.08 in) in length (**Figure 5-10C** through **Figure 5-10F**). The tuff has been locally zeolitized (**Figure 5-10E,F**) Samples obtained from this unit have a rhyolitic whole-rock chemical composition of 76.04 to 76.93 weight percent SiO_2, 12.4 to 12.88 weight percent Al_2O_3, 4.28 to 4.37 weight percent Na_2O, and 3.65 to 3.88 weight percent K_2O (**Table 5-1**). The tuff also contains relatively high amounts of barium (1,417.65 to 1,418.57 ppm Ba), moderate amounts of zirconium (442.09 to 466 ppm Zr), yttrium (48.94 to 75 ppm Y), and niobium (24.82 to 25.57 ppm Nb). The unit is equivalent to Dinner Creek Welded Ash-flow Tuff of Kittleman and others (1965); Dinner Creek Welded Tuff of Greene and others (1972); unit Td, Dinner Creek Tuff of Ferns and others (1993); and unit 1 of the Dinner Creek Tuff of Streck and others (2015). The unit is assigned a middle or early Miocene age on the basis of stratigraphic position and $^{40}Ar/^{39}Ar$ ages of 15.9 ± 0.09 Ma to 16.16 ± 0.02 Ma obtained by Streck and others (2015).

Figure 5-10. Outcrop and petrographic description of the Dinner Creek Tuff (Tmdc) exposed in the map area. (A) Typical closed basin morphology. Basin shown is <1 hectare (2.5 acres) in size and as much as 6 m (20 ft) deep (43.825881, -118.984249 WGS84 geographic coordinates; 340448.7568mE, 4854447.5926mN WGS84 UTM Zone 11 coordinates). *(Figure continued on following pages.)*

(Figure 5-10, continued) **Outcrop and petrographic description of the Dinner Creek Tuff (Tmdc) exposed in the map area. (B) Dinner Creek Tuff locally exhibits a horizontal platy compaction foliation. Hammer for scale is 28 cm (11 in) in length (43.805775, -118.969684 WGS84 geographic coordinates; 341566.7673mE, 4852186.5301mN WGS84 UTM Zone 11 coordinates).** *(Figure continued on following pages.)*

(Figure 5-10, continued) **Outcrop and petrographic description of the Dinner Creek Tuff (Tmdc) exposed in the map area. (C) Pinkish light gray crystal- and lithic-poor tuff. Quarter for scale is 24 mm (0.96 in) in diameter (43.795459, -118.965808 WGS84 geographic coordinates; 341851.2831mE, 4851033.3388mN WGS84 UTM Zone 11 coordinates).** *(Figure continued on following pages.)*

(Figure 5-10, continued) **Outcrop and petrographic description of the Dinner Creek Tuff (Tmdc) exposed in the map area. (D) Light purple to pinkish tan crystal-poor tuff with abundant rounded lithic fragments. Quarter for scale is 24 mm (0.96 in) in diameter (43.769447, -118.875946 WGS84 geographic coordinates; 349015.3128mE, 4847976.4986mN WGS84 UTM Zone 11 coordinates).** *(Figure continued on following page.)*

(Figure 5-10, continued) **Outcrop and petrographic description of the Dinner Creek Tuff (Tmdc) exposed in the map area. (E) Photomicrograph of crystal fragment of plagioclase feldspar (pl; 0.4 mm), quartz (qz; 0.3 mm), and surrounded pumice fragment in a groundmass of devitrified glass shards in plane-polarized light. Scale bar is 1 mm (0.04 in) in length. Sample number HBH066-17. (F) Same view as (E) under cross-polarized light. Zeolitization of the pumice fragment and polysynthetic twinning of plagioclase feldspar are evident.**

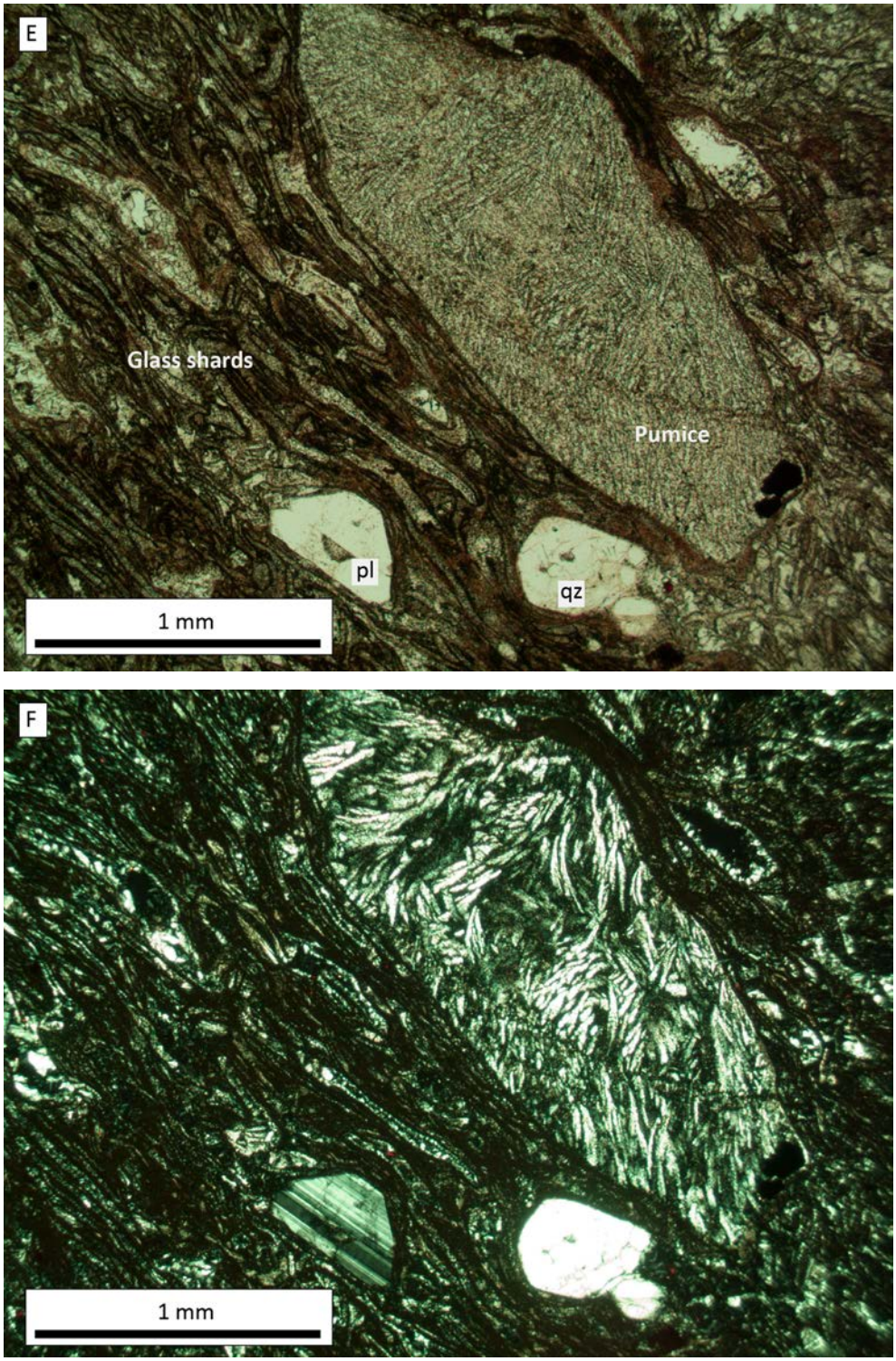

Tmb **basalt-basaltic andesite (lower Miocene[?])**—Aphyric to olivine-, clinopyroxene-, and plagioclase-microporphyritic basalt and basaltic trachy-andesite underlies the ~16 Ma Dinner Creek Tuff (**Tmdc**) in the southeastern corner of the map area (**Figure 5-11A** through **Figure 5-11G;** Plate 1). The unit consists of a flow-on-flow succession of discontinuous basalt and basaltic trachy-andesite lava flows, exposed as rubbly outcrop surrounded by red iron-oxidized soils (**Figure 5-11A**). The total thickness in the map area is approximately 73 m (240 ft), with individual flows as much as 10 m (32 ft) thick. The basal contact of the unit is poorly exposed. Hand samples are medium gray (N5) to pale-red purple (5RP 6/2) containing ~40 to 50 percent by volume subhedral plagioclase laths and range in size up to 2 mm (0.08 in) in length. (**Figure 5-11B** and **Figure 5-11E**). Anhedral clinopyroxene, exhibiting poikilitic textures, is present up to 30 percent by volume (**Figure 5-11C,D** and **Figure 5-11F,G**). Some lavas contain olivine up to 10 percent by volume and commonly altered to iddingsite. The geochemical analysis shows individual lavas have a basalt or basaltic trachy-andesite composition, with 16.63 to 16.85 weight percent Al_2O_3, 1.52 to 1.58 weight percent TiO_2, 6.38 to 6.84 weight percent MgO, and 0.22 to 0.36 weight percent P_2O_5. These samples also contain 80.59 to 177.42 ppm zirconium, 25.4 to 34.1 ppm yttrium, and 11.78 to 21.19 ppm Nb niobium. **Tmb** lavas have reversed magnetic polarity (Appendix) and are considered to be part of the Columbia River Basalt Group on the basis of stratigraphic position; they may correlate with the Steens Basalt and the Picture Gorge Basalt exposed outside of the map area (Camp and others, 2013; Cahoon and Streck, 2017; S. L. Isom and M. J. Streck, unpub. data, 2017). The basalt and basaltic trachy-andesite lavas in the Devine Ridge North quadrangle are likely equivalent to the basalt-basaltic andesite (Tmb) unit of Niewendorp and others (2018) and Houston and others (unpub. data, 2018). The unit is assigned an early Miocene[?] age on the basis of its stratigraphic position below the ~16 Ma Dinner Creek Tuff (**Tmdc**) and above the 24.75 Ma andesite (**Toa**).

Figure 5-11. Outcrop and petrographic description of the basalt-basaltic andesite (Tmb) exposed in the southeastern area of the map. (A) Basalt weathers to boulders and red iron-oxidized soil (43.755243, -118.883018 WGS84 geographic coordinates; 348410.2071mE, 4846411.8904mN WGS84 UTM Zone 11 coordinates). *(Figure continued on following pages.)*

(Figure 5-11, continued) **Outcrop and petrographic description of the basalt-basaltic andesite (Tmb) exposed in the southeastern area of the map. (B) Plagioclase microphenocrysts (white arrows) are as much as 1 mm (0.4 in) and are surrounded by a black aphanitic groundmass. Reflectance in the aphanitic groundmass suggests the occurrence of plagioclase microlites. Locally, the basalt is poorly exposed (43.755243, -118.883018 WGS84 geographic coordinates; 348410.2071mE, 4846411.8904mN WGS84 UTM Zone 11 coordinates).** *(Figure continued on following pages.)*

(Figure 5-11, continued) **Outcrop and petrographic description of the basalt-basaltic andesite (Tmb) exposed in the southeastern area of the map. (C) Photomicrograph under plane-polarized light of microphenocrystic subhedral plagioclase feldspar (Pl) laths, poikilitic clinopyroxene (Cpx), and opaque crystals, likely magnetite or ilmenite. Scale bar is 0.5 mm (0.02 in) in length. (D) Same view as (C) under cross-polarized light.** *(Figure continued on following pages.)*

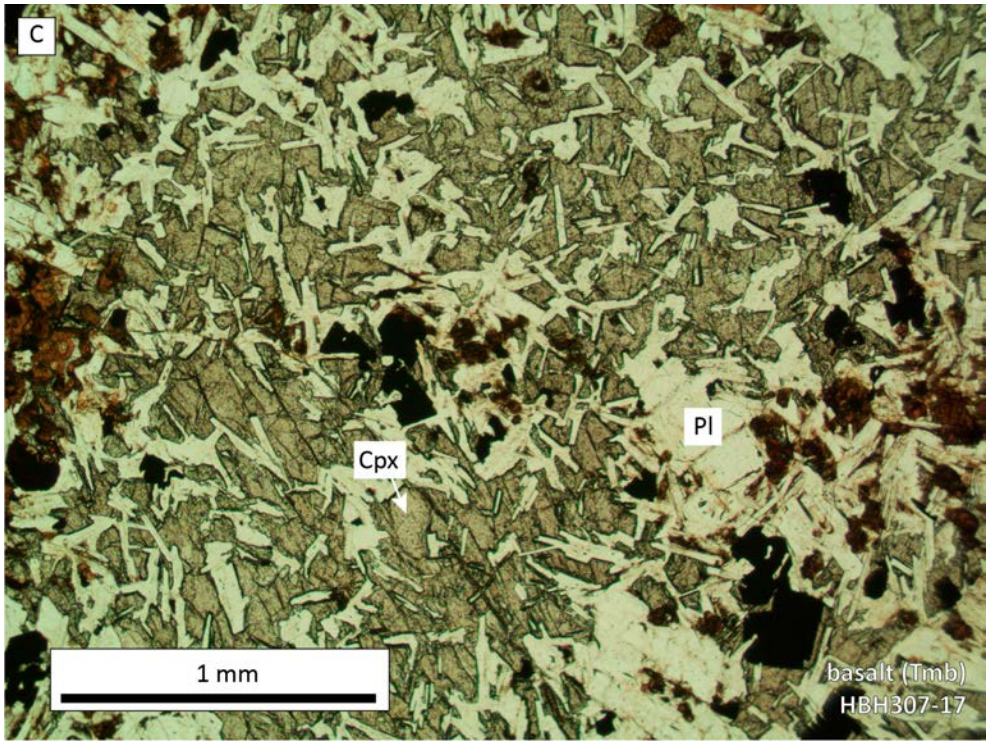

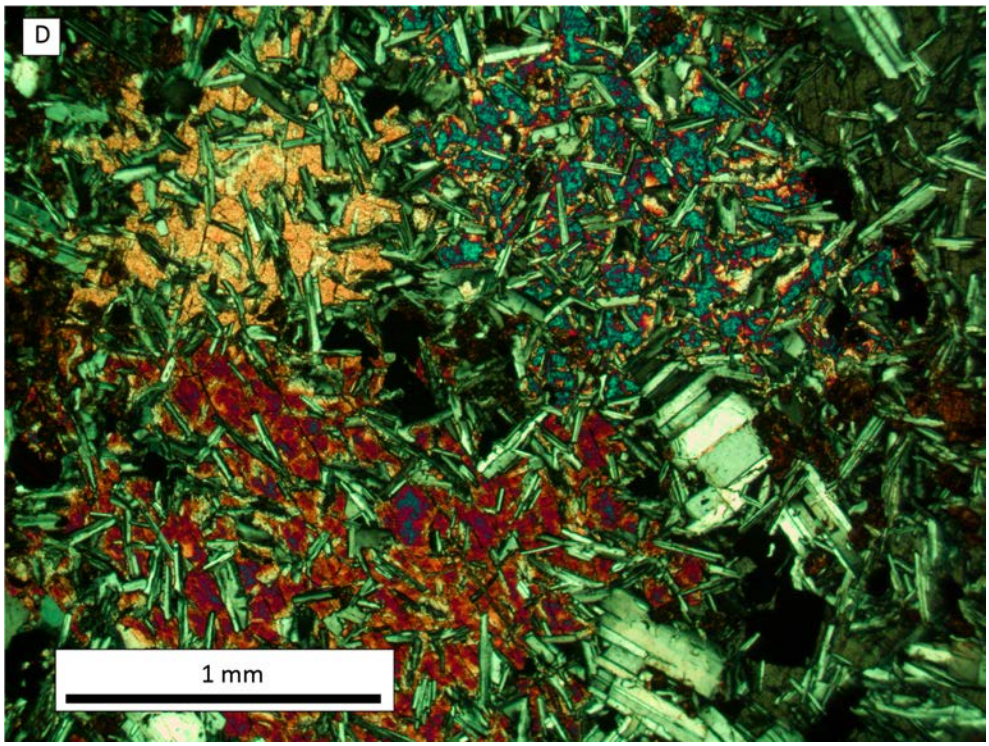

(Figure 5-11, continued) **Outcrop and petrographic description of the basalt-basaltic andesite (Tmb) exposed in the southeastern area of the map. (E) Black holocrystalline, microporphyritic basalt containing visible subhedral plagioclase laths (43.754799, -118.882835 WGS84 geographic coordinates; 348423.8694mE, 4846362.2335mN WGS84 UTM Zone 11 coordinates).** *(Figure continued on following page.)*

(Figure 5-11, continued) **Outcrop and petrographic description of the basalt-basaltic andesite (Tmb) exposed in the southeastern area of the map. (F) Photomicrograph under plane-polarized light of basalt containing subhedral phenocrysts of plagioclase (Pl) laths, and clinopyroxene (Cpx). Opaque crystals (magnetite or ilmenite) minor in abundance. Larger (0.75 mm; 0.3 in) plagioclase and subhedral clinopyroxene phenocrysts are surrounded by a groundmass of microcrystalline plagioclase, clinopyroxene, olivine and opaque minerals. Scale bar is 0.5 mm (0.02 in) in length. (G) Same view as (F) under cross-polarized light.**

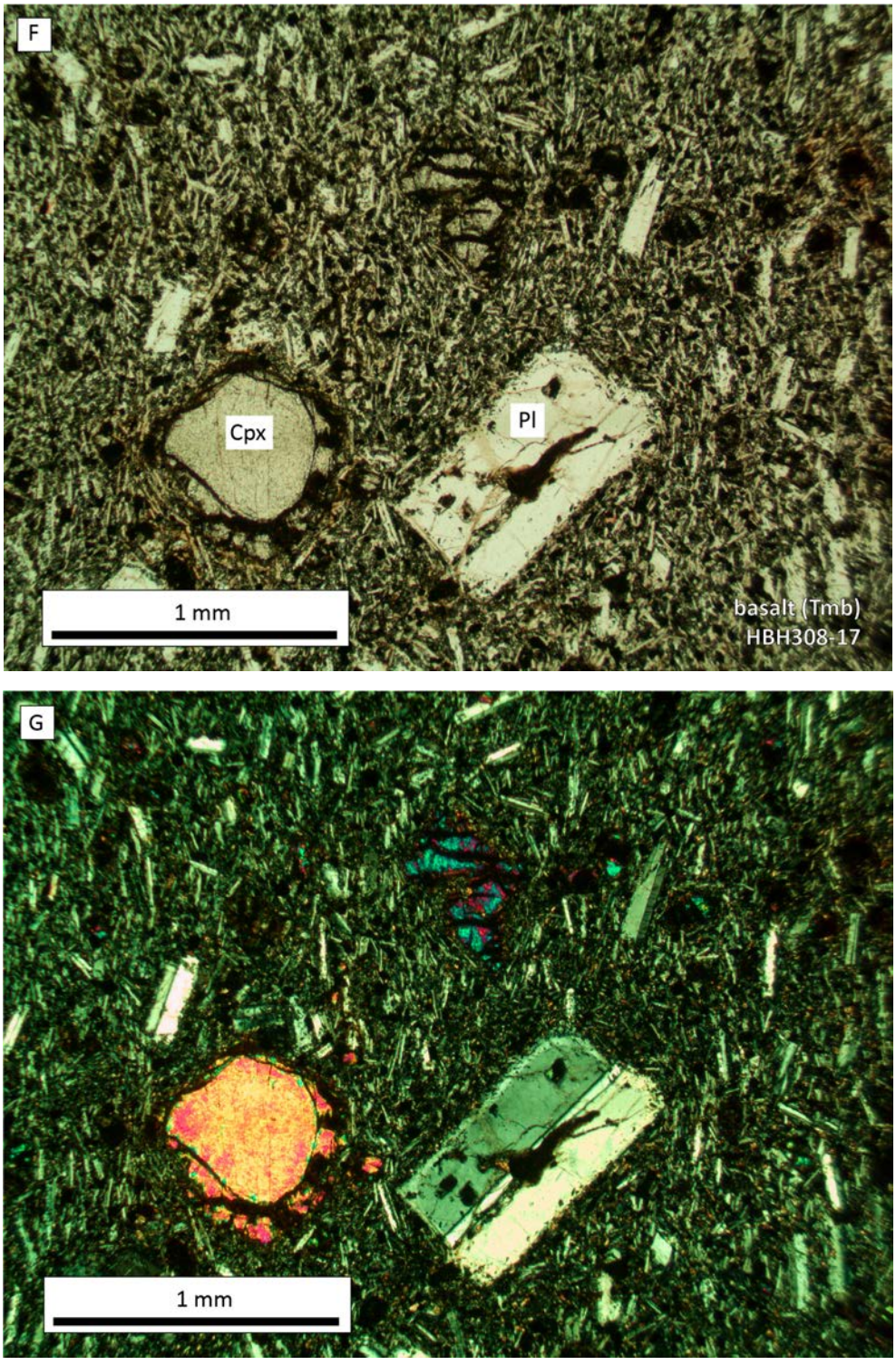

Toa **andesite (upper Oligocene)**—Plagioclase, hornblende, clinopyroxene andesite (**Toa**) is exposed in the northern and southeastern parts of the study area (**Figure 5-12**; Plate 1). Plagioclase and hornblende phenocrysts are conspicuous. Basal contact is not exposed. Individual lava flows range from 5 to 10 m (16 to 32 ft) thick, with a collective total exposed thickness as much as 76 m (250 ft) (**Figure 5-12A,** Plate 1). In hand sample, individual flows are medium gray (N5) containing ~60 percent subhedral lath-shaped plagioclase microphenocrysts as much as 1 mm (0.04 in) in length **(Figure 5-12B,C**). Petrographic inspection reveals plagioclase, hornblende, clinopyroxene, and biotite phenocrysts (1 mm c-axis, 0.04 in) within a groundmass of feldspar microlites (**Figure 5-12D** through **Figure5-12I**). Geochemical analysis of samples obtained from individual flows shows that the rock has an andesitic chemical composition, with a 62.66 weight percent SiO_2, 1.31 weight percent TiO_2, 3.69 weight percent MgO, 0.41 weight percent P_2O_5 , and low amounts of zirconium (140.36 ppm Zr), yttrium (35.82 ppm Y), and niobium (8.56 ppm Nb) (**Table 5-1**). The andesite has reversed magnetic polarity (Appendix). The unit is assigned an upper Oligocene age on the basis of stratigraphic position and an $^{40}Ar/^{39}Ar$ age of 24.75 ± 0.15 Ma obtained (Appendix, 40Ar39ArAnalyticalData folder).

Figure 5-12. Outcrop and petrographic description of andesite (Toa) exposed in the map area. (A) Plagioclase, biotite, hornblende andesite exhibiting moderately strong platy jointing. Hammer for scale is 28 cm (11 in) in length (43.871423, -118.92783 WGS84 geographic coordinates; 345103.3414mE, 4859398.5789mN WGS84 UTM Zone 11 coordinates). *(Figure continued on following pages.)*

(Figure 5-12, continued) **Outcrop and petrographic description of andesite (Toa) exposed in the map area. (B) Plagioclase phenocryst surrounded by fine-grained groundmass of subhedral plagioclase. Hammer for scale is 28 cm (11 in) in length (43.871423, -118.92783 WGS84 geographic coordinates; 345103.3414mE, 4859398.5789mN WGS84 UTM Zone 11 coordinates). (C) Plagioclase, hornblende and biotite phenocrysts are up to 2 mm (0.07 in) in size and are surrounded by an aphanitic groundmass. Quarter for scale is 2.5 cm (0.96 in) in diameter (43.871423, -118.92783 WGS84 geographic coordinates; 345103.3414mE, 4859398.5789mN WGS84 UTM Zone 11 coordinates).** *(Figure continued on following pages.)*

(Figure 5-12, continued) **Outcrop and petrographic description of andesite (Toa) exposed in the map area. (D) Photomicrograph of andesite showing subhedral hornblende (Hbl) phenocryst (c-axis 1.5 mm; 0.06 in) set in a microphenocrystic groundmass of plagioclase feldspar (Pl) and clinopyroxene (Cpx), under plane-polarized light. (E) Same view as in (D) under cross-polarized light.** *(Figure continued on following pages.)*

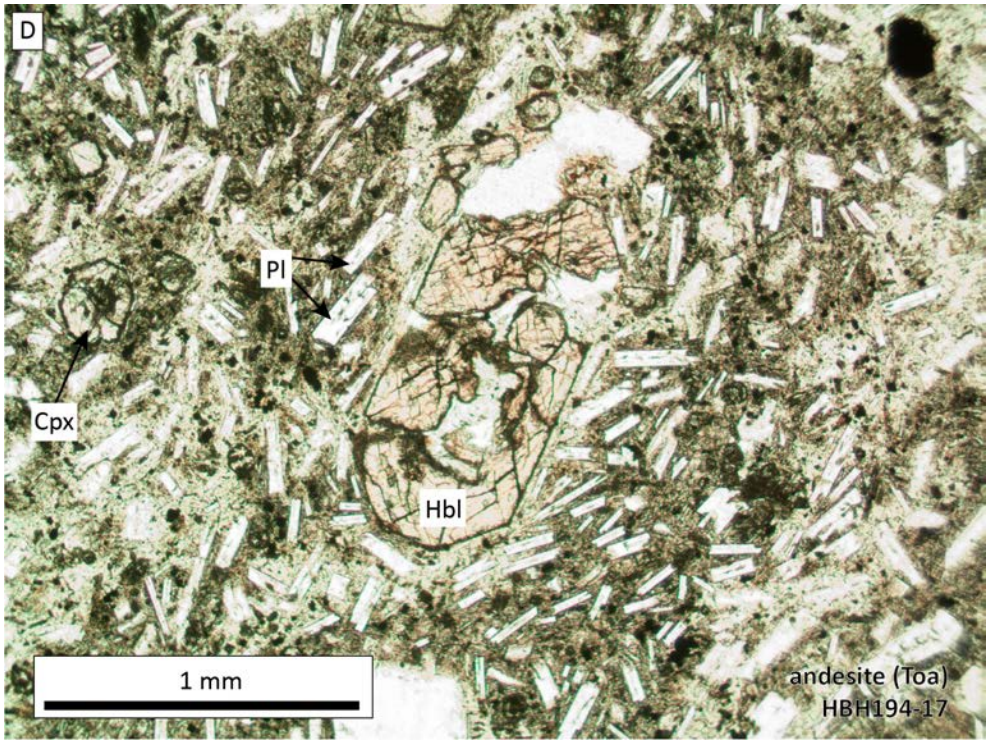

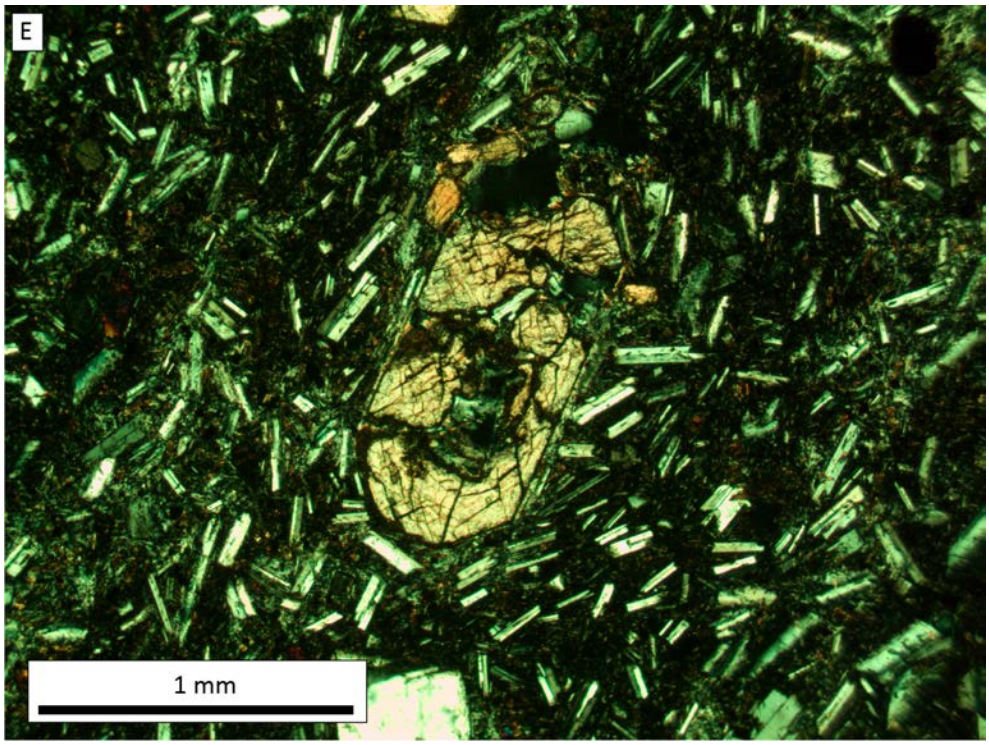

(Figure 5-12, continued) **Outcrop and petrographic description of andesite (Toa) exposed in the map area. (F) Photomicrograph of sparse plagioclase phenocryst (Pl) (c-axis: 2 mm; 0.08 in), under plane-polarized light. Cpx is clinopyroxene. (G) Same view as (F) under cross-polarized light.** *(Figure continued on following pages.)*

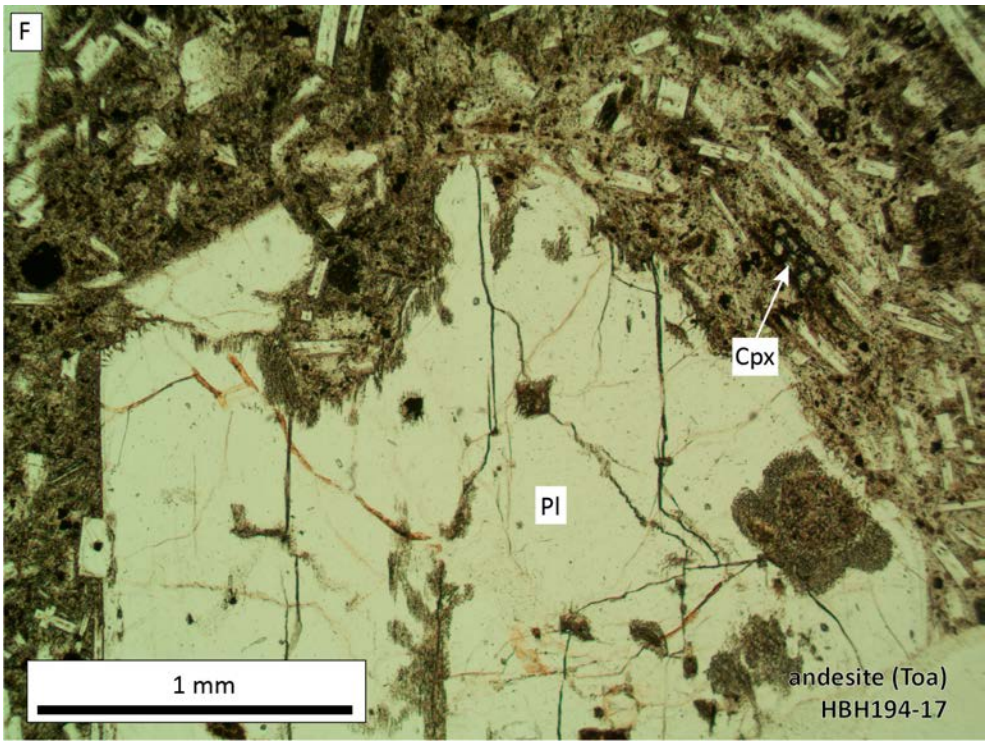

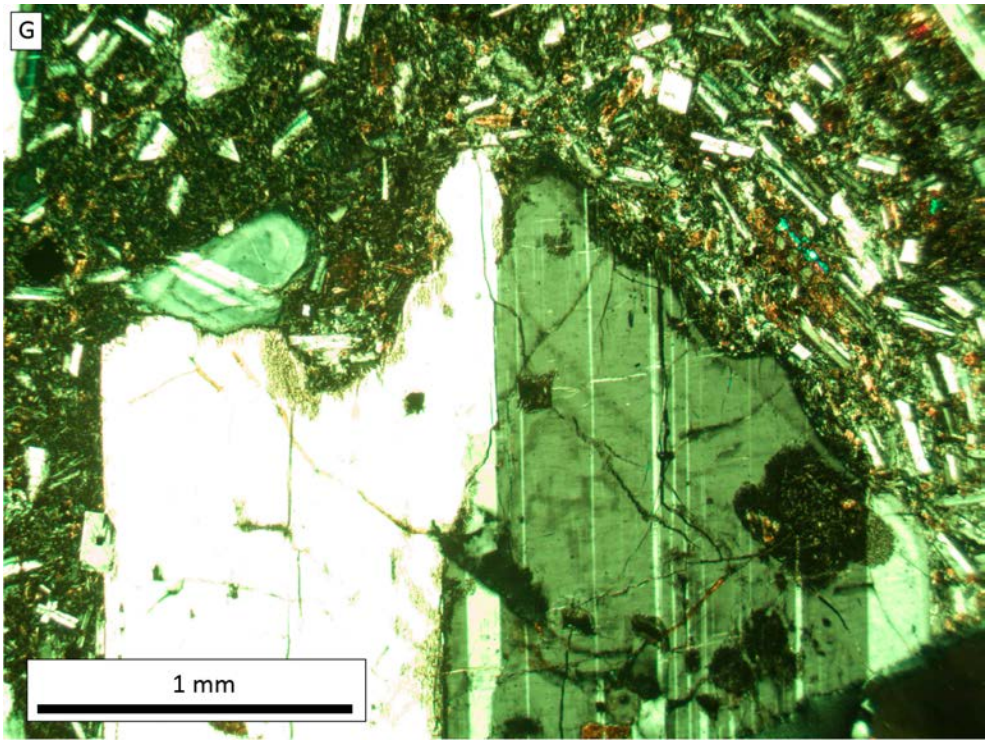

(Figure 5-12, continued) **Outcrop and petrographic description of andesite (Toa) exposed in the map area. (H) Photomicrograph of plagioclase (Pl) and clinopyroxene (Cpx) phenocrysts in a microporphyritic groundmass of plagioclase feldspar opaque crystals, under plane-polarized light. Plagioclase phenocrysts exhibit sieve texture. (I) Same view as (H) under cross-polarized light.** *(Figure continued on following pages.)*

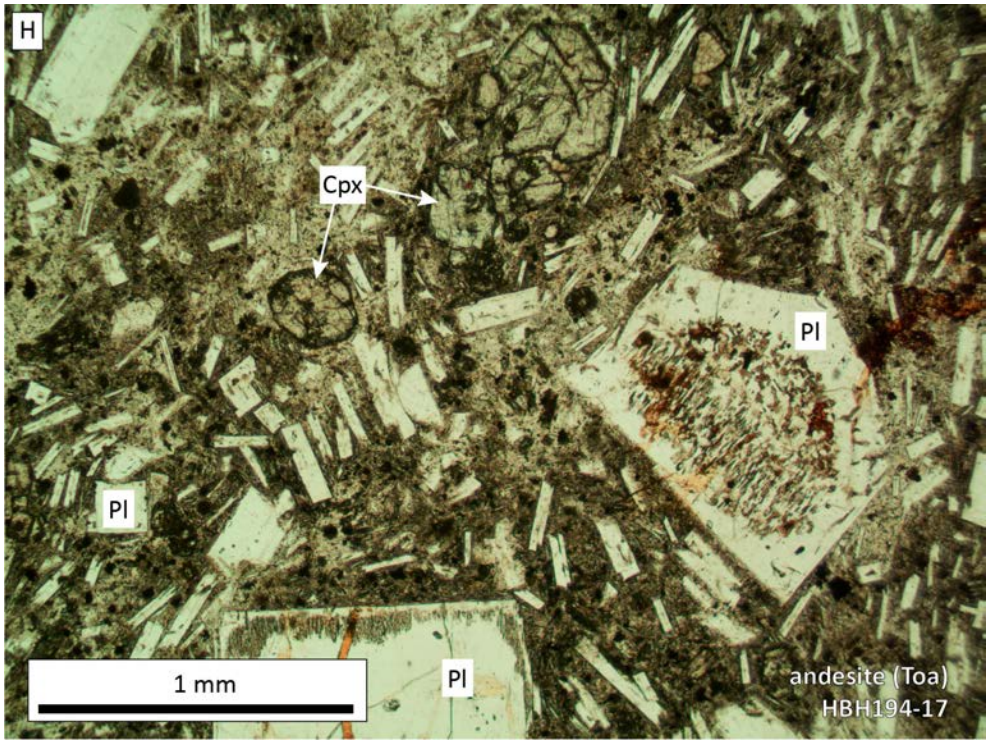

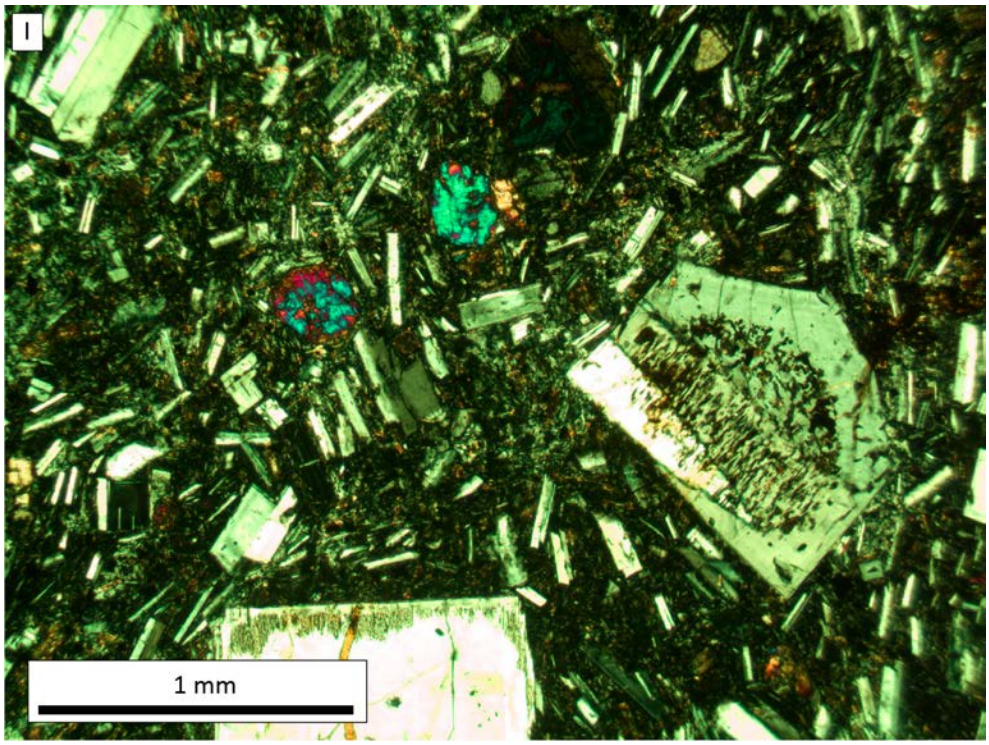

(Figure 5-12, continued) **Outcrop and petrographic description of andesite (Toa) exposed in the map area. (J) Photomicrograph of plagioclase (Pl) and clinopyroxene (Cpx) phenocrysts in a microporphyritic groundmass of plagioclase feldspar opaque crystals, under plane-polarized light. (K) Same view as (J) under cross-polarized light. Cpx - clinopyroxene; Pl - plagioclase feldspar.**

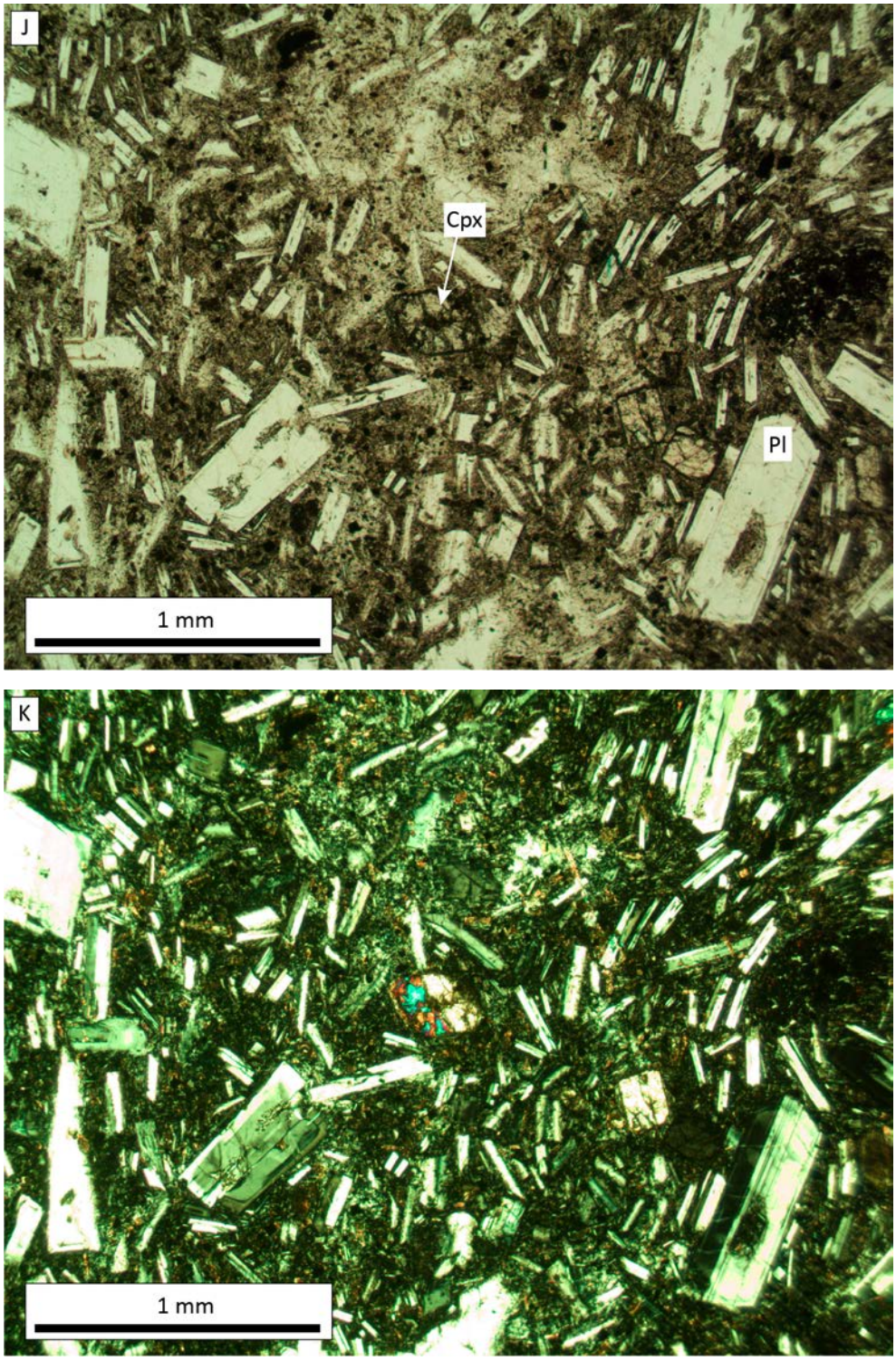

Angular unconformity to disconformity

Tor **rhyolite (upper Oligocene[?])**—Quartz-sanidine rhyolitic dikes and plug-like bodies exposed in the northeastern and southeastern parts of the map area (**Figure 5-13A** through **Figure 5-13D**; Plate 1). In hand sample the rhyolite is light to medium light gray (N7 to N6) with 20 to 25 percent feldspar and quartz phenocrysts (**Figure 5-13B**). Petrologic inspection reveals subhedral to euhedral feldspar (sanidine), biotite, and quartz phenocrysts ranging in size from 0.5 to 1.5 mm (0.02 to 0.6 in). Phenocrysts are set in a very fine grained microcrystalline groundmass of feldspar and quartz (**Figure 5-13C,D**). Locally, the small rhyolite pluglike bodies are silicified, containing numerous chalcedony-filled fractures. McGrane (1985) noted that both rhyolitic and quartz porphyry dikes are spatially, temporally, and genetically related to the epithermal gold mineralization at the Idol City District. The rhyolite is assigned an upper Oligocene age on the basis of stratigraphic position.

Figure 5-13. Outcrop and petrographic description of rhyolite (Tor) exposed in the eastern area of the map. (A) Rhyolite, exhibiting poorly developed flow foliations (43.843789, -118.88995 WGS84 geographic coordinates; 348076.7543mE, 4856259.0673mN WGS84 UTM Zone 11 coordinates). (B) In hand sample phenocrysts are aligned parallel to the flow foliation orientation (43.843789, -118.88995 WGS84 geographic coordinates; 348076.7543mE, 4856259.0673mN WGS84 UTM Zone 11 coordinates). *(Figure continued on following pages.)*

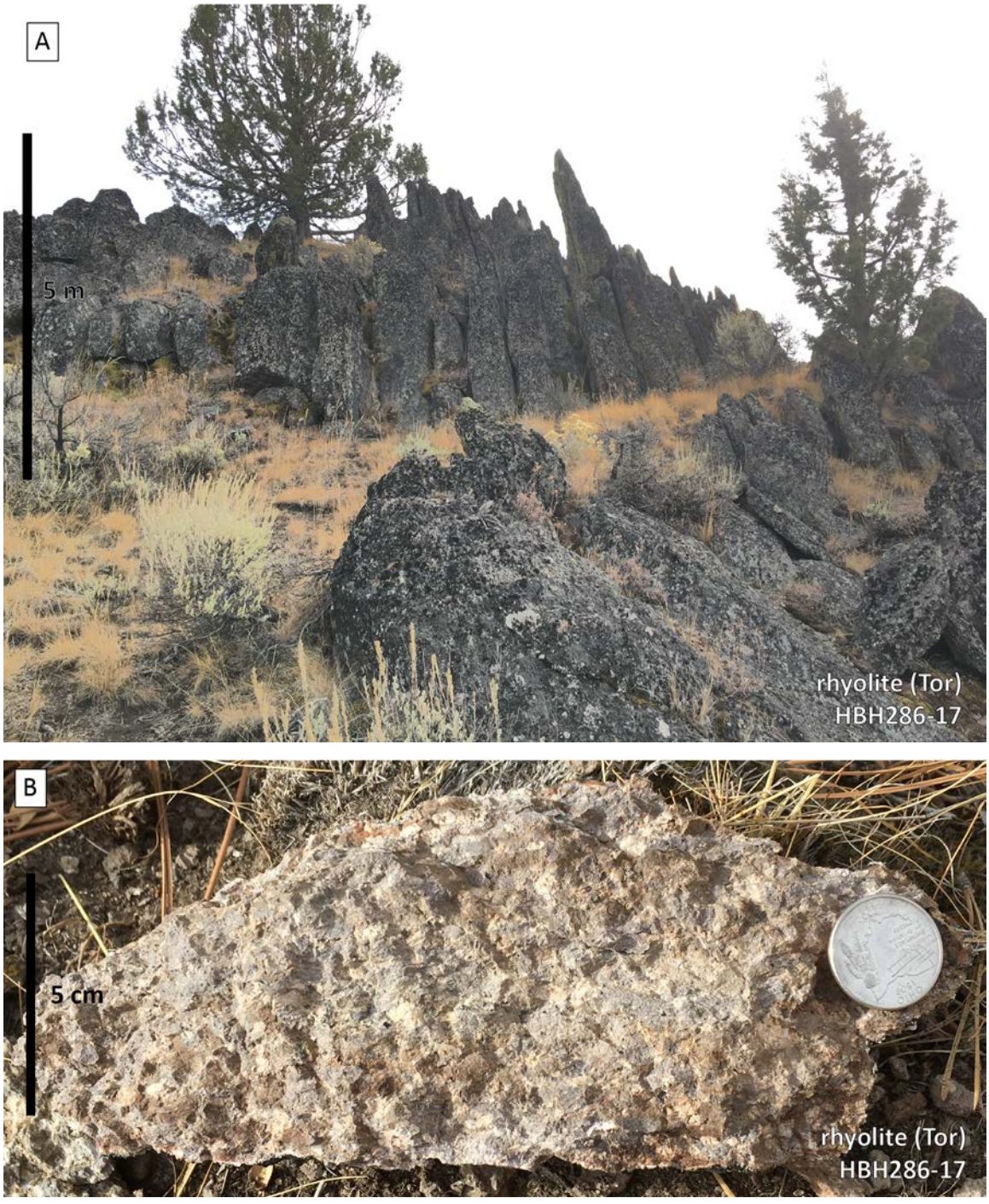

(Figure 5-13, continued) **Outcrop and petrographic description of rhyolite (Tor) exposed in the eastern area of the map. (C) Photomicrograph of subhedral feldspar and biotite (opaque minerals) phenocrysts (c-axis <0.5 mm; 0.02 in) set in a very fine-grained groundmass of feldspar and quartz, under plane-polarized light. (D) Same view as in (C) under cross-polarized light.**

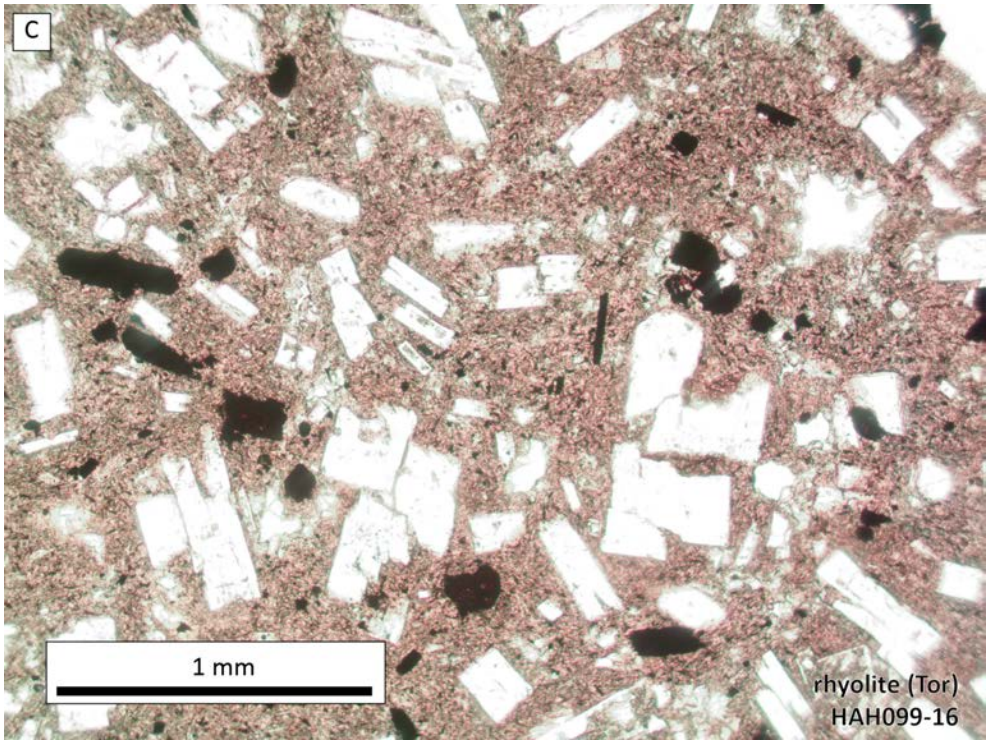

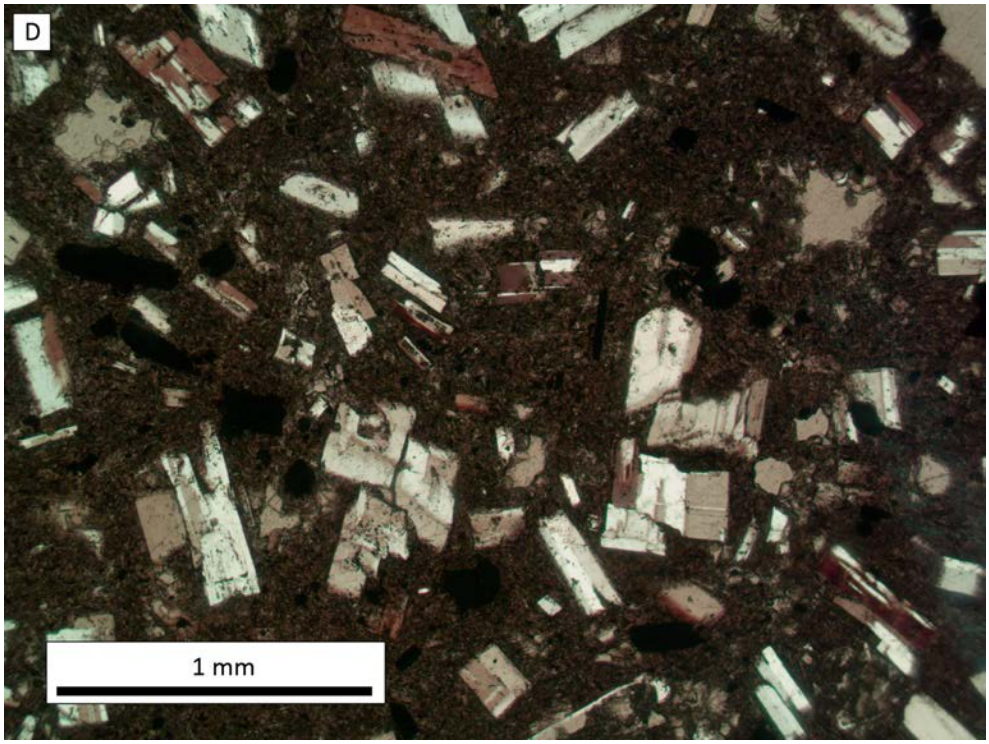

Toda **dacite (upper Oligocene[?])**—Plagioclase- hornblende- biotite- and quartz-phyric dacite (**Toda**) exposed in the northwestern and eastern part of the map area (**Figure 5-14A** through **Figure 5-14Q**; Plate 1). **Toda** rocks are the oldest rocks in the study area and are stratigraphically overlain by basalt-basaltic andesite (**Tmb**), andesite (**Toa**), and Devine Canyon Ash-flow Tuff (**Tmtd**). The unit is exposed as rubbly outcrops, typically producing boulders at the surface (**Figure 5-14A,B**). Alternatively, good exposures of dacite locally exhibit well-developed horizontal to contorted flow foliation (**Figure 5-14C,D**). The basal contact of the dacite is not exposed in the quadrangle, so is queried where shown in cross section (Plate 1). Total exposure in the map area suggests the unit may exceed 300 m (1,000 ft) in composite thickness. Typically, the dacite is dark gray (N3) and commonly contains ~25 percent plagioclase laths (~5 mm [0.19 in]) and minor quartz (<1 mm [0.039 in]) set in a fine-grained groundmass. Petrographic inspection of the microcrystalline groundmass reveals euhedral to subhedral plagioclase, hornblende, biotite, and clinopyroxene (<1 mm [0.02 in] c-axis) in a groundmass of dominantly plagioclase and pyroxene microlites (**Figure 5-14L** through **Figure5-14Q**). Geochemical analysis of samples obtained from individual flows shows that the rock has dacitic chemical compositions from 63.17 to 69.81 weight percent SiO_2 and moderate amounts of weight percent TiO_2 (0.40 to 0.96), 0.25 to 2.84 weight percent MgO, and 0.12 to 0.33 weight percent P_2O_5, and low amounts of Zr (96.08 to 171.97 ppm), Y (8.57 to 60.10 ppm), and Nb (3.76 to 10.6 ppm). Geochemical analysis of samples obtained from individual flows shows that the rock has an andesitic chemical composition, with a 62.66 weight percent SiO_2, 1.31 weight percent TiO_2, 3.69 weight percent MgO, 0.41 weight percent P_2O_5 , and low amounts of zirconium (140.36 ppm Zr), yttrium (35.82 ppm Y), and niobium (8.56 ppm Nb)

In the map area, field observations identified at least four textures in the dacite: 1) abundant (~20%) large (10 mm [0.40 in]) plagioclase feldspar phenocrysts in an aphanitic groundmass (**Figure 5-14E**); 2) 5 mm (0.20 in) plagioclase and <1 mm (0.01 in) hornblende phenocrysts in a microcrystalline groundmass of smaller (5 mm [0.20 in]) plagioclase laths (**Figure 5-14F**); 3) light gray groundmass with abundant <2 mm euhedral plagioclase phenocrysts (**Figure 5-14G**); 3) rare (<3%), 7 to 10 mm (0.27 to 0.40 in) plagioclase phenocrysts in a black aphanitic groundmass (**Figure 5-14H**); and 4) red and black flow-banded dacite with a distinctive spherulitic texture (**Figure 5-14I** through **Figure 5-14K**; HBH271-17, HBH272-17). HBH271-17 has a total alkali [6.13 wt. % $Na_2O + K_2O$] vs. silica [64.79 wt. % SiO_2] plot classification of dacite.

In thin section, euhedral to subhedral plagioclase, ±hornblende, ±biotite, and ±clinopyroxene (<1 mm [0.02 in] c-axis) phenocrysts within a groundmass of dominantly plagioclase, pyroxene, ±hornblende, ±biotite microlites (**Figure 5-14L** through **Figure 5-14Q**). Textural differences and wide-ranging geochemical compositions suggest the dacite (**Toda**) may be composed of a thick and compositionally varied assemblage of domes and/or flows. Subdivision of the dacite into field-identifiable individual units may be possible with further work.

This unit has a normal magnetic polarity and is assigned an upper Oligocene age on the basis of stratigraphic position. The dacite is equivalent to the dacite described by Houston and others (unpub. data, 2018) and Niewendorp and others (2018) in the adjacent Harney and Devine Ridge South 7.5′ quadrangles, respectively.

Figure 5-14. Outcrop and petrographic description of dacite (Toda) exposed in the map area. (A) Common outcrop of dacite boulders. Dacite with a phaneritic groundmass weathers to a granular texture (43.796955, -118.965406 WGS84 geographic coordinates; 341887.5948mE, 4851198.6916mN WGS84 UTM Zone 11 coordinates). *(Figure continued on following pages.)*

(Figure 5-14, continued) **Outcrop and petrographic description of dacite (Toda) exposed in the map area. (B) Light-gray dacite with an aphanitic groundmass weathers to a smooth texture. (43.804059, -118.945841 WGS84 geographic coordinates; 343480.1533mE, 4851950.5849mN WGS84 UTM Zone 11 coordinates). (C) Well-developed horizontal laminated flow foliation is common in the dacite (43.77972, -118.917501 WGS84 geographic coordinates; 345697.1621mE, 4849194.0899mN WGS84 UTM Zone 11 coordinates).** *(Figure continued on following pages.)*

(Figure 5-14, continued) **Outcrop and petrographic description of dacite (Toda) exposed in the map area. (D) Locally, flow foliation is vertically aligned and often contorted (43.866577, -118.935238 WGS84 geographic coordinates; 344495.5572mE, 4858874.296mN WGS84 UTM Zone 11 coordinates).** *(Figure continued on following pages.)*

(Figure 5-14, continued) **Outcrop and petrographic description of dacite (Toda) exposed in the map area. (E) Dacite with abundant feldspar phenocrysts in an aphanitic groundmass. Quarter for scale is 24 mm (0.96 in) in diameter (43.761297, -118.942668 WGS84 geographic coordinates; 343623.9329mE, 4847195.1921mN WGS84 UTM Zone 11 coordinates).** *(Figure continued on following pages.)*

(Figure 5-14, continued) **Outcrop and petrographic description of dacite (Toda) exposed in the map area. (F) Fine-grained dacite with feldspar and hornblende phenocrysts. Quarter for scale is 24 mm (0.96 in) in diameter (43.814971, -118.964179WGS84 geographic coordinates; 342033.798mE, 4853197.3574mN WGS84 UTM Zone 11 coordinates). (G) Dacite containing larger feldspar phenocrysts set in a groundmass of microcrystalline feldspar crystals. Quarter for scale is 24 mm (0.96 in) in diameter (43.811278, -118.938527 WGS84 geographic coordinates; 344087.2185mE, 4852738.5249mN WGS84 UTM Zone 11 coordinates).** *(Figure continued on following pages.)*

(Figure 5-14, continued) **Outcrop and petrographic description of dacite (Toda) exposed in the map area. (H) Dacite with rare feldspar phenocrysts in an aphanitic groundmass. Quarter for scale is 24 mm (0.96 in) in diameter (43.852698, -118.96546 WGS84 geographic coordinates; 342030.3557mE, 4857390.0296mN WGS84 UTM Zone 11 coordinates). (I) Red and black banded dacite. Black bands are microcrystalline (< 0.5 mm; 0.2 in). Banded dacite may be equivalent to the red and black banded dacite of King Mountain (Tmkm) of S. L. Isom and M. J. Streck (unpub. data, 2017). Quarter for scale is 24 mm (0.96 in) in diameter (43.767241, -118.911716 WGS84 geographic coordinates; 346130.6569mE, 4847797.3604mN WGS84 UTM Zone 11 coordinates).** *(Figure continued on following pages.)*

(Figure 5-14, continued) **Outcrop and petrographic description of dacite (Toda) exposed in the map area. (J) Dacite exhibiting spherulitic texture, fresh surface. Quarter for scale is 24 mm (0.96 in) in diameter (43.767241, -118.911716WGS84 geographic coordinates; 346130.6569mE, 4847797.3604mN WGS84 UTM Zone 11 coordinates). (K) Dacite exhibiting abundant spherulites (HBH271-17). Within the same exposure the spherulitic dacite (Figure 5-14J and K; HBH271-17) grades into the red and black dacite (HBH272-17) shown in Figure 5-14I. Quarter for scale is 24 mm (0.96 in) in diameter (43.767241, -118.911716WGS84 geographic coordinates; 346130.6569mE, 4847797.3604mN WGS84 UTM Zone 11 coordinates).** *(Figure continued on following pages.)*

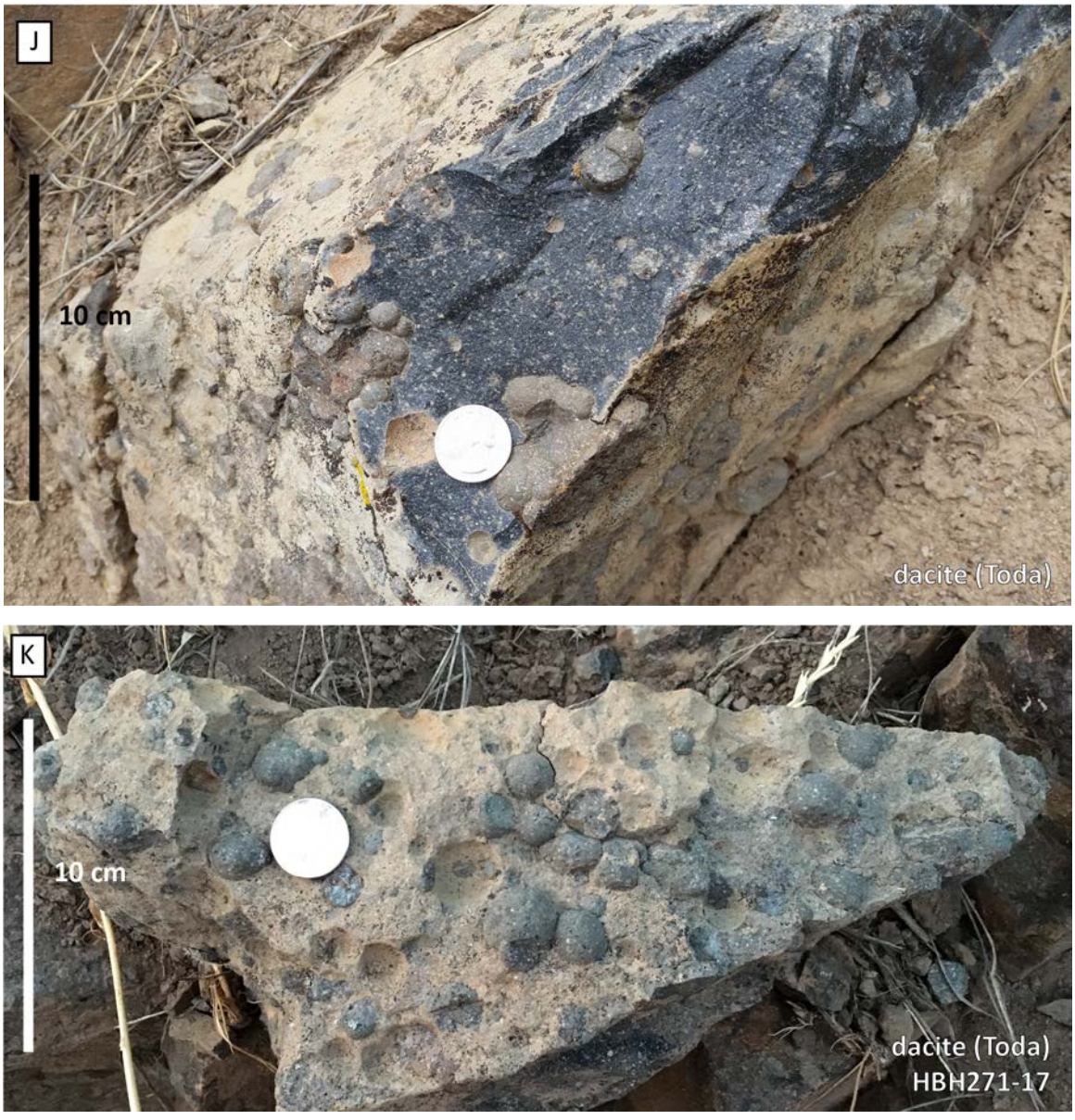

(Figure 5-14, continued) **Outcrop and petrographic description of dacite (Toda) exposed in the map area. (L) Photomicrograph of dacite pictured in (E), showing a large (7 mm; 0.27 in) feldspar phenocryst set in a microphenocrystic groundmass of plagioclase feldspar and minor clinopyroxene, under plane-polarized light. (M) Same view as in (L) under cross-polarized light.** *(Figure continued on following pages.)*

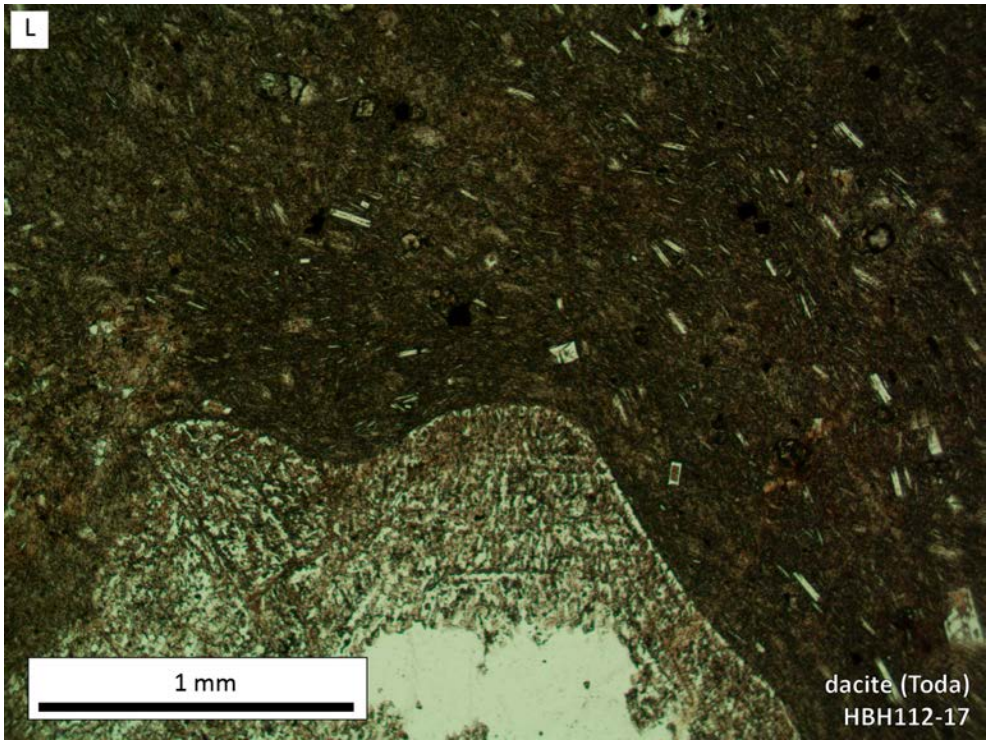

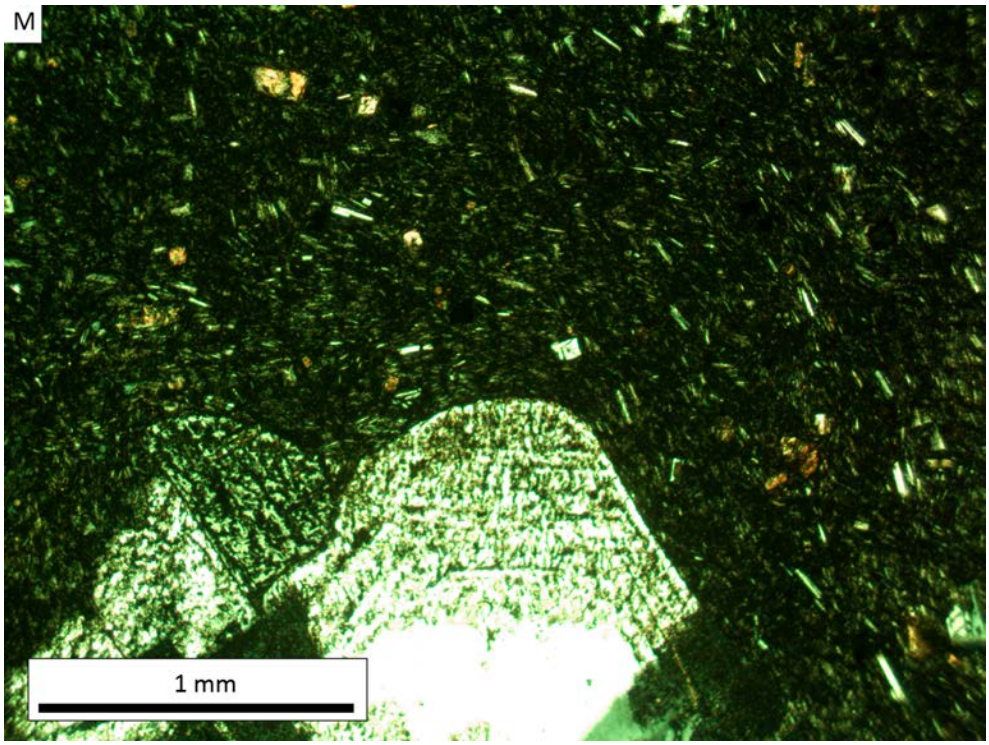

(Figure 5-14, continued) **Outcrop and petrographic description of dacite (Toda) exposed in the map area. (N) Photomicrograph of dacite pictured in (F), showing subhedral hornblende and clinopyroxene phenocrysts (c-axis 1 mm; 0.04 in) set in a microphenocrystic groundmass of plagioclase feldspar and clinopyroxene, under plane-polarized light. (O) Same view as in (N) under cross-polarized light.** *(Figure continued on following page.)*

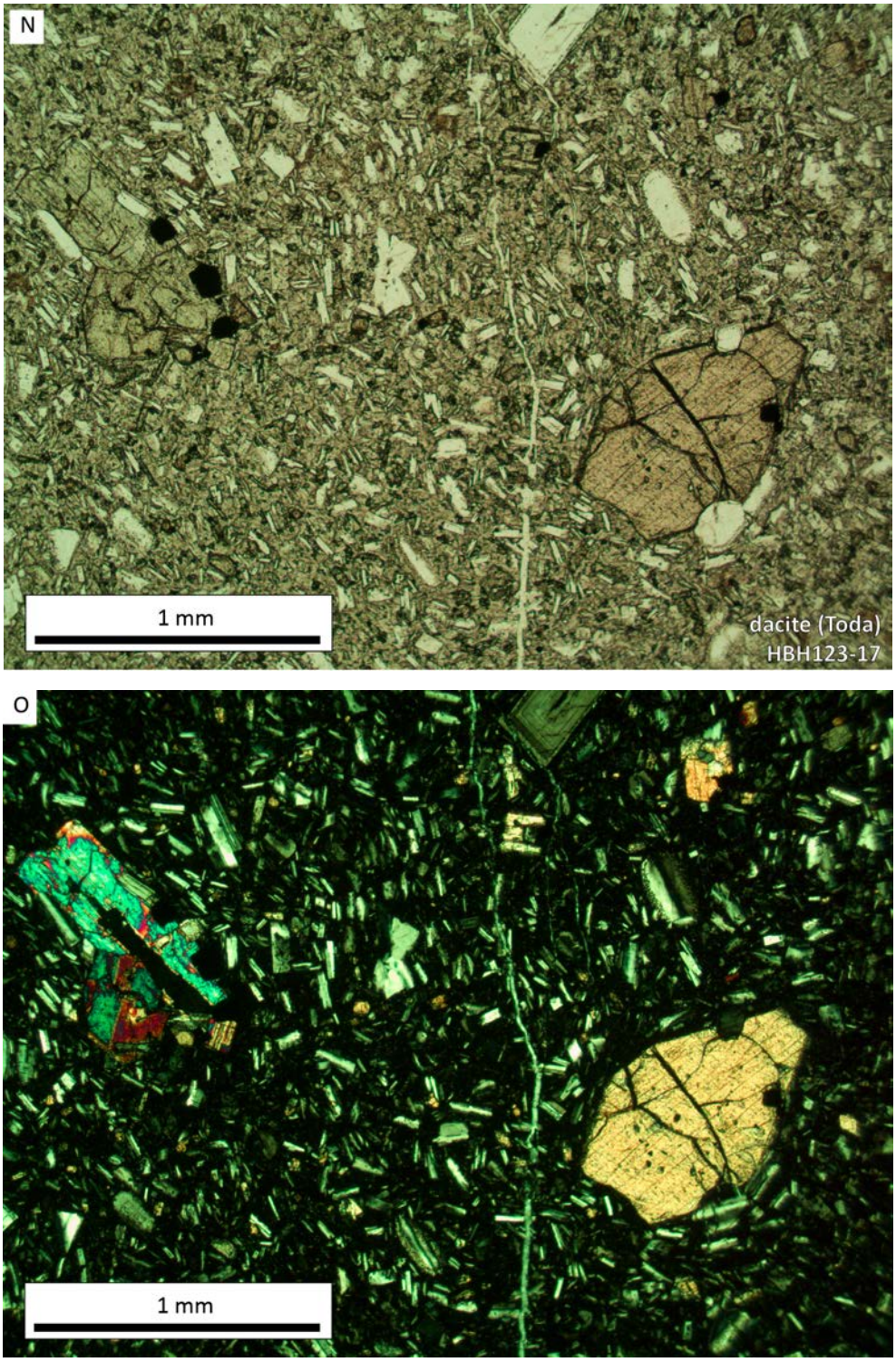

(Figure 5-14, continued) **Outcrop and petrographic description of dacite (Toda) exposed in the map area. (P) Photomicrograph of dacite, with large (c-axis 1 mm; 0.04 in) biotite and plagioclase feldspar phenocrysts with smaller (0.35 mm; 0.1 in) anhedral clinopyroxene phenocryst in a microphenocrystic groundmass of plagioclase feldspar and clinopyroxene, under plane-polarized light. (Q) Same view as in (P) under cross-polarized light.**

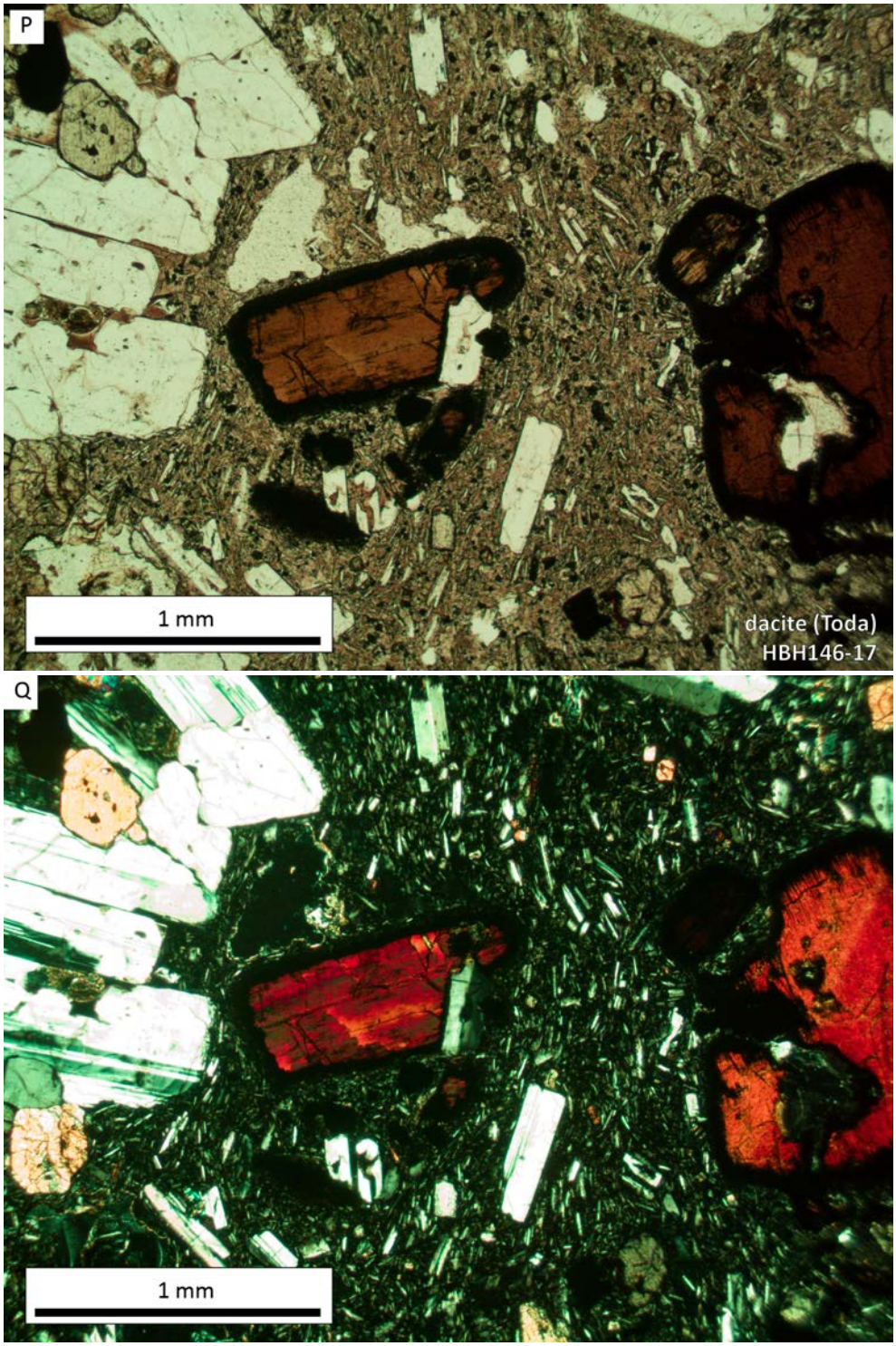

6.0 STRUCTURE

6.1 Introduction

Structure in the quadrangle is defined by the mapped distribution of geologic units, faults, topographic lineaments (as observed in the field, 10-m DEMs, and 2016 NAIP photographs), folds, and bedding attitudes (Plate 1; Appendix). Primary structural features (e.g., slickensides or fault breccia) are rarely observed in the field. Fault zones, such as those shown on Plate 1, are recognized from offset between geologic contacts and lithologies, missing units, topographic lineaments as indicators of possible movement, breccia, alignment of springs, and subsurface lithologic data obtained from water wells.

In the field, primary structural features are recognized from displacement of geologic contacts, change in bedding attitudes, excessive unit thickening, repeated sections, missing units, and topographic lineaments as indicators of possible displacement. Lack of exposure at key locations made fault piercing point determinations difficult. Besides direct evidence, structure was further interpreted by comparing stratigraphic position and attitudes between different fault blocks. Gentle folding and normal faulting, some exhibiting oblique displacement, were recognized by using these methods.

The northern region of the Harney Basin is underlain by a southward dipping stratigraphic section, cut by a predominant set of steeply dipping, right-lateral normal oblique north-striking faults. Direct observations of horizontal to gently inclined slickensides within shear fracture zones suggest a number of these faults have strike-slip or oblique-slip movement (**Figure 6-1A,B**). To a lesser extent, the area is cut by a number of northwest-striking and east-northeast–striking normal and normal oblique faults that, interpreted as Riedel shears, conjugate to the strike-slip faults (**Figure 6-1A,B;** Plate 1). A major north-northwest-trending dextral fault zone bisects the quadrangle, referred to here as the Trout Creek fault zone. Windows of older upper Oligocene stratigraphy (**Toa**, **Toda**, **Tor**) surrounded by younger rocks suggest the development of a significant paleo-topography prior to the deposition of the early Miocene Devine Canyon Ash-flow Tuff (**Tmtd**). The faults cut all Oligocene and Miocene aged rocks but are much less common in the late Miocene and younger rocks, suggesting that faulting may have been reactivated several times along selected structures through the late Miocene. The following discussion will present the spatial and temporal distribution of faults and folds in the quadrangle.

6.2 Faulting in the Devine Ridge North quadrangle

The Trout Creek fault is a major north-northwest-trending structure that bisects the quadrangle parallel to the Trout Creek drainage (**Figure 6-1; Figure 6-2;** Plate 1). In the southeastern part of the quadrangle several major fault structures, including the Soldier Creek fault zone of Devine Ridge South 7.5′ Quadrangle (Brown and others, 1980; Niewendorp and others, 2018), Upper Rattlesnake Creek fault (Houston and others, unpub. data, 2018), and upper Mill Creek fault (Houston and others, unpub. data, 2018), both located in Harney 7.5′ quadrangle, converge into the Trout Creek fault. The Idol City District, an epithermal gold deposit, is located at this zone of convergence. To the north, along the trace of the fault, synthetic splay faults (horsetail splays) widen the fault zone, forming a broad valley occupied by Trout Creek (**Figure 6-2;** Plate 1). Across the valley, east of the fault, the basal contact of the Rattlesnake Tuff (**Tmtr**) is exposed at an elevation of 5,309 ft. To the west and across the fault zone, the upper part of the Rattlesnake Tuff (**Tmtr**) is exposed at a lower elevation (4,754 ft) revealing approximately 550 ft of normal, down to the west, displacement. Locally, individual fault blocks in proximity to the fault zone are moderately tilted to the west approximately 10 to 35 degrees. Along the fault, oblique or strike-slip

displacements are difficult to quantify. However, offset of contacts and the relative rotation of individual fault blocks suggest the Trout Creek fault zone may have strike-slip displacement characterized as horsetail splays of en echelon synthetic faults with positive or negative fault duplexes or flower structure. West of the Trout Creek fault zone many northwest-striking and a lesser number of N-S striking normal faults occur. These faults are dominantly down-on-the-west with displacement estimated at 10 to 30 m (32 to 98 ft).

Figure 6-1. Observations of faulting in the Devine Ridge North 7.5’ quadrangle. (A) Oblique right-lateral slip faults cutting dacite (Toda), showing sense of normal (white arrows) and strike-slip (minus, away from observer; plus, toward observer) displacement. Highly sheared and fractured rock contains numerous slickensides with slickenline orientations, fault breccia, and gouge. Breccia fragments and fault gouge are altered (argillic alteration) by hydrothermal fluids related to the Idol City epithermal gold deposit. View looking south (43.759466, -118.887258 WGS84 geographic coordinates; 348079.6234mE, 4846888.614mN WGS84 UTM Zone 11 coordinates). *(Figure continued on following pages.)*

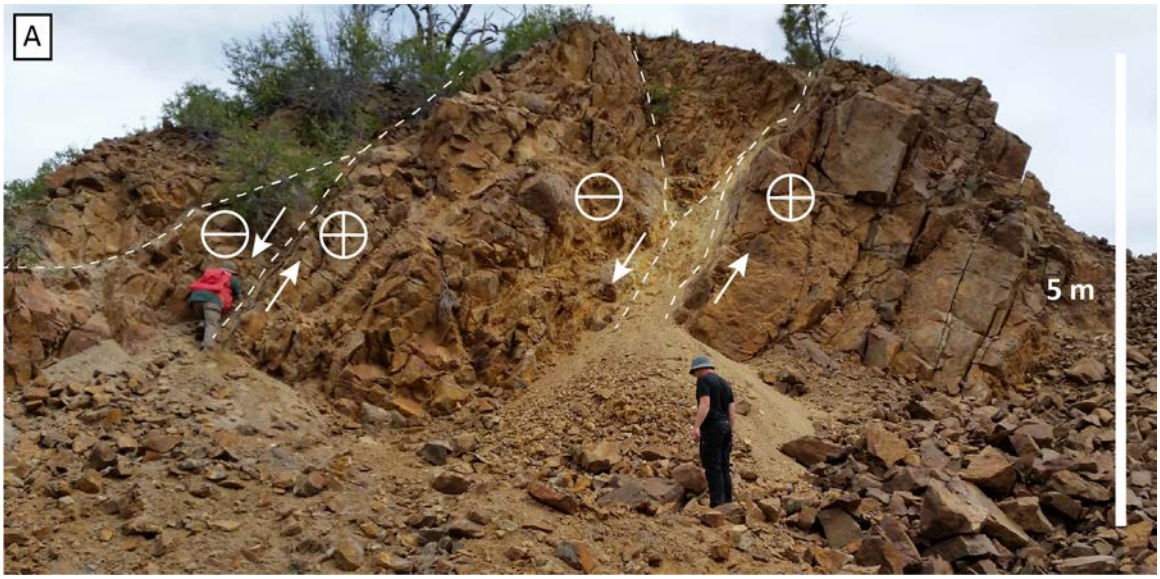

(Figure 6-1, continued) **Observations of faulting in the Devine Ridge North 7.5’ quadrangle. (B) Southwest-striking steeply west dipping oblique-slip fault, showing gently inclined (S43W-87W; rake = 25 degrees) slickenlines along the fault surface (white arrows). View looking north (43.781367, -118.897431 WGS84 geographic coordinates; 347316.4298mE, 4849339.8217mN WGS84 UTM Zone 11 coordinates).** *(Figure continued on following page.)*

(Figure 6-1, continued) **Observations of faulting in the Devine Ridge North 7.5' quadrangle. (C) Fault (N43W-50NE), showing normal displacement (80 cm [2.6 ft]; white arrows) of the basal contact of Devine Canyon Ash-flow Tuff (Tmtd) and the Tuffaceous sedimentary rocks (Tmst). View looking east (43.865144, -118.931998 WGS84 geographic coordinates; 344752.1475mE, 4858709.0071mN WGS84 UTM Zone 11 coordinates).**

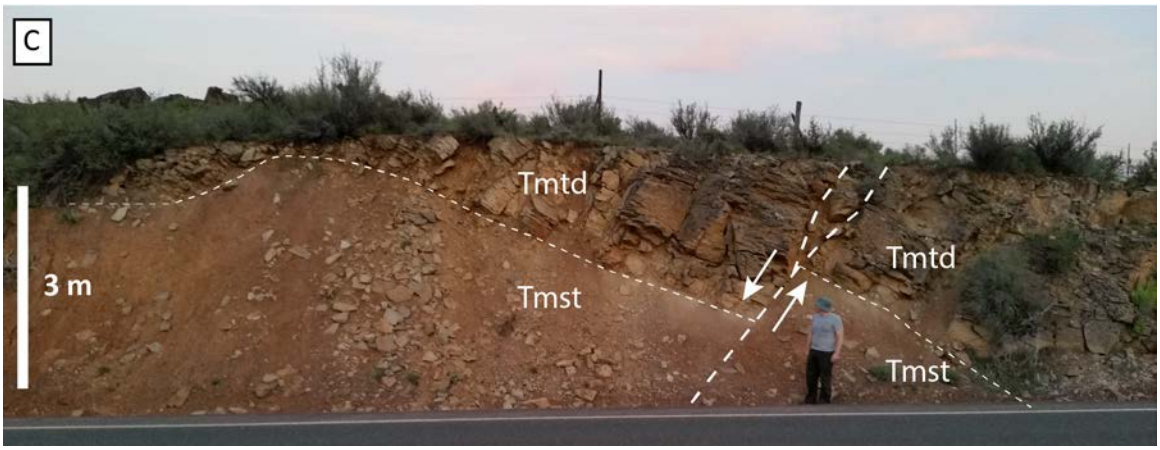

6.3 Fold structure in the Devine Ridge North quadrangle

Greene and others (1972) and Brown and others (1980) showed two gently south-southwest plunging anticlines (**Figure 6-2**; Plate 1). Primary field evidence for folding is limited to a region that is highly faulted by both the Trout Creek and Soldier Creek fault zones. This region of the map has very limited occurrences of primary sedimentary bedding planes.

Figure 6-2. Structure map for the Devine Ridge North 7.5′ quadrangle, showing the distribution of faults (black lines) and folds (blue lines) (after Brown and others [1980] and Greene and others [1972]). Basemap: 10-m hillshade DEM.

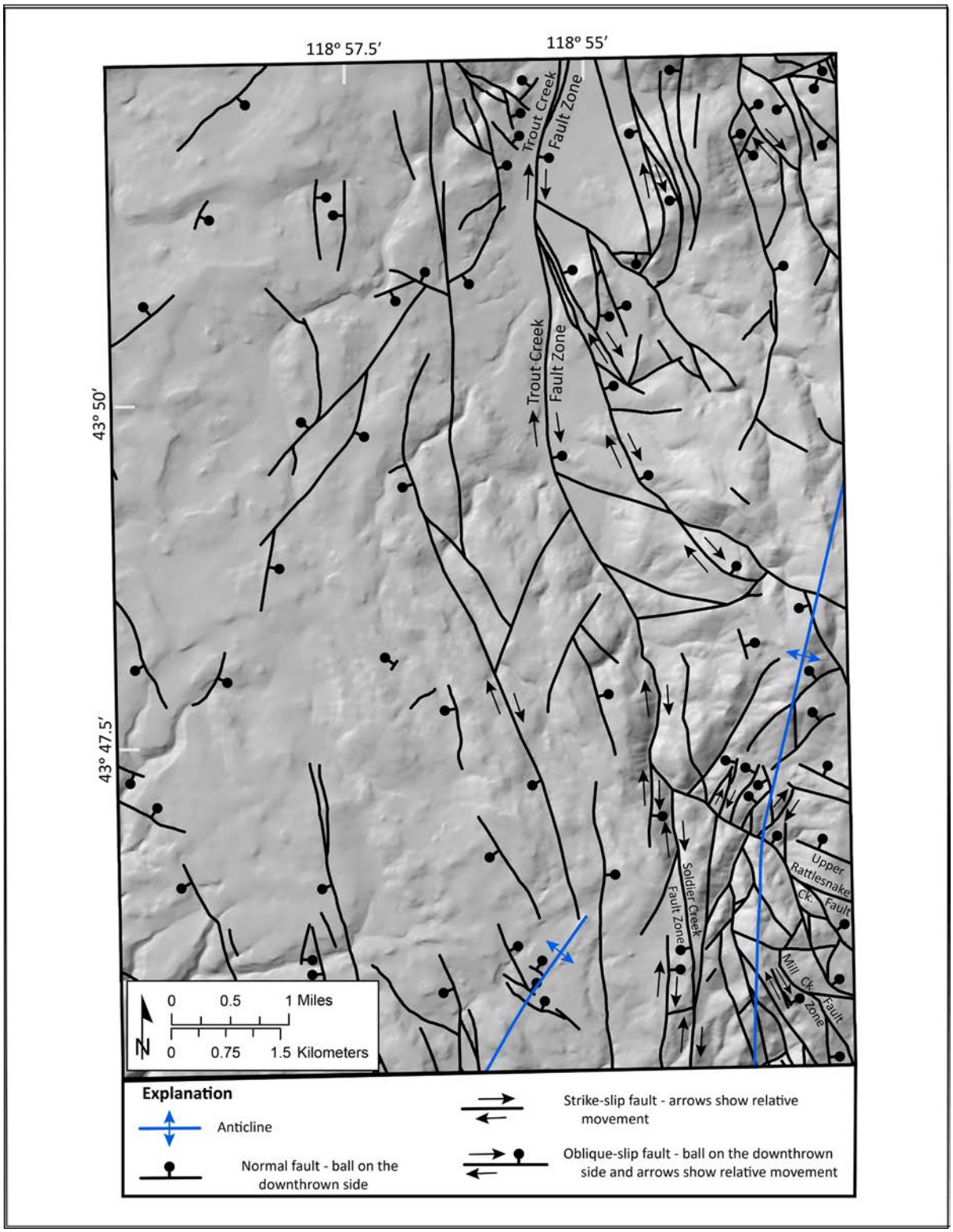

7.0 GEOLOGIC HISTORY

Cenozoic volcanic rocks, sedimentary rocks, and surficial deposits exposed in the Devine Ridge North 7.5′ quadrangle record the volcanic, depositional, and deformational history of the northern Harney Basin region since the late Oligocene (Plate 1). The upper Miocene and upper Oligocene volcanic rocks represent a bimodal suite of eruptive products. High-angle normal faults and oblique right-lateral normal faults cut all rocks in the study area. Faulting was both contemporaneous with and followed deposition of the 7.05 Ma Rattlesnake Tuff. The following discussion presents the major geologic events in the Devine Ridge North 7.5′ quadrangle.

7.1 Late Miocene to late Oligocene (<25 Ma to 9.63 Ma)

Based on stratigraphic relationships, dacite is the oldest rock type in the study area. The dacite is overlain by a high-barium 24.75 ± 0.15 Ma andesite in the quadrangle. Additionally, the dacite is intruded by rhyolitic dikes and irregular bodies in the southwestern part of the quadrangle. The chronologic relationship between the andesite and intrusive rhyolite dikes are not known, owing to the lack of exposed cutting relationships. Lode ores of the Idol City District, an epithermal gold deposit, are hosted in the dacite (**Toda**) and rhyolitic dikes (**Tor**). McGrane (1985) reported ages of 21 ± 0.9 Ma (K/Ar) on sericite alteration and 19 ± 0.08 Ma (K/Ar) on a rhyolite dike within the Idol City District. However, altered and mineralized rocks are locally overlain by nonmineralized "fresh" 24.75 Ma andesite (**Toa**), suggesting the secession of the hydrothermal ore fluids occurred prior to the late Oligocene. This chronologic contradiction in the age of the Idol City District hydrothermal system merits additional geological investigation. Later eruptive phases, including basalt-basaltic andesite (**Tmb**) and Dinner Creek Tuff (**Tmdc**), were deposited onto partially eroded and faulted paleo-surface.

7.2 Late Miocene (<9.63 Ma to 7.05 Ma)

During the late Miocene, the early mafic phase was followed by an alternating sequence of tuffaceous sedimentary rocks and felsic ash-flow tuffs (**Figure 5-1**; Plate 1). An interval of sedimentation in the basin was interrupted by three cataclysmic ash-flow eruptions that created the 9.63 Ma Devine Canyon Ash-flow Tuff, 8.41 Ma Prater Creek Ash-flow Tuff, and 7.05 Ma Rattlesnake Tuff. The Devine Canyon Ash-flow Tuff and the Prater Creek Ash-flow Tuff are interbedded with the tuffaceous sedimentary unit (**Tmst**) and provide excellent stratigraphic and chronologic control. The Rattlesnake Tuff conformably overlies the tuffaceous sedimentary rocks and is the youngest (non-surficial) rock unit exposed in the study area and is one of the most far-traveled ash-flow tuffs known in the world with a reconstructed dense rock equivalent volume of 280 km^3 (67 mi^3; Streck and Grunder, 1995). Caldera sources related to all three tuffs are not exposed but are thought to occur in the Harney Basin (Walker, 1970; Greene, 1973; Parker, 1974; Walker, 1979; Streck and Grunder, 1995; Khatiwada and Keller, 2015).

8.0 GEOLOGIC RESOURCES

8.1 Aggregate materials and industrial minerals

Aggregate in the form of crushed rock and gravel is the major mineral resource mined in the Harney Basin area. Niewendorp and Geitgey (2009) provided regional locations for aggregate and crushed rock resources (https://www.oregongeology.org/milo/index.htm). In the study area, sand, gravel, and crushed rock quarry sites are sited mainly in dacite (**Toda**), andesite (**Toa**), basalt-basaltic andesite (**Tmb**), Prater Creek Ash-flow Tuff (**Tmtp**), Rattlesnake Tuff (**Tmtr**), and alluvial deposits (**Qa**). Presently, all quarries in the Devine Ridge North quadrangle are small pit-run sources located on private lands and on lands administered by the Oregon Department of Transportation or the U.S. Forest Service. This material is used locally as pit-run resource for road construction and maintenance. However, certain localities may provide material suitable for decorative stone and for use as riprap for stabilization and erosion control purposes. Sand and gravel resources are limited and restricted to unconsolidated alluvial deposits (**Qa**, **Qao**) in Trout Creek drainage. No industrial minerals are known to occur in the map area (Niewendorp and Geitgey, 2009).

Discovery of placer gravels in 1891, in the southeastern part of the map area, led to the identification and development of an epithermal gold deposit (McGrane, 1985), and beginning of mining in the Idol City District (**Figure 8-1A** through **Figure 8-1H;** Niewendorp and Geitgey, 2009). The Idol City District extends southward into the Devine Ridge South 7.5′ quadrangle, where the district is defined by zones of hydrothermally altered (argillic) and brecciated silicified rock (**Figure 8-1G**). McGrane (1985) reported that a small dredge recovered 17,000 ounces of gold from ~280,000 tons of gravel, mined at a grade of 0.061 oz./ton located in Trout Creek. Production records indicate that approximately 20,000 oz. of gold were recovered from the placers (McGrane, 1985; **Figure 8-1A**). Mining quickly shifted from placer to lode ores, where several prospects, shafts, and underground works developed the deposit (**Figure 8-1B** through **Figure 8-1F**). The lodes are hosted in dacite (**Toda**), rhyolitic dikes (**Tor**), and hydrothermal breccia zones within these units. The degree of alteration varies within the district, with the most intense alteration and mineralization occurring along breccia zones (tourmaline breccias, stockwork breccias, and rubble breccias). The four types of alteration recognized include tourmalinitic, sericitic, argillic (**Figure 8-1G**), and propylitic. Precious and base metal ores are present. McGrane (1985) reported soil samples with as much as 1.9 ppm gold and "significant" gold grades for certain drill core intercepts. McGrane (1985) also reported that in the disseminated ore body, lead, zinc, and copper grades rarely exceed 0.5 percent and silver grades are rarely greater than 0.5 oz./ton. However, high grades centered on brecciated zones had grades of 15 percent combined lead-zinc and 3-4 oz./ton silver (McGrane, 1985). McGrane (1985) reported that most of the rock yielded minor amounts of gold and that the high-grade zones were never located. Fluid inclusion derived temperature data indicate ore fluids were approximately 300 degrees C.

McGrane (1985) concluded from drill core and fluid inclusion homogenization temperature analysis that mineralization occurred at ~300 degrees C (572 degrees F) in response to boiling triggered by explosive brecciation events at a shallow depth of 315 m (1,033 ft). Altered and mineralized rocks are overlain by nonmineralized fresh andesite, providing a chronologic and stratigraphic constraint on the spatial and temporal distribution of mineralization. Peripheral to the deposit, colorless, white, to bluish-gray chalcedony occurs as the dominate vein filling material and as vesicle lining. Common open space cryptocrystalline silica includes massive or banded and to a lesser extent botryoidal textures. The presence of chalcedony and open space textures indicate that the emplacement depths were shallow and

fluid temperatures were low (< 180°C). Supergene enrichment occurred in the district to a minor extent (**Figure 8-1H**). Locally, the presence of malachite along fractures in post-ore nonmineralized rock (Dinner Creek Tuff; **Figure 8-1H**) indicate that secondary enrichment continued post-ore emplacement as meteoric waters transported and precipitated the soluble minerals into younger downfaulted nonmineralized rocks.

New mapping by C. Niewendorp (Niewendorp and others, 2018) identified additional hydrothermally altered breccias to the south in Devine Ridge South 7.5′ quadrangle. Additionally, to the north and downstream from the district, unmined older alluvium (**Qao**) and strath-terrace deposits (**Qt**) adjacent to Trout Creek may merit further mineral resource (placer) potential investigation. Additional mapping and analytical data are required to understand better the spatial and temporal zoning of hydrothermal alteration and mineralization in the Idol City epithermal gold deposit.

Figure 8-1. Idol City District. (A) Hydraulic mining placer deposit, circa 1941 (photograph courtesy of Western History Room, Harney County Library, from a manuscript donated by Carol Martin Winters) (43.780614, -118.896584 WGS84 geographic coordinates; 347382.6808mE, 4849254.631mN WGS84 UTM Zone 11 coordinates). *(Figure continued on following pages.)*

(Figure 8-1, continued) **Idol City District. (B) The town of Idol City, circa 1975 (photograph courtesy of Western History Room, Harney County Library, from a manuscript donated by Carol Martin Winters) (43.777122, -118.892927 WGS84 geographic coordinates; 347668.0368mE, 4848860.08181mN WGS84 UTM Zone 11 coordinates).** *(Figure continued on following pages.)*

(Figure 8-1, continued) **Idol City District. (C) Head frame at the Idol City District, late 1980s (photograph courtesy of Western History Room, Harney County Library, from a manuscript donated by Carol Martin Winters) (43.777122, -118.892927 WGS84 geographic coordinates; 347668.0368mE, 4848860.08181mN WGS84 UTM Zone 11 coordinates).** *(Figure continued on following pages.)*

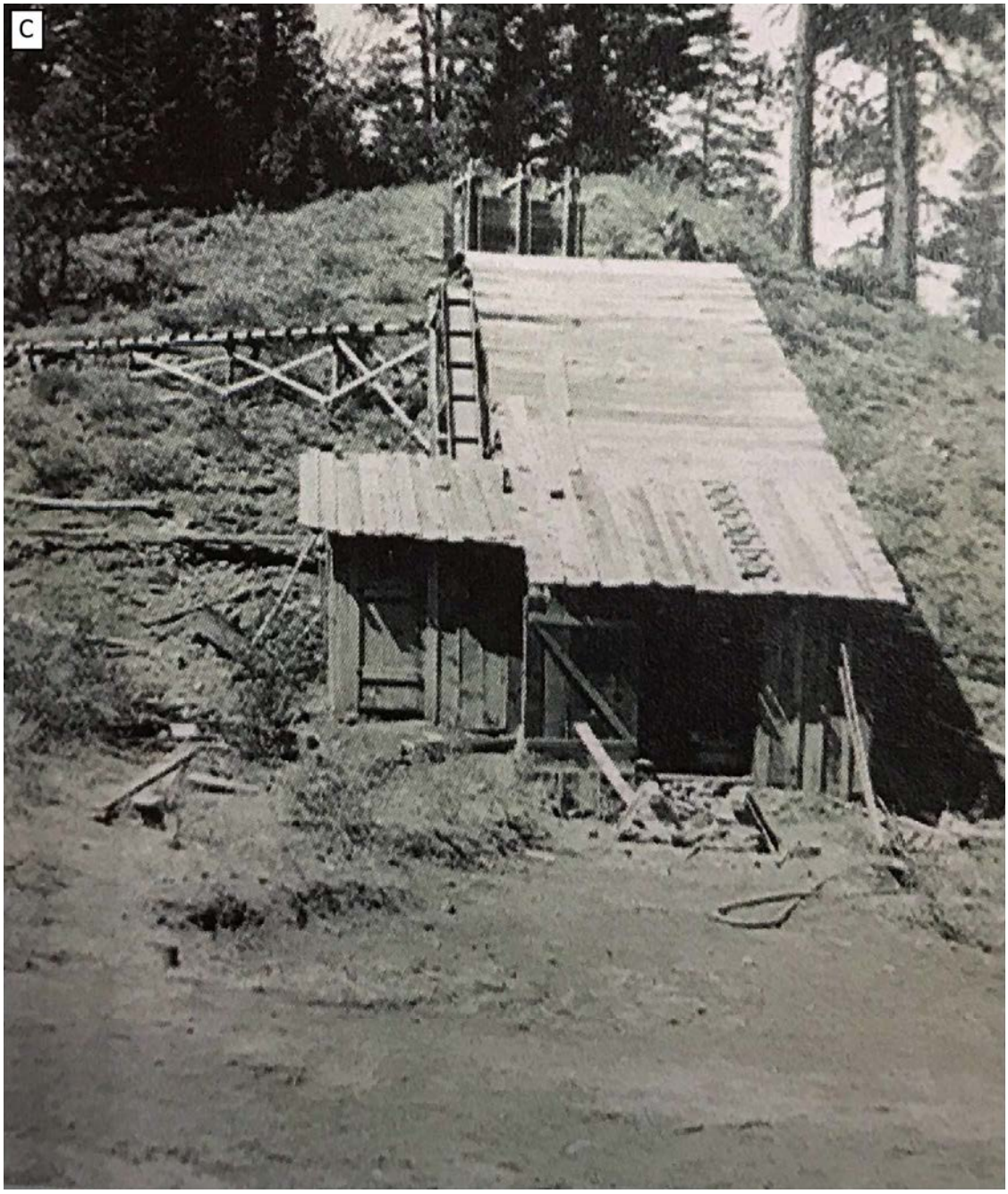

(Figure 8-1, continued) **Idol City District. (D) Reclaimed head frame and main shaft location (43.777122, -118.892927 WGS84 geographic coordinates; 347668.0368mE, 4848860.08181mN WGS84 UTM Zone 11 coordinates). (E) Trammel used to process auriferous gravels eroded from lode veins of the epithermal gold deposit, Idol City District (43.780614, -118.896584 WGS84 geographic coordinates; 347382.6808mE, 4849254.631mN WGS84 UTM Zone 11 coordinates).** *(Figure continued on following pages.)*

(Figure 8-1, continued) **Idol City District. (F) Trout Creek placer gravels and tailings (43.780614, -118.896584 WGS84 geographic coordinates; 347382.6808mE, 4849254.631mN WGS84 UTM Zone 11 coordinates). (G) Typical argillic alteration of wall rock in proximity to fault structures in the Idol City District (43.759466, -118.887258 WGS84 geographic coordinates; 348079.6234mE, 4846888.614mNWGS84 UTM Zone 11 coordinates).** *(Figure continued on following page.)*

(Figure 8-1, continued) **Idol City District. (H) Malachite, secondary enrichment in younger post ore rocks (43.769469, -118.875938 WGS84 geographic coordinates; 349016.0254mE, 4847978.9091mN WGS84 UTM Zone 11 coordinates).**

8.2 Energy resources

Geothermal resources have not been identified in the Devine Ridge North 7.5′ quadrangle area and, to the knowledge of the authors, no geothermal exploration has occurred in the map area (https://www.oregongeology.org/gtilo/index.htm).

No oil and gas exploration wells have been drilled in the Devine Ridge North 7.5′ quadrangle. To the south in Harney Basin, a limited number of exploratory wells were drilled from the late 1940s into the late 1970s. Many wells report multiple shows of gas. All wells were abandoned shortly after completion. Well location and drilling logs are available at https://www.oregongeology.org/mlrr/oilgas-logs.htm.

8.3 Water resources

A full discussion of the geologic controls on surface and groundwater resources in the Devine Ridge North 7.5′ quadrangle is beyond the scope of this report. However, field observations and preliminary findings on geologic parameters controlling water resources within the study area are briefly summarized below (**Figure 8-2A** through **Figure8-2C**). The reader is referred to previous hydrogeologic investigations conducted by Piper and others (1939), Leonard (1970), Walker (1979), Whitehead (1994), and Gonthier (1985) for more in-depth discussions.

Unconsolidated to partly consolidated alluvial sand and gravel deposits preserved in terraces and floodplains (**Qa**, **Qao**) and on alluvial and debris fans (**Qaf**) likely contain groundwater that typically saturates sediments just above the underlying bedrock platform and is usually in hydraulic connection with nearby streams (**Figure 8-2B;** Plate 1; Piper and others, 1939; Leonard, 1970). The deposits are typically thin (<10 m [30 ft]) and likely sinuous, but may be very permeable, except where they contain large amounts of clay and silt (Piper and others, 1939; Leonard, 1970). Alluvial wells developed in permeable sand and gravel intervals with yields depending on annual precipitation, as compared to relatively impermeable silt-rich sedimentary intervals, are likely favorable targets (Piper and others, 1939).

In the Devine Ridge North 7.5′ quadrangle, perennial springs appear to cluster along faults and contacts. Seeps or springs in proximity to a significant reduction of slope, not related to a lithologic contact, might suggest a shallower hydraulic connection associated with snowmelt and rainfall recharge.

The location of perennial springs along faults and contacts in the study area concentrates groundwater flow where permeability is favorable (**Figure 8-2C**). Based on location of springs, water-bearing horizons in the study area are generally found at the basal contacts of **Tmtr**, **Tmtp**, and **Tmtd** rock types (Plate 1). These horizons serve as lateral pathways for groundwater flow. Tuffaceous sedimentary rocks (**Tmst**) between ash-flow tuffs appear to act as either confining units or porous media serving as a pathway for lateral transport of groundwater depending on percent clays (**Figure 8-2A**). In the southeastern part of the study area, clay alteration of the rocks and precipitation of chalcedony in fractures associated with the Idol City epithermal gold deposit likely disrupt groundwater flow. Elsewhere, variability in the alteration and percent fault gouge along faults may leave limited permeable zones that serve as ideal groundwater pathways.

A majority of the water wells (n=6) are drilled to an average depth of more than 66 m (217 ft) and encounter first water at an average depth of 43 m (144 ft; Appendix). The deepest well (HARN-51008; Appendix) was drilled to a depth of 94 m (310 ft) into “fractured basalt” mapped as dacite (**Toda**). From the drillers’ report, all other wells terminated in either sedimentary rocks or basalt. Permeable layers within the sedimentary rocks as well as near-surface volcanic rocks may be targets for groundwater resources. Locally, unconsolidated to partly consolidated alluvial sand and gravel sequences in proximity to Trout Creek and its tributaries may contain groundwater in hydraulic connection with nearby streams and are likely groundwater targets (Plate 1; Piper and others, 1939; Leonard, 1970). Within the map area there are some examples where seeps or springs occur along the Trout Creek shear zone or associated faults. However, the volume and quality of groundwater along the Trout Creek shear zone and associated faults remain poorly understood.

Figure 8-2. Springs and seeps in the map area. (A) A seasonal seep in tuffaceous sedimentary rocks. The seep occurs in two separate layers of siltstone and sandstone separated by a bed of finer-grained sedimentary rock. Water bottle is 25 cm (10 in) in length (43.772346, -119.002485 WGS84 geographic coordinates; 338838.5143mE, 4848536.992mN WGS84 UTM Zone 11 coordinates). (B) Agricultural pond excavated into alluvial deposits (Qa) containing shallow groundwater. Excavation is approximately 1 m (3 ft) deep and 10 m (32 ft) in diameter (43.805978, -118.954222 geographic coordinates; 342811.18 mE, 4852179.67 mN WGS84 UTM Zone 11 coordinates). *(Figure continued on following page.)*

(Figure 8-2, continued) **Springs and seeps in the map area. (C) Perennial spring located in proximity to a projected concealed fault. The surface expression of the spring is approximately 12 m (40 ft) in diameter (43.871019, -118.898478 WGS84 geographic coordinates; 347460.7303mE, 4859299.1285mN WGS84 UTM Zone 11 coordinates).**

9.0 GEOLOGIC HAZARDS

9.1 Landslide hazards

The downslope movement of rock and soil, in the form of landslides, rock falls, and debris flows, may present a geologic hazard to residents, infrastructure, and transportation corridors in the Devine Ridge North 7.5′ quadrangle.

9.1.1 Simple and colluvial landslides

Seven landslide deposits (**Qls**) were recognized and mapped in the study area. Those landslide deposits (**Qls**) recognized cover approximately 1.5 percent of the map area and are of limited size, covering less than 4.7 hectares (11.6 acres) to larger composite features covering areas as much as 80 hectares (200 acres). Most mapped landslide deposits are deep-seated earthflow-type features that occur along major drainages, originating on sparsely vegetated, moderate to steep slopes underlain by weakly consolidated rocks of the tuffaceous sedimentary rocks (**Tmst**; Plate 1). Many of these slides can be attributed to the

combined influences of parallel topographic slope and faulting or bedding dip, undercutting by streams, heavy precipitation, groundwater conditions, and rock type. The generally weakly consolidated nature of the tuffaceous sedimentary rocks (**Tmst**) makes this unit especially prone to landslides on gently to steeply inclined slopes. Future landslides should be expected in **Tmst** particularly in areas of changing vegetation resulting from rangeland fires or changes in land use that may alter local groundwater conditions.

Unstable colluvium (wedges of soil and rock) mantles few slopes in the study area. These deposits typically form when weathered rock particles, ranging in size from clay to boulders, accumulate along a hillside. When the mass of the accumulated material reaches a critical size, a triggering event such as heavy rainfall or a seismogenic event may initiate the rapid downslope movement of this mass. Areas denuded by fire or other anthropogenic vegetative removal can especially be at risk from such events.

9.1.2 Rock fall

Rock fall and rockslide hazards may be present in the study area where steep slopes and cliff exposures of **Toda**, **Toa**, **Tmb**, **Tmtd**, **Tmtp**, and **Tmtr** occur (Plate 1). Potential natural triggering mechanisms for rock fall events include freeze/thaw cycles, heavy rainfall, earthquakes, or extensive devegetation due to fire (Beaulieu, 1977).

9.1.3 Alluvial fan deposits

Alluvial fan and debris fan (**Qaf**) deposits in the study area have been mapped along Trout Creek and its tributaries (Plate 1). Rapidly moving landslides in the form of debris flows may be expected on both alluvial and debris fans that lie at the mouth of steep-sided, colluvium-filled canyons and upland drainages. The potential for inundation of fan areas by rapidly moving debris flows increases during episodes of intense rainfall that occur after soils have been saturated by fall and early winter rainfall. Redirected drainage and poor construction practices are human activities that could initiate debris flows. Debris flows have the potential to threaten life and may cause extensive damage to property and transportation corridors.

10.0 ACKNOWLEDGMENTS

This project and publication were supported through the STATEMAP component of the National Cooperative Geologic Mapping Program under cooperative agreement number G17AC00210. Additional funds were provided by the State of Oregon. XRF geochemical analyses were prepared and analyzed by Dr. Scott Boroughs at the GeoAnalytical Lab at Washington State University, Pullman. The authors appreciate informative discussions and field trips with Ivan Gall, Justin Iverson, Jerry Grondin, and many other geologists who provided their expertise on stratigraphy in the Harney Basin. The authors acknowledge many area landowners who provided local knowledge and graciously allowed access to private holdings within the study area. The first author greatly appreciated the assistance from DOGAMI staff John Bauer, Nancy Calhoun, and Deb Schueller for numerous insightful discussions and detailed internal reviews. Cartography for the map plates was provided by Jon Franczyk. Critical and insightful external reviews by Darrick Boschmann and Mark Ferns greatly enriched the final manuscript, geodatabase, and geologic maps.

11.0 REFERENCES

Beaulieu, J. D., 1977, Geologic hazards of parts of northern Hood River, Wasco, and Sherman Counties, Oregon: Oregon Department of Geology and Mineral Industries Bulletin 91, 95 p. 11 pl., scale 1:62,500. https://www.oregongeology.org/pubs/B/B-091.pdf

Boschmann, D. E., 2012, Structural and volcanic evolution of the Glass Buttes area, High Lava Plains, Oregon: Corvallis, Oreg., Oregon State University, M.S. thesis, 100 p. https://ir.library.oregonstate.edu/concern/graduate_thesis_or_dissertations/47429d66f

Brown, C. E., and Thayer, T. P., 1966, Geologic map of the Canyon City quadrangle, northeastern Oregon: U.S. Geological Survey Miscellaneous Geologic Investigations Map I-447, 1 pl., scale 1:250,000.

Brown, D. E., 1982, Map showing geology and geothermal resources of the southern half of the Burns 15 minute quadrangle, Oregon: Oregon Department of Geology and Mineral Industries Geological Map Series GMS-20, 1 pl., scale 1:24,000. https://www.oregongeology.org/pubs/gms/GMS-020.pdf

Brown, D. E., McLean, G. D., and Black, G. L., 1980, Preliminary geology and geothermal resource potential of the northern Harney Basin, Oregon: Oregon Department of Geology and Mineral Industries Open-File Report 80-6, 52 p., 4 pl., scale 1:62,500. Zipped file: https://www.oregongeology.org/pubs/ofr/O-80-06.zip

Butler, R. F., 1992, Origins of natural remanent magnetism, chap. 3 *of* Paleomagnetism: Magnetic domains to geologic terranes: Boston, Mass., Blackwell Scientific Publications, p. 31–63. Available from https://websites.pmc.ucsc.edu/~njarboe/pmagresource/ButlerPaleomagnetismBook.pdf

Cahoon, E. B., and Streck, M. J., 2017, Picture gorge basalt, eastern Oregon: Extended distribution and petrogenetic connections to Steens basalt and Strawberry Volcanics: Geological Society of America Abstracts with Programs, v. 49, no. 6. doi: 10.1130/abs/2017AM-304582. https://gsa.confex.com/gsa/2017AM/webprogram/Paper304582.html

Camp, V. E., Ross, M. E., and Hanson, W. E., 2003, Genesis of flood basalts and Basin and Range volcanic rocks from Steens Mountain to the Malheur River Gorge, Oregon: Geological Society of America Bulletin, v. 115, no. 1, p. 105–128. https://doi.org/10.1130/0016-7606(2003)115<0105:GOFBAB>2.0.CO;2

Camp, V. E., Ross, M. E., Duncan, R. A., Jarboe, N. A., Coe, R. S., Hanan, B. B., and Johnson, J. A., 2013, The Steens Basalt: Earliest lavas of the Columbia River Basalt Group, *in* Reidel, S. P., Camp, V. E., Ross, M. E., Wolff, J. A., Martin, B. S., Tolan, T. L., and Wells, R. E., The Columbia River Flood Basalt Province: Geological Society of America Special Paper 497, p. 87–116. https://doi.org/10.1130/2013.2497(04)

Cande, S. C., and Kent, D. V., 1992, A new geomagnetic polarity time scale for the Late Cretaceous and Cenozoic: Journal of Geophysical Research, v. 97, no. B10, p. 13,917–13,951. https://doi.org/10.1029/92JB01202

Cohen, K. M., Finney, S. C., Gibbard, P. L., and Fan, J.-X., 2018, The ICS International Chronostratigraphic Chart: Episodes, v. 36, no. 3, 199–204. Available at http://www.stratigraphy.org/ICSchart/Cohen2013_Episodes.pdf

Donath, F. A., 1962, Analysis of basin-range structure, south-central Oregon: Geological Society of America Bulletin, v. 73, p. 1–16. https://doi.org/10.1130/0016-7606(1962)73[1:AOBSSO]2.0.CO;2

Duncan, R.A., Hooper, P. R., Rehacek, J., Marsh, J. S., and Duncan, A. R., 1997, The timing and duration of the Karoo igneous event, southern Gondwana: Journal of Geophysical Research, v. 102, no. B8, p. 18,127–18,138.

Ferns, M. L., and McClaughry, J. D., 2013, Stratigraphy and volcanic evolution of the middle Miocene to Pliocene La Grande–Owyhee eruptive axis in eastern Oregon, *in* Reidel, S. P., Camp, V. E., Ross, M. E., Wolff, J. A., Martin, B. S., Tolan, T. L., and Wells, R. E., eds., The Columbia River Flood Basalt Province: Geological Society of America Special Paper 497, p. 401–427. https://doi.org/10.1130/2013.2497(16)

Ferns, M. L., Brooks, H. C., Evans, J. G., and Cummings, M. L., 1993, Geologic map of the Vale 30 × 60 minute quadrangle, Malheur County, Oregon, and Owyhee County, Idaho: Oregon Department of Geology and Mineral Industries Geologic Map Series GMS-77, 1 pl., scale 1:100,000. https://www.oregongeology.org/pubs/gms/GMS-077.pdf

Ford, M. T., Grunder, A. L., and Duncan, R. A., 2013, Bimodal volcanism of the High Lava Plains and northwestern Basin and Range of Oregon: Distribution and tectonic implications of age-progressive rhyolites: Geochemistry, Geophysics, Geosystems, v. 14, no. 8, p. 2837–2857. https://doi.org/10.1002/ggge.20175

Geological Society of America Rock-Color Chart Committee, 1991, Rock color chart, 7th printing: Boulder, Colo.

Gillespie, M. R., and Styles, M. T., 1999, BGS rock classification scheme, v. 1, Classification of igneous rocks: Keyworth, U.K., British Geological Survey Research Report RR 99-06 (reformatted), 52 p. http://nora.nerc.ac.uk/3223/1/RR99006.pdf

Gonthier, J. B., 1985, A description of aquifer units in eastern Oregon: U.S. Geological Survey Water-Resources Investigations Report 84-4095, 39 p., 4 pl., scale 1:500,000. https://doi.org/10.3133/wri844095

Gradstein, F. M., and others. 2004, A geologic time scale 2004: Cambridge University Press, 589 p.

Gray, J. J., Peterson, N. V., Clayton, J., and Baxter, G. L., 1983, Geology and mineral resources of 18 BLM Wilderness Study Areas, Harney and Malheur Counties, Oregon: Oregon Department of Geology and Mineral Industries Open-File Report O-83-2. https://www.oregongeology.org/pubs/ofr/O-83-02.pdf

Greene, R. C., 1972, Preliminary geologic map of the Burns and West Myrtle Butte 15-minute quadrangles, Oregon: U.S. Geological Survey Miscellaneous Field Studies Map MF-320, scale 1:62,500. https://ngmdb.usgs.gov/Prodesc/proddesc_2743.htm

Greene, R. C., 1973, Petrology of the welded tuff of Devine Canyon, southeast Oregon: U.S. Geological Survey Professional Paper 797, 26 p. https://doi.org/10.3133/pp797

Greene, R. C., Walker, G. W., and Corcoran, R. E., 1972, Geologic map of the Burns quadrangle, Oregon: U.S. Geological Survey Miscellaneous Geologic Investigations Map I-680, scale 1:250,000. https://ngmdb.usgs.gov/Prodesc/proddesc_9455.htm

Haddock, G. H., 1967, The Dinner Creek welded ash-flow tuff of the Malheur Gorge area: Eugene, Oreg., University of Oregon, Ph.D. thesis, 111 p.

Hallsworth, C. R., and Knox, R. W. O'B., 1999, BGS rock classification scheme, v. 3, Classification of sediments and sedimentary rocks: Keyworth, U.K., British Geological Survey Research Report RR 99-03, 44 p. http://nora.nerc.ac.uk/3227/1/RR99003.pdf

Iademarco, M. J., 2009, Volcanism and faulting along the northern margin of Oregon's High Lava Plains: Hampton Butte to Dry Mountain: Corvallis, Oreg., Oregon State University, M.S. thesis, 158 p., 1 pl. https://ir.library.oregonstate.edu/concern/graduate_thesis_or_dissertations/t435gj391

Isom, S. L., 2017, Compositional and physical gradients in the magmas of the Devine Canyon Tuff, eastern Oregon: constraints for evolution models of voluminous high-silica rhyolites: Portland, Oreg., Portland State University, M.S. thesis, 147 p. https://pdxscholar.library.pdx.edu/open_access_etds/3885/

Johnson, D. M., Hooper, P. R., and Conrey, R. M., 1999, XRF analysis of rocks and minerals for major and trace elements on a single low dilution Li-tetraborate fused bead: Advances in X-ray Analysis, v. 41, p. 843–867. Available at: https://s3.wp.wsu.edu/uploads/sites/2191/2017/06/Johnson-Hooper-and-Conrey.pdf

Johnson, J. A., 1994, Geologic map of the Krumbo Reservoir quadrangle, Harney County, southeastern Oregon: U.S. Geological Survey Miscellaneous Field Studies Map MF-2267, 11 p., 1 pl., scale 1:24,000. https://pubs.er.usgs.gov/publication/mf2267

Johnson, J. A., 1996, Geologic map of the Page Springs quadrangle, Harney County, southeastern Oregon: U.S. Geological Survey Open-File Report OF-96-675, 1 pl., scale 1:24,000. https://ngmdb.usgs.gov/Prodesc/proddesc_18672.htm

Johnson, J.A., Hooper, P.R., Hawkesworth, C. J., and Binger, G. B., 1998a, Geologic map of the Stemler Ridge quadrangle, Malheur County, southeastern Oregon: U.S. Geological Survey Open-File Report OF-98-105, 1 pl., scale 1:24,000. https://ngmdb.usgs.gov/Prodesc/proddesc_16445.htm

Johnson, J. A., Hawkesworth, C. J., Hooper, P. R., and Binger, G. B., 1998b, Major- and trace-element analyses of Steens Basalt, southeastern Oregon: U.S. Geological Survey Open-File Report 98-482, 30 p. https://doi.org/10.3133/ofr98482

Jordan, B. T., Streck, M. J., and Grunder, A. L., 2002, Bimodal volcanism and tectonism of the High Lava Plains, Oregon, *in* Moore, G. W., ed., Field guide to geologic processes in Cascadia, Field trips to accompany the 98th Annual Meeting of the Cordilleran Section of the Geological Society of America, May 13–15, 2002, Corvallis, Oregon: Oregon Department of Geology and Mineral Industries Special Paper 36, p. 23–46. https://www.oregongeology.org/pubs/sp/SP-36.pdf

Jordan, B. T., Grunder, A. L., Duncan, R. A., and Deino, A. L., 2004, Geochronology of age-progressive volcanism of the Oregon High Lava Plains: Implications for the plume interpretation of Yellowstone: Journal of Geophysical Research, v. 109, no. B10, B10202, 19 p. https://doi.org/10.1029/2003JB002776

Khatiwada, M., and Keller, G. R., 2015, An integrated geophysical imaging of the upper crustal features in the Harney Basin, southeast Oregon: Geosphere, v. 11, no. 1, p. 185–200. https://doi.org/10.1130/GES01046.1

Kittleman, L. R., Green, A. R., Hagood, A. R., Johnson, A. M., McMurray, J. M., Russell, R. G., and Weeden, D. A., 1965, Cenozoic stratigraphy of the Owyhee region, southeastern Oregon: University of Oregon, Museum of Natural History Bulletin, no. 1, 45 p.

Langer, V. W., 1991, Geology and petrologic evolution of the silicic to intermediate volcanic rocks underneath Steens Mountain basalt, SE Oregon: Corvallis, Oreg., Oregon State University, M.S. thesis, 109 p., 1 pl., scale 1:24,000. https://ir.library.oregonstate.edu/concern/graduate_thesis_or_dissertations/p8418q421

Lawrence, R. D., 1976, Strike-slip faulting terminates the Basin and Range province in Oregon: Geological Society of America Bulletin, v. 87, no. 6, p. 846–850. https://doi.org/10.1130/0016-7606(1976)87<846:SFTTBA>2.0.CO;2

Le Bas, M. J., and Streckeisen, A. L., 1991, The IUGS systematics of igneous rocks: Journal of the Geological Society, v. 148, no. 5, p. 825–833. https://doi.org/10.1144/gsjgs.148.5.0825

Le Bas, M. J., Le Maitre, R. W., Streckeisen, A., and Zanettin, B., 1986, A chemical classification of volcanic rocks based on the total alkali-silica diagram: Journal of Petrology, v. 27, no. 3, p. 745–750. https://doi.org/10.1093/petrology/27.3.745

Le Maitre, R. W., and others, 1989, A classification of igneous rocks and glossary of terms: Recommendations of the International Union of Geological Sciences Subcommission on the Systematics of Igneous Rocks: Oxford, Blackwell, 193 p.

Le Maitre, R. W. (ed.), and others, 2004, Igneous rocks: a classification and glossary of terms: recommendations of the International Union of Geological Sciences, Subcommission on the Systematics of Igneous Rocks: Cambridge, Cambridge University Press, 236 p.

Leonard, A. R., 1970, Ground-water resources in Harney Valley, Harney County, Oregon: Salem, Oreg., Oregon Water Resources Department, Ground Water Report 16, 65 p., 3 pl., scale 1:125,000. https://www.oregon.gov/owrd/wrdreports/gw_report_16_harney.pdf

Mackenzie, W. S., Donaldson, C. H., and Guilford, C., 1997, Atlas of igneous rocks and their textures (7th ed.): Addison Wesley Longman, 148 p.

MacLeod, N. S., Walker, G. W., and McKee, E. H., 1976, Geothermal significance of eastward increase in age of upper Cenozoic rhyolitic domes in southeastern Oregon, *in* Second United Nations Symposium on the Development and Use of Geothermal Resources, v. 1: Washington D.C., Government Printing Office, p. 465–474.

McGrane, D, J., 1985, Geology of the Idol City area: a volcanic-hosted, disseminated precious-metal occurrence in east-central Oregon: Missoula, Mont., University of Montana, M.S. thesis, 88 p. https://scholarworks.umt.edu/etd/7536

Meigs, A., and others, 2009, Geological and geophysical perspectives on the magmatic and tectonic development, High Lava Plains and northwest Basin and Range, *in* O'Connor, J. E., Dorsey, R. J., and Madin, I. P., GSA Field Guide 15, Volcanoes to Vineyards: Boulder, Colo., Geological Society of America. https://doi.org/10.1130/2009.fld015(21)

Milliard, J. B., 2010, Two-stage opening of the northwestern Basin and Range in eastern Oregon: Evidence from the Miocene Crane Basin: Corvallis, Oreg., Oregon State University, M.S. thesis, 82 p.

Minor, S. A., Rytuba, J. J., Grubensky, M. J., Meulen, D. B. V., Goeldner, C. A., and Tegtmeyer, K. J., 1987a, Geologic map of the High Steens and Little Blitzen Gorge Wilderness Study areas, Harney County, Oregon: U.S. Geological Survey Miscellaneous Field Studies Map MF-1876, 1 pl., scale 1:24,000. https://ngmdb.usgs.gov/Prodesc/proddesc_7460.htm

Minor, S. A., Rytuba, J. J., Vander Meulen, D. B., Grubensky, M. J., and Tegtmeyer, K. J., 1987b, Geologic map of the Wildhorse Lake quadrangle, Harney County, Oregon: U.S. Geological Survey Miscellaneous Field Studies Map MF-1915, 1 pl., scale 1:24,000. https://ngmdb.usgs.gov/Prodesc/proddesc_5480.htm

NCGMP (USGS National Cooperative Geologic Mapping Program), 2010, NCGMP09—Draft standard format for digital publication of geologic maps, version 1.1, *in* Soller, D. R., ed., Digital Mapping Techniques '09—Workshop Proceedings: U.S. Geological Survey Open-File Report 2010–1335, p. 93–146. https://pubs.usgs.gov/of/2010/1335/pdf/usgs_of2010-1335.pdf

Niem, A. R., 1974, Wright's Point, Harney County, Oregon: an example of inverted topography: Ore Bin, v. 36, no. 3, 33–49. https://www.oregongeology.org/pubs/OG/OBv36n03.pdf

Niewendorp, C. A., and Geitgey, R. P., 2009, Mineral information layer for Oregon (MILO), release 2, GIS files. https://www.oregongeology.org/milo/index.htm

Niewendorp, C. A., Duda, C. J. M., Houston, R. A., and McClaughry, J. D., 2018, Geologic map of the Devine Ridge South 7.5 minute quadrangle, Harney County, Oregon: Oregon Department of Geology and Mineral Industries Geologic Map Series GMS-120, 65 p., 1 pl., scale 1:24,000.

Ogg, J. G., Ogg, G., and Gradstein, F. M., 2008, The concise geologic time scale: Cambridge University Press, 150 p.

Parker, D. J., 1974, Petrology of selected volcanic rocks of the Harney Basin, Oregon: Corvallis, Oreg., Oregon State University, Ph.D. dissertation, 153 p., 1 pl. https://ir.library.oregonstate.edu/concern/graduate_thesis_or_dissertations/r494vn606

Piper, A. M., Robinson, T. W., and Park C. F., 1939, Geology and ground-water resources of the Harney Basin, Oregon: U.S. Geological Survey Water Supply Paper 841, 189 p., 1 pl., scale 1:125,000. https://pubs.er.usgs.gov/publication/wsp841

Robertson, S., 1999, BGS rock classification scheme, v. 2, Classification of metamorphic rocks: Keyworth, U.K., British Geological Survey Research Report RR 99-02, 24 p. http://nora.nerc.ac.uk/id/eprint/3226/1/RR99002.pdf

Russell, I. C., 1884, A geological reconnaissance in southern Oregon: U.S. Geological Survey Annual Report 4 (1882-1883), p. 431–464. https://doi.org/10.3133/ar4

Sheppard, R. A., 1994, Zeolitic diagenesis of tuffs in Miocene lacustrine rocks near Harney Lake, Harney County, Oregon: U.S. Geological Survey Bulletin 2108, 28 p. https://pubs.usgs.gov/bul/2108/report.pdf

Sherrod, D. R., and Johnson, J. A., 1994, Geologic map of the Irish Lake quadrangle, Harney County, south-central Oregon: U.S. Geological Survey Miscellaneous Field Studies Map MF-2256, 1 sheet, scale 1:24,000. https://ngmdb.usgs.gov/Prodesc/proddesc_5877.htm

Smith, G. A., 1986a, Stratigraphy, sedimentology, and petrology of Neogene rocks in the Deschutes Basin, central Oregon: a record of continental margin volcanism and its influence on fluvial sedimentation in an arc-adjacent basin: Corvallis, Oreg., Oregon State University, Ph.D. dissertation, 467 p, 3 pl., scale 1:24,000.

Smith, G. A., 1986b, Stratigraphy, sedimentology, and the petrology of Neogene rocks in the Deschutes Basin, central Oregon: A record of continental-margin volcanism and its influence on fluvial sedimentation in an arc-adjacent basin: Richland, Wash., U.S. Department of Energy Basalt Waste Isolation Project, Rockwell Hanford Operations Publication RHO-BW-SA-555 P, 1 pl., scale 1:24,000.

Smith, J. V., and MacKenzie, W. S., 1958, The cooling history of high-temperature sodium-rich feldspars, pt. 4 *of* The alkali feldspars: Am. Mineralogist, v. 43, no. 9-10, p. 872–889.

Smith, R. L., and Roe, W. P., 2015, Oregon geologic data compilation [OGDC], release 6 (statewide): Oregon Department of Geology and Mineral Industries Digital Data Series OGDC-6, geodatabase. https://www.oregongeology.org/pubs/dds/p-OGDC-6.htm

Streck, M. J., 1994, Volcanology and petrology of the Rattlesnake Ash-Flow Tuff, eastern Oregon: Corvallis, Oreg., Oregon State University, Ph.D. dissertation, 184 p.

Streck, M., and Ferns, M., 2004, The Rattlesnake Tuff and other Miocene silicic volcanism in eastern Oregon, chap. 1 *of* Haller, K. M., and Wood, S. H., Geological field trips in southern Idaho, eastern Oregon, and northern Nevada: U.S. Geological Survey Open-File Report 2004-1222, p. 4–19. https://pubs.usgs.gov/of/2004/1222/

Streck, M. J., and Grunder, A. L., 1995, Crystallization and welding variations in a widespread ignimbrite sheet; the Rattlesnake Tuff, eastern Oregon, USA: Bulletin of Volcanology, v. 57, no. 3, p. 151–169. https://doi.org/10.1007/BF00265035

Streck, M. J., Ferns, M. L., and McIntosh, W., 2015, Large, persistent rhyolitic magma reservoirs above Columbia River Basalt storage sites: The Dinner Creek Tuff Eruptive Center, eastern Oregon: Geological Society of America, Geosphere, v. 11, no. 2, 226–235. doi:10.1130/GES01086.1

Thompson, G. A., and Burke, D. B., 1974, Regional geophysics of the Basin and Range province: Ann. Rev. Earth Planet. Sci., v. 2, 213-238. https://doi.org/10.1146/annurev.ea.02.050174.001241

Thormahlen, D. J., 1984, Geology of the northwest one-quarter of the Prineville quadrangle, central Oregon: Corvallis, Oreg., Oregon State University, M.S. thesis, 106 p. 1 pl., scale 1:24,000.

Trench, D., 2008, The termination of the Basin and Range Province into a clockwise rotating region of transtension and volcanism, central Oregon: Corvallis, Oreg., Oregon State University, M.S. thesis, 64 p.

Walker, G. W., 1970, Cenozoic ash-flow tuffs of Oregon: Ore Bin, v. 32, no. 6, 97–115. https://www.oregongeology.org/pubs/OG/OBv32n06.pdf

Walker, G. W., 1977, Geologic map of Oregon east of the 121st meridian: U.S. Geological Survey Miscellaneous Investigations Map I-902, 2 sheets, scale 1:500,000. https://ngmdb.usgs.gov/Prodesc/proddesc_9795.htm

Walker, G. W., 1979, Revisions to the Cenozoic stratigraphy of Harney Basin, southeastern Oregon: U.S. Geological Survey Bulletin 1475, 35 p., 1 pl. https://doi.org/10.3133/b1475

Walker, G. W., and MacLeod, N. S., 1991, Geologic map of Oregon: U.S. Geological Survey, scale 1:500,000. https://ngmdb.usgs.gov/Prodesc/proddesc_16259.htm

Walker, G. W., and Repenning, C. A., 1965, Reconnaissance geologic map of the Adel quadrangle, Lake, Harney, and Malheur Counties, Oregon: U.S. Geological Survey, Miscellaneous Geologic Investigations Map IMAP-446, 1 pl., scale 1:250,000. https://doi.org/10.3133/i446

Wallace, R. E., and Calkins, J. A., 1956, Reconnaissance geologic map of the Izee and Logdell quadrangles, Oregon: U.S. Geological Survey Miscellaneous Field Studies Map MF-82, scale 1:62,500. https://ngmdb.usgs.gov/Prodesc/proddesc_2988.htm

Watkins, N. D., and Baksi, A. K., 1974, Magnetostratigraphy and oroclinal folding of the Columbia River, Steens, and Owyhee basalts in Oregon, Washington, and Idaho: American Journal of Science, v. 274, no. 2, 148–189. doi: 10.2475/ajs.274.2.148

Wentworth, C. K., 1922, A scale of grade and class terms of clastic sediments: Journal of Geology, v. 30, no. 5, p. 377–392.

Whitehead, R. L., 1994, Ground water atlas of the United States: Segment 7, Idaho, Oregon, Washington: U.S. Geological Survey Hydrologic Atlas 730-H, 31 p. https://doi.org/10.3133/ha730H

12.0 APPENDIX

This appendix contains a summary of the geodatabase along with a description of analytical and field methods and the list of attribute fields for spreadsheets (see page 7 of this report). The appendix is divided into two sections:

- Section 12.1 describes the digital databases included with this publication.
- Section 12.2 contains a summary of analytical and field methods. Accompanying tables, explain the fields listed in various spreadsheets.

12.1 Geographic Information Systems (GIS) database

Geodatabase specifications

Digital data created for the Devine Ridge North 7.5′ quadrangle are stored in an Esri format geodatabase. The geodatabase structure follows that outlined by the U.S. Geological Survey (USGS) National Cooperative Geologic Mapping Program 2009 draft standard format for digital publication of geologic maps, version 1.1 (NCGMP, 2010). The following information describes the overall database structure, the feature classes, and supplemental tables (**Figure 12-1**, **Figure 12-2**, **Figure 12-3**, **Table 12-1**, and **Table 12-2**).

The data are stored in a file geodatabase feature dataset (GeologicMap). Accessory file geodatabase tables (DataSources, DescriptionOfMapUnits, Glossary) were created by using ArcGIS version 10.2.2 (SP 1). The GeologicMap feature dataset contains all the spatially oriented data (feature classes) created for the Devine Ridge South 7.5′ quadrangle. The file geodatabase tables are used to hold additional geologic attributes.

Figure 12-1. Devine Ridge North 7.5′ quadrangle geodatabase feature dataset and data tables.

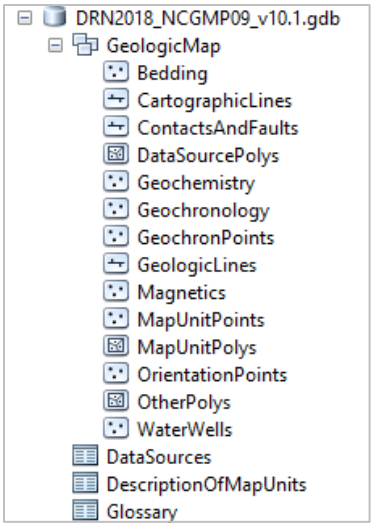

Geodatabase feature class specifications

Each feature class within the GeologicMap feature dataset in the geodatabase contains detailed metadata. Please see the metadata for detailed information such as process descriptions, accuracy specifications, and entity attribute descriptions.

Figure 12-2. Devine Ridge North 7.5’ quadrangle geodatabase feature classes and descriptions.

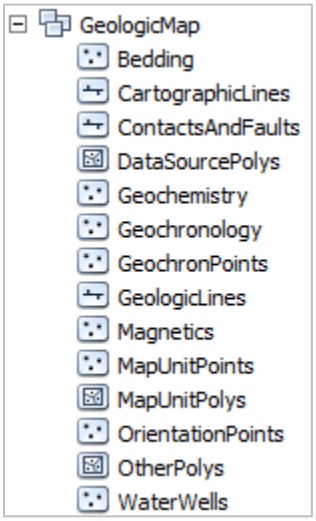

Table 12-1. Feature class description.

Name	Description
Bedding	This feature class represents point locations in the quadrangle where bedding measurements were made or were compiled from previous studies. These data are also contained in the bedding (strike and dip) spreadsheet described in more detail below.
CartographicLines	Vector lines that have no real-world physical existence and do not participate in map-unit topology. The feature class includes cross section lines used for cartography for the quadrangle.
ContactsAndFaults	The vector lines in this feature class contains geologic content including contacts and fault locations used to create the map unit polygon boundaries. The existence and location confidence values for the contacts and faults are provided in the feature class attribute table.
DataSourcePolys	This feature class contains polygons that delineate data sources for all parts of the geologic map. These sources may be a previously published map, new mapping, or mapping with a certain technique. For a map with one data source, for example all new mapping, this feature class contains one polygon that encompasses the map area.
Geochemistry	This feature class represents point locations where whole-rock samples have been analyzed by X-ray fluorescence (XRF) techniques in the quadrangle. Includes data collected by the authors during this study or compiled from previous studies. These data are also contained in the geochemistry spreadsheet described in more detail below.
Geochronology	This feature class represents point locations where 40Ar/39Ar isotopic ages have been obtained for rock samples in the quadrangle. Data collected by the authors during the course of this study. These data are also contained in the geochronology spreadsheet described in more detail below.
GeochronPoints	This feature class represents point locations where 40Ar/39Ar isotopic ages have been obtained for rock samples in the quadrangle. Complete analytical data are shown in the analysis-specific table Geochronology.
GeologicLines	These vector lines represent known fold axis locations in the quadrangle. The existence and location confidence for the fold axes are provided in the feature class attribute table.
Magnetics	This feature class represents point locations where measurements of natural remanent magnetization have been obtained for strongly magnetized lavas in the quadrangle. Includes data collected by the authors during the course of this study. These data are also contained in the magnetic polarity spreadsheet described in more detail below.
MapUnitPoints	This feature class represents points used to generate the MapUnitPolys feature class from the ContactsAndFaults feature class.
MapUnitPolys	This polygon feature class represents the geologic map units as defined by the authors.

OrientationPoints	This feature class represents point locations in the quadrangle where bedding measurements were made or were compiled from previous studies. These data are also contained in the bedding (strike and dip) spreadsheet described in more detail below.
OtherPolys	This feature class depicts the reference map for the quadrangle study area.
WaterWells	This feature class represents point locations of water wells in the quadrangle. Includes data obtained by the authors from the Oregon Department of Water Resources (OWRD). These data are also contained in the WaterWells spreadsheet described in more detail below.

Geodatabase table specifications

Figure 12-3. Devine Ridge North 7.5' quadrangle geodatabase data tables.

Table name description

Table 12-2. Accompanying tables.

Name	Description
DataSources	Data table that contains information about data sources used to compile the geology of the area.
DescriptionOfMapUnits	Data table that captures the content of the Description of Map Units (DMU), or equivalent List of Map Units and associated pamphlet text, included in a geologic map.
Glossary	Data table that contains information about the definitions of terms used in the geodatabase.

Geodatabase projection specifications

All spatial data are stored in the Oregon Statewide Lambert Conformal Conic projection. The datum is NAD83 HARN. The linear unit is international feet. See detailed projection parameters below:

Projection: Lambert_Conformal_Conic
False_Easting: 1312335.958005
False_Northing: 0.000000
Central_Meridian: -120.500000
Standard_Parallel_1: 43.000000
Standard_Parallel_2: 45.500000
Latitude_Of_Origin: 41.750000
Linear Unit: Foot (0.304800)

Geographic Coordinate System: GCS_North_American_1983_HARN
Angular Unit: Degree (0.0174532925199433299)
Prime Meridian: Greenwich (0.000000000000000000)
Datum: D_North_American_1983_HARN
Spheroid: GRS_1980
Semimajor Axis: 6378137.000000000000000000
Semiminor Axis: 6356752.314140356100000000
Inverse Flattening: 298.257222101000020000

Geologic map

This report is accompanied by a map plate displaying the surficial and bedrock geology at a scale of 1:24,000 and geologic cross sections (Plate 1 facsimile below) for the Devine Ridge North 7.5′ quadrangle. The map plate was generated from detailed geologic data (scale of 1:8,000 or better) contained in the accompanying Esri format geodatabase. Both bedrock and surficial geologic interpretations can be recovered from the geodatabase and can be used to create a variety of additional thematic maps.

Plate 1. Reproduction of the geologic map of the Devine Ridge North 7.5′ quadrangle, Harney County, Oregon. Plate dimensions are 34 by 45 inches. See digital folder for map plate.

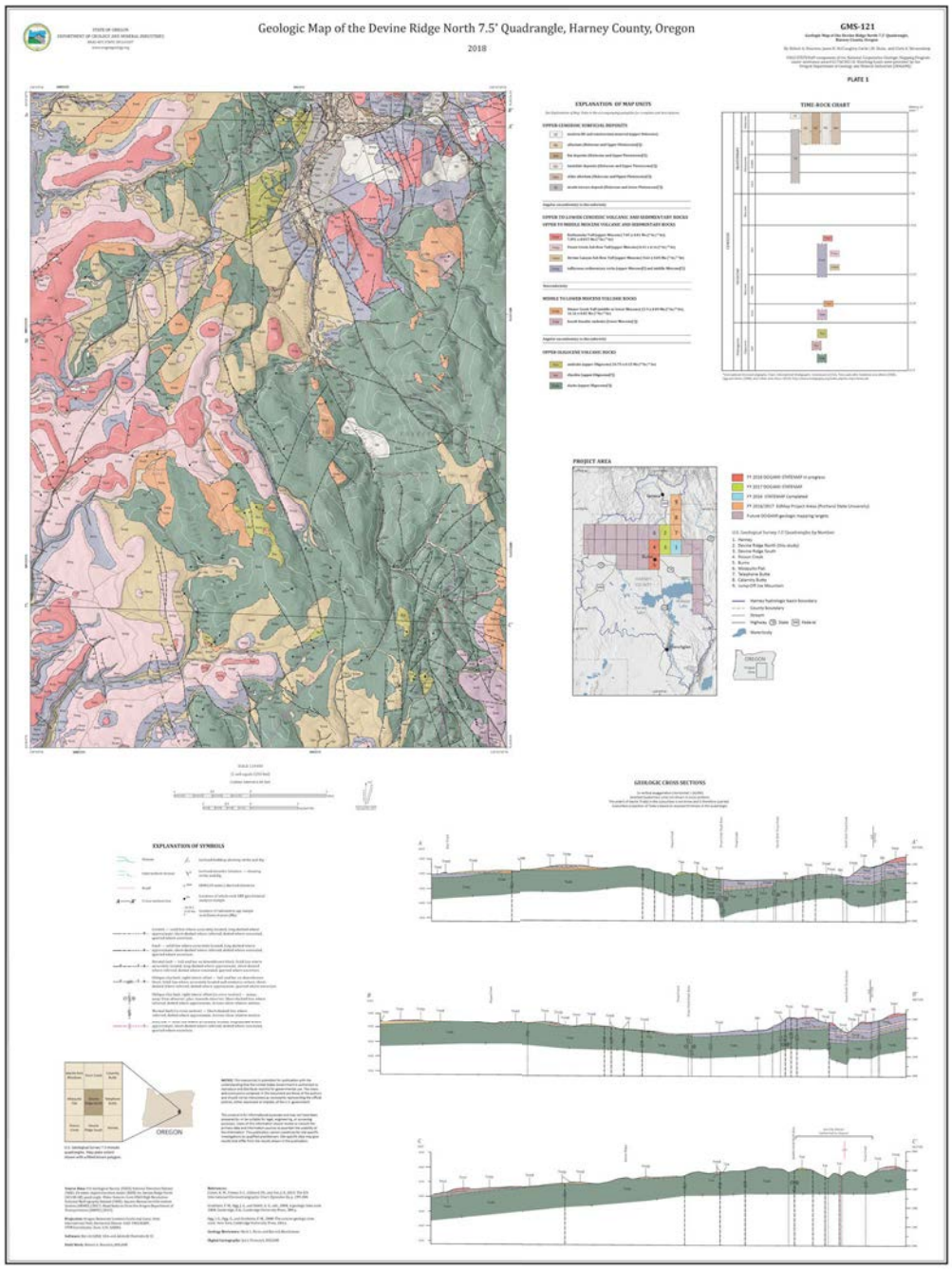

12.2 Methods

Geochemical analytical methods

Geologic mapping in the Devine Ridge North 7.5′ quadrangle was supported by numerous new and compiled X-ray fluorescence (XRF) geochemical analyses of whole-rock samples. Descriptive rock unit names for igneous rocks are based on normalized major element analyses plotted on the total alkalis ($Na_2O + K_2O$) versus silica (SiO_2) diagram (TAS) of Le Bas and others (1986), Le Bas and Streckeisen (1991), and Le Maitre and others (1989, 2004). New and compiled XRF-geochemical analyses are included in the geodatabase, as a separate shapefile named DRN2018_Geochemistry.shp, and as a Microsoft Excel® spreadsheet named DRN2018_Geochemistry.xlsx. **Table 12-3** describes the fields listed in the spreadsheet. The locations of all geochemical samples are given in five coordinate systems: UTM Zone 11 (datum = NAD 27, NAD 83, units = meters), Geographic (datum = NAD 27, NAD 83, units = decimal degrees), and Oregon Lambert (datum = NAD 83, HARN, units = international feet).

Samples denoted by lab abbreviation WSU were analyzed by XRF at the Washington State University GeoAnalytical Lab, Pullman, Washington. Analytical procedures for the Washington State University GeoAnalytical Lab are described by Johnson and others (1999) and can be obtained online at https://s3.wp.wsu.edu/uploads/sites/2191/2017/06/Johnson-Hooper-and-Conrey.pdf. Notes for spreadsheet: nd, no data; ¥ original field sample locations in UTM Zone 11 (datum = NAD 83) coordinates.

Table 12-3. Geochemistry spreadsheet field names and descriptions.

Field	Description
SAMPLE_NO	A unique number identifying the sample. E.g., 18 DRNCN 17.
MAP_NO	A unique number identifying the sample on the map plates.
QUADRANGLE	The USGS 7.5' quadrangle in which the sample is located. E.g., Devine Ridge North.
ELEV_FT	Elevation of sample location in feet. E.g., 1928.
UTMN_NAD27	Meters north in NAD 27 UTM projection, zone 11.
UTME_NAD27	Meters east in NAD 27 UTM projection, zone 11.
LAT_NAD27	Latitude in NAD 27 geographic coordinates.
LONG_NAD27	Longitude in NAD 27 geographic coordinates.
UTMN_NAD83	Meters north in NAD 83 UTM projection, zone 11.
UTME_NAD83	Meters east in NAD 83 UTM projection, zone 11.
LAT_NAD83	Latitude in NAD 83 geographic coordinates.
LONG_NAD83	Longitude in NAD 83 geographic coordinates.
N_83HARN	Feet north in Oregon Lambert NAD 83, HARN, international feet.
E_83HARN	Feet east in Oregon Lambert NAD 83, HARN, international feet.
TERRANE_GR	Geologic group that the sample is assigned to. See GeologicMap, MapUnitPolys in the geodatabase. E.g., Columbia River Basalt Group. See pamphlet and DescriptionOfMapUnits table in the geodatabase.
FORMATION	Geologic formation that the sample is assigned to. See GeologicMap, MapUnitPolys in the geodatabase. E.g., Dalles Formation. See pamphlet and DescriptionOfMapUnits table in the geodatabase.
MEMBER	Geologic member that the sample is assigned to. See GeologicMap, MapUnitPolys in the geodatabase. E.g., Frenchman Springs. See pamphlet and DescriptionOfMapUnits table in the geodatabase.
MAP_UNIT_N	Geologic unit that the sample is assigned to. See GeologicMap, MapUnitPolys in the geodatabase. E.g., Basalt of Gingko. See pamphlet and DescriptionOfMapUnits table in the geodatabase.
MAP_UNIT_L	Unique label identifying the geologic unit that the sample is assigned to. See GeologicMap, MapUnitPolys in the geodatabase. E.g., Tmtr. See pamphlet and DescriptionOfMapUnits table in the geodatabase.
TAS_LITHOLOGY	Rock name assigned based on the total alkalis ($Na_2O + K_2O$) versus silica (SiO_2) diagram (TAS) of Le Bas and others (1986), Le Bas and Streckeisen (1991), and Le Maitre and others (1989). E.g., Basalt, Rhyolite.
[MAJOR ELEMENTS]	SiO_2, Al_2O_3, TiO_2, FeO*, MnO, CaO, MgO, K_2O, Na_2O, P_2O_5. In wt.%.
[TRACE ELEMENTS]	Ni, Cr, Sc, V, Ba, Rb, Sr, Zr, Y, Nb, Ga, Cu, Zn, Pb, La, Ce, Th, Nd, U, and Co. In ppm.
LOI	Value for loss on ignition as reported by lab.
FE_2O_3	Iron (III) oxide or ferric oxide reported in original analysis.
FeO	Iron (II) oxide or ferrous oxide reported in original analysis.
REFERENCE	Publication reference, keyed to the reference list in this report.
METHOD	Analytical method used by laboratory that analyzed the sample. E.g., XRF.
LABORATORY	Analytical laboratory that analyzed the sample. E.g., F & M.
NOTES	Special information (e.g., alteration) about certain samples.
VOLCANIC_F	Volcanic field that the unit is assigned to. In igneous provinces, a well-defined area covered with volcanic rocks with a common geologic history.

Geochronology analytical methods

One new $^{40}Ar/^{39}Ar$ isotopic age has been obtained for a rock in the Devine Ridge North 7.5' quadrangle during the course of this study. The sample was prepared and analyzed at the College of Oceanic and Atmospheric Sciences, Oregon State University, Corvallis. Duncan and others (1997) described the $^{40}Ar/^{39}Ar$ methodology used at Oregon State University. Original data sheets for the new $^{40}Ar/^{39}Ar$ isotopic age are located in the digital folder named 40Ar39ArAnalyticalData. The geochronological datum is included in the geodatabase, as a separate shapefile named DRN2018_Geochronology, and as a Microsoft Excel® spreadsheet named DRN2018_Geochronology.xlsx. **Table 12-4** describes the fields listed in the spreadsheet. The location of the radiometric age is given in five coordinate systems: UTM Zone 11 (datum = NAD 27, NAD 83, units = meters), Geographic (datum = NAD 27, NAD 83, units = decimal degrees), and Oregon Lambert (datum = NAD 83, HARN, units = international feet). Notes for spreadsheet: na, not applicable; nd, no data.

Table 12-4. Geochronology spreadsheet field names and descriptions.

Field	Description
SAMPLE_NO	A unique number identifying the sample.
CORE_ID	A unique number identifying a drill core from which the sample was obtained.
QUADRANGLE	The USGS 7.5' quadrangle in which the sample is located.
ELEV_FT	Elevation of sample location in feet.
UTMN_NAD27	Meters north in NAD 27 UTM projection, zone 11.
UTME_NAD27	Meters east in NAD 27 UTM projection, zone 11.
LAT_NAD27	Latitude in NAD 27 geographic coordinates.
LONG_NAD27	Longitude in NAD 27 geographic coordinates.
UTMN_NAD83	Meters north in NAD 83 UTM projection, zone 11.
UTME_NAD83	Meters east in NAD 83 UTM projection, zone 11.
LAT_NAD83	Latitude in NAD 83 geographic coordinates.
LONG_NAD83	Longitude in NAD 83 geographic coordinates
N_83HARN	Feet north in Oregon Lambert NAD 83, HARN, international feet
E_83HARN	Feet east in Oregon Lambert NAD 83, HARN, international feet
TERRANE_GR	Geologic group that the sample is assigned to. See GeologicMap, MapUnitPolys in the geodatabase.
FORMATION	Geologic formation that the sample is assigned to. See GeologicMap, MapUnitPolys in the geodatabase.
MEMBER	Geologic member that the sample is assigned to. See GeologicMap, MapUnitPolys in the geodatabase.
MAP_UNIT_N	Geologic unit that the sample is assigned to. See GeologicMap, MapUnitPolys in the geodatabase.
MAP_UNIT_L	Unique label identifying the geologic unit that the sample is assigned to. See GeologicMap, MapUnitPolys in the geodatabase.
VOLCANIC_FIELD	Volcanic field that the unit is assigned to. In igneous provinces, a well-defined area covered with volcanic rocks with a common geologic history.
LITHOLOGY	Rock type analyzed.
POLARITY	Natural remanent magnetization of the sample analyzed.
AGE_MA	Age determined for the sample in millions of years.
ERROR_MA	Error in age determination in millions of years.
REP_ERROR	Error in age determination in years before present.
METHOD_see_text_appendix	Analytical method used by laboratory that analyzed the sample.
MATERIAL_DATED	Type of material analyzed.
REFERENCE_see_text_report	Publication reference, keyed to the reference list in this report.
LABORATORY	Analytical laboratory that analyzed the sample.
NOTES	Special information (e.g., alteration) about certain samples.

Natural remanent magnetization (magnetic polarity) methods

Field measurements of natural remanent magnetization (the magnetic field of a sample measured when induced magnetic fields are absent or zeroed out by probe; Butler, 1992) were determined from strongly magnetized lavas exposed in the Devine Ridge North 7.5′ quadrangle during the course of this study in order to distinguish between flow units with normal and reversed magnetic polarity. Magnetic polarity also serves as a check on the permissible age of radiometrically dated samples, when compared to the paleomagnetic time scale of Cande and Kent (1992). This method of constraining radiometric ages by magnetic polarity determinations is most effective when the analytical error is less than 0.20 m.y. Larger errors reported for radiometric ages may overlap so many polarity subchrons that no constraint is provided by knowing a sample's magnetic polarity. Magnetic polarity values reported were determined using a Macintyre Electronic Design Associates (MEDA), Inc. μMag handheld digital fluxgate magnetometer. The measured point data are included in the geodatabase, as a separate shapefile named DRN2018_ Magnetics, and as a Microsoft Excel® spreadsheet named DRN2018_Magnetics.xlsx. **Table 12-5** describes the fields listed in the spreadsheet. The locations of these point data are given in five coordinate systems: UTM Zone 11 (datum = NAD 27, NAD 83, units = meters), Geographic (datum = NAD 27, NAD 83, units = decimal degrees), and Oregon Lambert (datum = NAD 83, HARN, units = international feet).

The natural remanent magnetization (magnetic polarity) of strongly magnetized lavas was determined using the following method:

A north-pointing arrow and near-horizontal line were drawn on and around (to the extent possible) an approximately fist-sized equidimensional sample that was then removed from the outcrop (**Figure 12-4a**).

The magnetometer was placed on the most level ground available in a relatively magnetically clean area. The probe was then placed in a fixed position in the horizontal plane and rotated to null the local magnetic field (μMag reads zero). This procedure was done incrementally beginning with minimum range sensitivity (2,000 mG [milliGauss]), increasing the sensitivity (20 mG) and re-rotating the probe until maximum sensitivity was reached. Magnetic polarity was then checked with the north end of a locked compass needle. Total field value will decrease when the compass needle is moved horizontally toward and remains parallel to the probe.

The polarity of a sample was determined by placing the oriented sample in a path parallel to the probe. The north-verging line drawn to represent the approximate magnetic pole of the sample was held horizontally (approximately) with the north end facing toward the probe at a distance of at least 10 times more than the measurement distance. A reading was then determined with the sample absent from the probe. The sample was then moved to a point (typically within 1 to 2 cm) toward the probe in order to cause a change of at least several times greater than the minimum resolution of the magnetometer (**Figure 12-4b**). A decrease in the total field value indicated normal-polarity (N); an increase in total field value indicated reversed-polarity (R).

The sample was then rotated backward (top away from the probe) about a horizontal axis approximately 45° to see if field strength increased as the sample's inclined magnetic field was rotated into parallel with the probe.

The polarity of 2 to 10 representative samples from different portions of an outcrop or from different outcrops was determined to verify the repeatability of results. Erratic results, due to re-magnetization resulting from lighting strikes, obscure post-emplacement alteration, or aberrant declination and inclination are reported as indeterminate (I).

Figure 12-4. Procedure for determining natural remanent magnetism of lavas. (a) Ideal sample is selected and oriented in outcrop. North arrow is drawn on upper surface; horizontal lines are drawn around the exposed edges of the sample. Fist-sized sample is then removed. (b) Magnetometer probe is placed in a fixed position in the horizontal plane and rotated to null the local magnetic field. Sample polarity is determined by moving the oriented sample into the path of the probe.

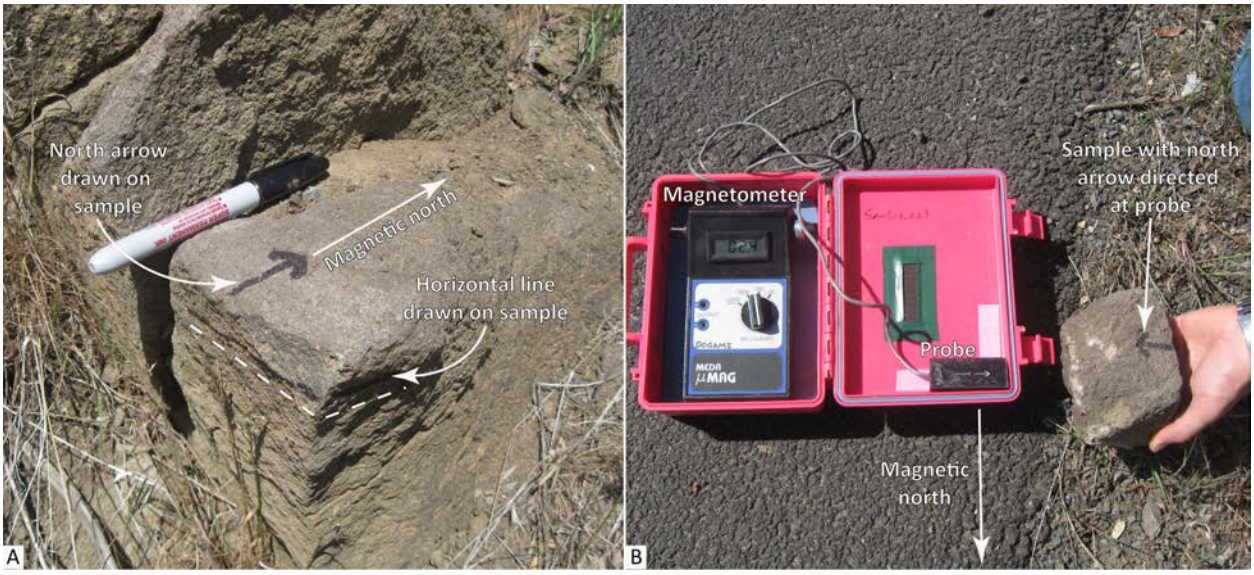

Table 12-5. Natural remanent magnetization (magnetic polarity) spreadsheet field names and descriptions.

Field	Description
SITE	A unique number identifying the sample. E.g., 18DFW.
NRM_see_t	N, R, I: Natural remanent magnetization of sample as determined from a portable fluxgate magnetometer. N is normal polarity, R is reverse polarity, and I is indeterminate.
QUADRANGLE	The USGS 7.5’ quadrangle in which the sample is located. E.g., Devine Ridge North.
ELEV_FT	Elevation of sample location in feet. E.g., 1928.
UTMN_NAD27	Meters north in NAD 27 UTM projection, zone 11.
UTME_NAD27	Meters east in NAD 27 UTM projection, zone 11.
LAT_NAD27	Latitude in NAD 27 geographic coordinates.
LONG_NAD27	Longitude in NAD 27 geographic coordinates.
UTMN_NAD83	Meters north in NAD 83 UTM projection, zone 11.
UTME_NAD83	Meters east in NAD 83 UTM projection, zone 11.
LAT_NAD83	Latitude in NAD 83 geographic coordinates.
LONG_NAD83	Longitude in NAD 83 geographic coordinates
N_83HARN	Feet north in Oregon Lambert NAD 83, HARN, international feet
E_83HARN	Feet east in Oregon Lambert NAD 83, HARN, international feet
TERRANE_GR	Geologic group that the sample is assigned to. See GeologicMap, MapUnitPolys in the geodatabase. E.g., Columbia River Basalt Group. See pamphlet and DescriptionOfMapUnits table in the geodatabase.
FORMATION	Geologic formation that the sample is assigned to. See GeologicMap, MapUnitPolys in the geodatabase. E.g., Dalles Formation. See pamphlet and DescriptionOfMapUnits table in the geodatabase.
MEMBER	Geologic member that the sample is assigned to. See GeologicMap, MapUnitPolys in the geodatabase. E.g., Frenchman Springs. See pamphlet and DescriptionOfMapUnits table in the geodatabase.
MAP_UNIT_N	Geologic unit that the sample is assigned to. See GeologicMap, MapUnitPolys in the geodatabase. E.g., Basalt of Gingko. See pamphlet and DescriptionOfMapUnits table in the geodatabase.
MAP_UNIT_L	Unique label identifying the geologic unit that the sample is assigned to. See GeologicMap, MapUnitPolys in the geodatabase. E.g., Twfg. See pamphlet and DescriptionOfMapUnits table in the geodatabase.
REFERENCE	Publication reference, keyed to the reference list in this report.
METHOD_see	Method used to determine magnetic polarity of the sample.
NOTES	Special information (e.g., alteration) about certain samples.
VOLCANIC_F	Volcanic field that the unit is assigned to. In igneous provinces, a well-defined area covered with volcanic rocks with a common geologic history.

Bedding (strike and dip)

Strike and dip measurements of inclined bedding were taken in the map area during this study by traditional compass and clinometer methods. Additional measurements have been compiled from previous workers. Strikes and dips are reported in both quadrant format (e.g., N30W, 15NE) and azimuthal format using the right-hand rule (e.g., 330, 15NE, American convention). Field measured bedding is coded by its appropriate Federal Geographic Data Committee (FGDC) reference number for geologic map symbolization. The measured point data are included in the geodatabase, as a separate shapefile named DRN2018_Bedding.shp, and as a Microsoft Excel spreadsheet named DRN2018_Bedding.xlsx. **Table 12-6** describes the fields listed in the spreadsheet. The locations of these point data are given in five coordinate systems: UTM Zone 11 (datum = NAD 27, NAD 83, units = meters), Geographic (datum = NAD 27, NAD 83, units = decimal degrees), and Oregon Lambert (datum = NAD 83, HARN, units = international feet). Strike and dip symbols can be properly drawn by the Esri ArcMap product by opening the layer properties, categoriing by type, choosing the appropriate symbol, and rotating the symbol based on the "Strike_Azi" field. (The advanced button allows you to select the rotation field). The rotation style should be set to geographic to maintain the right-hand rule property. Azimuths are given in true north; an additional clockwise correction of about 1.6 degrees is needed to plot strikes and dips properly on the Oregon Lambert conformal conic projection in this area. Notes for spreadsheet: nd, no data.

DOGAMI has developed a routine and model in Esri ArcGIS Model Builder™ to calculate 3-point solutions for SFM-derived bedding. The modeling process incorporates the use of (1) a 5-m SRM-derived DEM (Digital Elevation Model); (2) the registration of three non-collinear points picked along the trace of a geological plane or contact discernable from a 5-m SFM DEM; (3) updating these points with their SFM-derived elevation values; and (4) creating a TIN (triangular irregular network) facet of the three points. The aspect of the TIN facet is equivalent to the dip direction and the slope corresponds to the dip (0˚ to 90˚ degrees). The strike is then determined from the dip direction, subtracting or adding 90˚ based on the right-hand rule (described in paragraph 1 above).

The factors influencing the certainty of SFM-derived bedding are the subjectivity of the digitizer and the clarity of the feature presumed to be indicative of bedding. Where possible aerial photography, combined with a contextual knowledge of the geology of the area, was used to verify bedding features interpreted from the SFM. Agreement of the calculated strikes and dips over small areas, taken together with field measurements and data compiled from previous workers, was used as an accuracy gauge.

Table 12-6. Bedding (strike and dip) spreadsheet field names and descriptions.

Field	Description
STRUCTURE	Type of geologic structure from which feature was determined. E.g., Inclined bedding.
FGDC_REF	An attribute code assigned to each feature, derived from the Federal Geographic Data Committee (FGDC) digital standard for geologic map symbolization. E.g., 6.2.
QUADRANGLE	The USGS 7.5' quadrangle in which the sample is located. E.g., Devine Ridge North.
Elev_FT	Elevation of data location in feet. E.g., 22.
UTMN_NAD27	Meters north in NAD 27 UTM projection, zone 11.
UTME_NAD27	Meters east in NAD 27 UTM projection, zone 11.
LAT_NAD27	Latitude in NAD 27 geographic coordinates.
LONG_NAD27	Longitude in NAD 27 geographic coordinates.
UTMN_NAD83	Meters north in NAD 83 UTM projection, zone 11.
UTME_NAD83	Meters east in NAD 83 UTM projection, zone 11.
LAT_NAD83	Latitude in NAD 83 geographic coordinates.
LONG_NAD83	Longitude in NAD 83 geographic coordinates.
N_83HARN	Feet north in Oregon Lambert NAD 83, HARN, international feet.
E_83HARN	Feet east in Oregon Lambert NAD 83, HARN, international feet.
TERRANE_GR	Geologic group that the sample is assigned to. See GeologicMap, MapUnitPolys in the geodatabase. E.g., Columbia River Basalt Group.
FORMATION	Geologic formation that the sample is assigned to. See GeologicMap, MapUnitPolys in the geodatabase. E.g., Rattlesnake Tuff Formation.
MEMBER	Geologic member that the sample is assigned to. See GeologicMap, MapUnitPolys in the geodatabase.
MAP_UNIT_N	Geologic unit that the sample is assigned to. See GeologicMap, MapUnitPolys in the geodatabase. E.g., dacite.
MAP_UNIT_L	Unique label identifying the geologic unit that the sample is assigned to. See GeologicMap, MapUnitPolys in the geodatabase. E.g., Toda.
STRIKE_QUA	Strike direction of the inclined plane, stated in a north-directed quadrant format. E.g., N35E.
DIP	Amount of dip, degrees from horizontal, with direction. E.g., 45SE.
STRIKE_AZI	Strike direction of the inclined plane, as determined by employing the right-hand rule (American convention). E.g., 035.
DIP_AZIMUT	Azimuthal direction of dip. E.g., 125.
DIP_AMOUNT	Amount of dip, degrees from horizontal. E.g., 45.
REFERENCE	Publication reference, keyed to the reference list in this report.
Notes	Special information (e.g., lidar derived)
VOLCANIC_F	Volcanic field that the unit is assigned to. In igneous provinces, a well-defined area covered with volcanic rocks with a common geologic history.

Water well logs

The well log spreadsheet is derived from written drillers' logs provided by Oregon Department of Water Resources (OWRD). Well logs vary greatly in completeness and accuracy, so the utility of subsurface interpretations based upon these data can be limited. Water well logs compiled and used for interpretation during this study were not field located. The approximate locations were estimated using tax lot maps, street addresses (coordinates obtained from Google Earth™), and aerial photographs to plot locations on the map. The accuracy of the locations ranges widely, from errors of one-half mile possible for wells located only by section and plotted at the section centroid to a few tens of feet for wells located by address or tax lot number on a city lot with bearing and distance from a corner. At each mapped location the number of the well log is indicated. This number can be combined with the first four letters of the county name (e.g., HARN 5473), to retrieve an image of the well log from the OWRD website.

Point data are included in the geodatabase, as a separate shapefile named DRN2018_WaterWells.shp, and as a Microsoft Excel spreadsheet named DRN2018_WaterWells.xlsx. **Table 12-7** describes the fields listed in the spreadsheet. The locations of water well point data are given in six coordinate systems: UTM Zone 11 (datum = WGS 84, NAD 27, NAD 83, units = meters), Geographic (datum = NAD 27, NAD 83, units = decimal degrees), and Oregon Lambert (datum = NAD 83, HARN, units = international feet).

Lithologies in well intervals listed in the well log spreadsheet can alternate between consolidated and unconsolidated and may be listed as alternating between bedrock and surficial geologic units. This may occur where bedrock units are soft, where paleosols or weak zones lie within bedrock, or where cemented or partly cemented zones alternate with unconsolidated zones in surficial deposits.

Lithologic abbreviations used (alphabetical by group)

UNCONSOLIDATED SURFICIAL UNITS	
Abbreviation	**Description**
a	Ash
bd	Boulders
c	Clay
ch	Clay, hard (often logged as claystone but probably not bedrock)
g	Gravel
gc	Cemented gravel
gs	Gravel and sand (also sandy gravel)
m	Mud
s	Sand
sg	Sand and gravel (also gravelly sand)
st	Silt
ROCK, sedimentary	
ar	Argillite
bc	Breccia
cg	Conglomerate
cs	Claystone
pbs	Pebbly sandstone
sh	Shale
sts	Siltstone
ss	Sandstone
ROCK, igneous	
an	Andesite
b	Basalt
ba	Basaltic andesite
cd	Cinders
pu	Pumice
d	Diorite
gb	Gabbro
gr	Granite
l	Lava
r	Rhyolite
sc	Scoria
t	Tuff
v	Volcanic, undivided
vb	Volcanic breccia
Other	
af	Artificial fill
cl	Coal (lignite)
dg	Decomposed granite
o	Other (drillers unit listed in notes column of spreadsheet)
rk	Rock
sl	Soil
u	Unknown (typically used where a well has been deepened)

Table 12-7. Water well log spreadsheet field names and descriptions.

Field	*Description and Example
TRS	Two digits for township, two digits for range, and two for section; negative if township is south of Willamette baseline. Exception for township and range if they contain a decimal. E.g., −2132.503.
COUNTY	Harney County. E.g., HARN.
GRID	Well log number for wells. Wells in Harney County preceded by acronym HARN (e.g., HARN 53799). E.g., 53779.
WELL_EL_FT	Wellhead elevation in feet as given by Google Earth™ at corresponding WGS 84 location. E.g., 1978.
LOCATED_BY	Google Earth™ elevation for cursor location at a given address. E.g., Google.
	Google Earth™ elevation at house in vicinity of given address. E.g., House.
	Pad identifying approximate well location, visible in air photo. E.g., Pad.
	Approximate taxlot centroid or other best guess for well location using a combination of taxlot maps and aerial photographs. E.g., Taxlot.
	Owner name. E.g., Owner.
	Wells located by Oregon Water Resources Department (OWRD) using handheld GPS. E.g., OWRD.
	GPS coordinates of wellhead included with well log. E.g., GPS.
	Approximate quarter-quarter-section centroid. E.g., qq.
	Approximate quarter-section centroid. E.g., q.
	Approximate fit to sketch map included with well log. E.g., map
LITHOLOGY	Best interpretation of driller's log using abbreviations above. E.g., g.
BASE_FT	Record base of driller's interval or, if lithology abbreviation would not change, similar intervals, in feet below wellhead. E.g., 17.
TOP_FT	Calculated top of driller's interval or similar intervals, in feet below wellhead. E.g., 14.
TOP_EL_FT	Calculated elevation at top of driller's interval, or similar intervals, in feet above sea level. E.g., 86.
BASE_EL_FT	Calculated elevation at base of driller's interval, or similar intervals, in feet above sea level. E.g., 83.
BEDRK_LITH	Lists bedrock lithologies, when encountered, abbreviations listed above. E.g., b.
BEDRK_ELEV	Calculated elevation at which bedrock or soil over bedrock was first encountered, in feet above sea level. E.g., 1924.
TAX_LOT	Taxlot number. Where it is determined that a taxlot number is used more than once in the section then the appropriate subdivision of the section is indicated in the notes field. E.g., 800.
COLOR	Color of interval as reported by the well driller. E.g., green.
NOTES	Notes about the stratigraphic interval as originally described by the well driller.
MAP_LABEL	Geologic unit interpreted in subsurface based on drillers log and designated by map unit label used in accompanying geodatabase. Intervals labeled "suna" (surface unit not applicable) are those where the lithology as interpreted by the original drillers' log do not correspond; also denotes intervals in the subsurface where a precise unit label cannot be applied. E.g., Tb.
QUADRANGLE	The USGS 7.5' quadrangle in which the sample is located. E.g., Devine Ridge North.
UTMN_WGS84	Meters north in WGS84 UTM projection, zone 11.
UTME_WGS84	Meters east in WGS84 UTM projection, zone 11.
UTMN_NAD27	Meters north in NAD 27 UTM projection, zone 11.
UTME_NAD27	Meters east in NAD 27 UTM projection, zone 11.
LAT_NAD27	Latitude in NAD 27 geographic coordinates.
LONG_NAD27	Longitude in NAD 27 geographic coordinates.
UTMN_NAD83	Meters north in NAD 83 UTM projection, zone 11.
UTME_NAD83	Meters east in NAD 83 UTM projection, zone 11.
LAT_NAD83	Latitude in NAD 83 geographic coordinates.
LONG_NAD83	Longitude in NAD 83 geographic coordinates.
N_83HARN	Feet north in Oregon Lambert NAD 83, HARN, international feet.
E_83HARN	Feet east in Oregon Lambert NAD 83, HARN, international feet.

*Well location given in six coordinate systems calculated by reprojecting original WGS 84 UTM, zone 11 locations.